Comparison of Current Control Schemes for Single-Phase Grid-Connected PV Inverter with MPPT

DISSERTATION
SUBMITTED IN PARTIAL FULFILLMENT OF THE REQUIREMENTS
FOR THE AWARD OF THE DEGREE
OF

MASTER OF TECHNOLOGY
IN
POWER SYSTEMS

Submitted by:

Shobhit R.K. Sharma
2K18/PSY/08

Under the supervision of
Prof. Alka Singh

DEPARTMENT OF ELECTRICAL ENGINEERING
DELHI TECHNOLOGICAL UNIVERSITY
(Formerly Delhi College of Engineering)
Bawana Road, Delhi-110042

2020

DEPARTMENT OF ELECTRICAL ENGINEERING
DELHI TECHNOLOGICAL UNIVERSITY
(Formerly Delhi College of Engineering)
Bawana Road, Delhi-110042

CANDIDATE'S DECLARATION

I, Shobhit R.K. Sharma, Roll No. 2K18/PSY/08 student of M. Tech (Power Systems), hereby declare that the dissertation titled "Comparison of Current Control Schemes for Single-Phase Grid-Connected PV Inverter with MPPT" which is submitted by me to the Department of Electrical Engineering, Delhi Technological University, Delhi in partial fulfillment of the requirement for the award of the degree of Master of Technology, is original and not copied from any source without proper citation. This work has not previously formed the basis for the award of any Degree, Diploma Associate-ship, Fellowship or other similar title or recognition.

Place: New Delhi **Shobhit R.K. Sharma**

Date: 25-08-2020 **(2K18/PSY/08)**

DEPARTMENT OF ELECTRICAL ENGINEERING
DELHI TECHNOLOGICAL UNIVERSITY
(Formerly Delhi College of Engineering)
Bawana Road, Delhi-110042

CERTIFICATE

I hereby certify that the major project titled "**COMPARISON OF CURRENT CONTROL SCHEMES FOR SINGLE-PHASE GRID-CONNECTED PV INVERTER WITH MPPT**" which is submitted by SHOBHIT RK SHARMA, Roll No-2K18/PSY/08 ELECTRICAL ENGINEERING DEPARTMENT, Delhi Technological University, Delhi, in partial fulfilment of the requirement for the award of the degree of Master of Technology, is a record of the project work carried out by the students under my supervision. To the best of my knowledge this work has not been submitted in part or full for any Degree to this University or elsewhere.

Place: New Delhi

Date: 25-08-2020

PROF. ALKA SINGH
(SUPERVISOR)

Professor
Department of Electrical Engineering
Delhi Technological University

ABSTRACT

This project analyze and compares four current control schemes for a single-phase grid-connected PV inverter. The first two methods discussed are Synchronous Reference Frame (d-q) and Proportional Resonant (PR) based controllers. Both are linear regulators which uses Pulse Width Modulation (PWM) for the generation of the control signals. The PR controller provides high gain at a chosen frequency (also known as resonant frequency), due to which it is able to subdue the steady state error. Therefore, it can be successfully applied to the circuits where the controlled parameter is sinusoidal in nature with frequency of operation equal to that of resonant frequency. Whereas a PI controller suffers from steady state error and high sensitivity towards disturbance when used with sinusoidal input. To counteract this limitation of PI, the d-q transform is used to convert sinusoidal signals in stationary frame to DC signals in rotatory frame. This way the PI controller is able to bring the steady state error to zero.

The other two methods described are Fuzzy logic control (FLC) and Model predictive control (MPC). These are advanced control techniques which takes into account the non-linearity of power converters. FLC also works on DC parameters and therefore the controller structure is similar to that of d-q controller except that instead of PI, a fuzzy inference system (FIS) is used to do the job. MPC on the other hand uses the state space model of the system for predicting the future value of the controlled variables. This predicted value is utilized by the controller to find the required switching state, which is in accordance with a predefined cost function. The four schemes designed are compared based on their mathematical modeling, working principle, dynamic response to disturbances, and the ease of implementation.

The modeled system consists of PV, single phase H-bridge inverter, LCL-filter and an AC grid. Compared to the L and LC filter, the LCL filter has higher harmonic attenuation at the switching frequency and better decoupling from the grid impedance. However, it suffers from inherent resonance which may introduce instability in the system. To overcome this problem, a proper damping method is required to suppress the oscillations and this is achieved using either passive damping or active damping. The often used passive damping method is to connect a resistance in series with the filter capacitor. This method has been used so as to keep the control system simple and reduce sensor circuitry. However, it reduces efficiency of the overall system. The PWM technique which has been used is Bipolar Sinusoidal Pulse Width Modulation (SPWM). This is because as compared to Unipolar SPWM, it reduces the ground leakage current and thus provide galvanic isolation to the PV system from the AC grid.

The outer voltage control loop consists of a PI controller whose output acts as a reference for the inner current control loop. The outer loop regulates the PV voltage by comparing DC link capacitor voltage with the Perturb & Observe (P&O) MPPT algorithm to obtain maximum power from the modules. The effectiveness of the developed methods has been confirmed with the help of the simulation results. A 5 kVA grid-connected PV inverter is designed for this research on MATLAB/Simulink.

A hardware implementation of a single phase H-bridge inverter with an LC filter is also presented. It consists of H-bridge IGBT inverter, driver circuit, level shifter circuit, auxiliary power supply, and a micro-controller. A basic open loop operation is performed and validated with the simulation results.

ACKNOWLEDGEMENT

I am highly grateful to the Department of Electrical Engineering, Delhi Technological University (DTU) for giving me the opportunity to carry out this project work.

The constant guidance and encouragement received from my supervisor Prof. Alka Singh of Department of Electrical Engineering, DTU, has been of great help in carrying my present work and is acknowledged with reverential thanks.

I would also like to thank Mr. Hemant Saxena (PhD scholar), Mr. Amarendra Pandey (PhD scholar), Mr. Allu Bhargav (PhD scholar) and Mr. Dhruv Bhatia (M.Tech. Student) for their guidance and continuous support in completion of this project work.

Finally, I would like to express my gratitude to the faculty members of Electrical Engineering Department, DTU for their continuous support in my M. Tech. study at DTU.

Shobhit R.K. Sharma

2K18/PSY/08

M. Tech. (Power Systems)

Delhi Technological University

CONTENTS

List of Tables

List of Figures

List of Abbreviations

DC	Direct Cycle
AC	Alternating Cycle
PV	Photo-Voltaic
CSP	Concentrated Solar Power
MPP	Maximum Power Point
MPPT	Maximum Power Point Tracking
PWM	Pulse Width Modulation
SPWM	Sinusoidal Pulse Width Modulation
MATLAB	Matrix Laboratory
ESR	Equivalent Series Resistance
PI	Proportional-Integral
PR	Proportional Resonant
PLL	Phase Locked Loop
FLC	Fuzzy Logic Control
COG	Center of Gravity
MPC	Model Predictive Control
IGBT	Insulated Gate Bipolar Transistor
UART	Universal Asynchronous Receiver Transmitter
DTC	Direct Torque Control
DPC	Direct Power Control
ADC	Analog to Digital Converter
FOC	Field Oriented Control
VOC	Voltage Oriented Control
GPIO	General Purpose Input Output
GCC	Grid Connected Converter
THD	Total Harmonic Distortion
FFT	Fast Fourier Transform

Chapter 1

INTRODUCTION

1.1 Background

Energy is an important aspect in today's society for it is required to produce goods and perform mechanical work [1]. Conventional sources of energy such as coal, crude oil and natural gas are still predominantly used for the production of electricity, but Renewable resources use have also slowly increased a lot since 1970s [1]. As shown in Fig. 1.1, Global energy demand and technological advancement has contributed to the growth of the Renewable sources. Despite of converters energy efficiency going up, the global energy demand is predicted to shoot up until 2040, that too especially in third world countries [2].

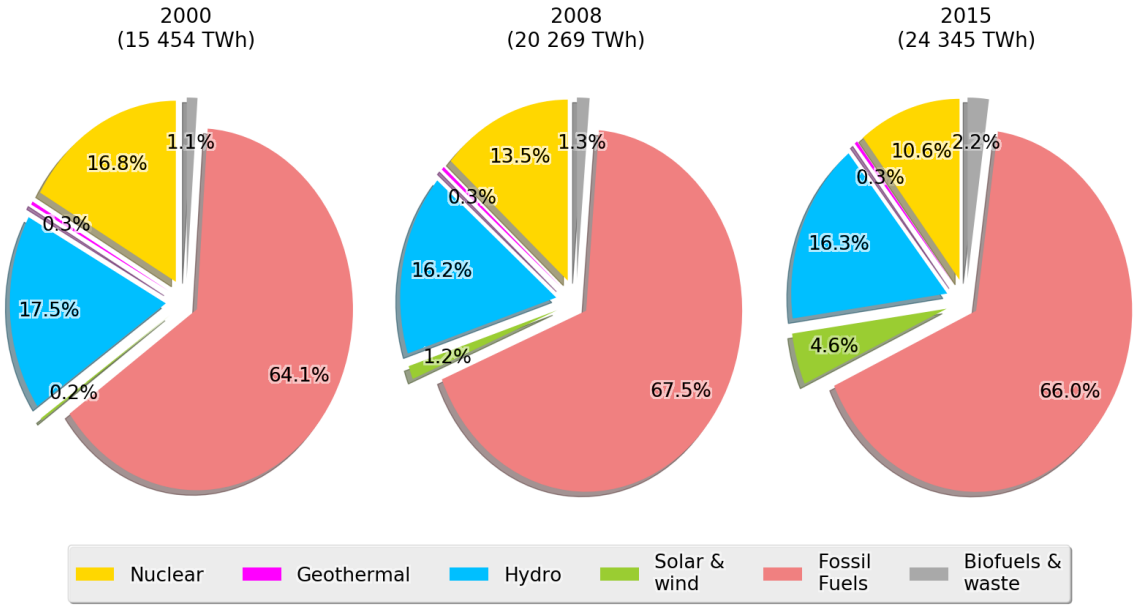

Figure 1.1: Global electricity production based on energy resources used [3][4][5].

The field of renewable energy resources is growing very fast and it is projected to increase by an average of 2.6% per year globally until 2040 [6]. Integration of utility and the renewable energy sources brings economic and environmental benefits. Though, the main challenge for integrated system is to offset the varying energy supply due to changing atmospheric conditions and economic competitiveness with the conventional sources [7]. Also clean energy resources have garnered interest from countries looking to reduce their carbon footprints [8].

Renewable energy sources are part of India's vision not only to bring clean and affordable energy within the reach of all people but also achieve social equity and address sustainability concerns. Tapping these energy sources has already put India on energy transition path with cleaner ecology, energy independence, and a stronger financial system. India has ensured that the best approaches are implemented for accelerating deployment, spurring innovative businesses and meeting the climate change mitigation goals.

With over 78 GW installed renewable power capacity, 65 GW at different stages of fruition, India is well on the way to attaining its target. Since 2014, solar power capacity has grown over 11 times and wind power capacity rose by 1.7 times. Now, India has the fifth largest renewable power installed capacity globally. However, this target is just the beginning, and by no means a ceiling of the ambition [9].

Creating an environment for developing renewable energy technologies indigenously and facilitating domestic manufacturing, handling intermittency of renewable power; improving forecasting technology; creating an efficient and resilient renewable power transmission infrastructure; and developing storage technologies are the challenges and we have been making focused efforts in their direction. Strategic research towards renewables includes improving performance and affordability of technologies; next generation photovoltaic, and energy storage technologies are high on the agenda. Coordinated research is being undertaken through R&D institutions, industry, and universities. We are exploring both domestic efforts and international experiences in these domains.

The National Electricity Plan 2018 has estimated renewable power capacity of 275 GW by 2027. There are other estimates suggesting that by the year 2030, an electric installed capacity of 860 GW with solar and wind power contributing about 500 GW would be required [9]. These will necessitate a significant departure from business as usual and would entail a new paradigm with support mechanisms, facilitate policies, and access to new technologies and investment. Mainstreaming of renewables in India's energy supply is part of India's 2030 vision and it is also committed to the global objective of realizing sustainable development and combating climate change.

1.2 Renewable energy

Conventional sources of energy and nuclear energy cannot sustain the global energy demand for long. This is due to the fact that the replenishing rate of these sources is very slow and thus cannot be used indefinitely [10]. In addition to that, they pollute the environment when employed to generate electricity. A better solution to above problems is the use of Renewable energy resources as they are environment friendly, have become economically viable and bring socio-economic benefits by creating employment. All this align with the idea of three pillar of sustainable development (i.e. economic, environmental and social sustainability).

Renewable energy resources are continuously replenished by the sun or other natural phenomena. Thermal, photo-chemical, and photo-electric energy directly use the sun. whereas Biomass, wind and hydro indirectly utilizes the sun energy. Geothermal and tidal energy are produced due to earth's crust and gravitational pull of the moon respectively. Fig.1.2 classifies the various types of renewable energy resources.

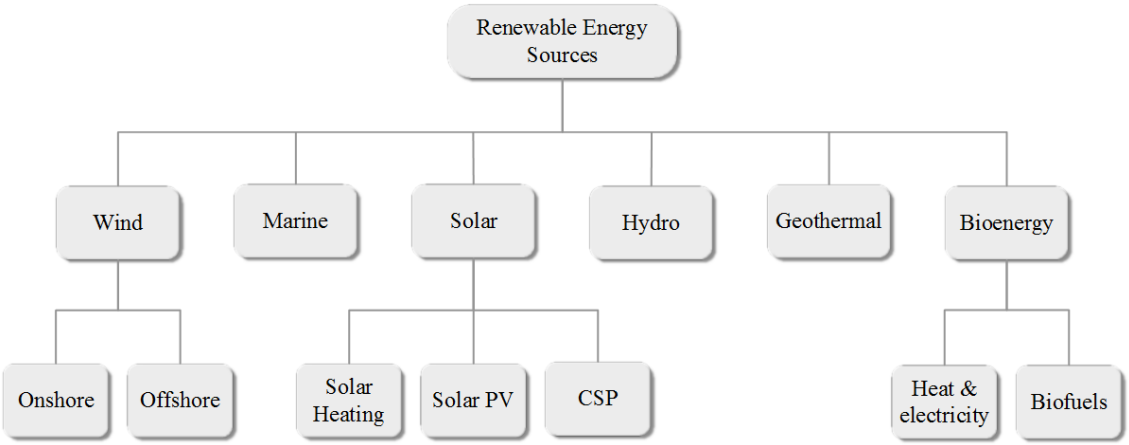

Figure 1.2: Renewable energy sources classification

The technologies of conventional energy resources have matured over a period of more than hundred years. Trillions of dollars have been invested for the purpose of research and development. In today's scenario a large investment is required to obtain marginal improvement, while renewable energy resources are in an innovation phase where small investment in R&D brings about great system efficiencies and economic viability.

The field of engineering which greatly contributes to the development of this technology is Power electronics. A DC-AC power electronic converter (inverter) is used to extract maximum energy from the PV system and deliver it to power grid or other AC loads. While in wind systems, the converter's job is to maximize energy extraction as well as regulate varying input wind power. All this is made possible by the knowledge of power electronics along with control system [11]. A common grid-connected topology for a solar energy system is shown in Fig. 1.3.

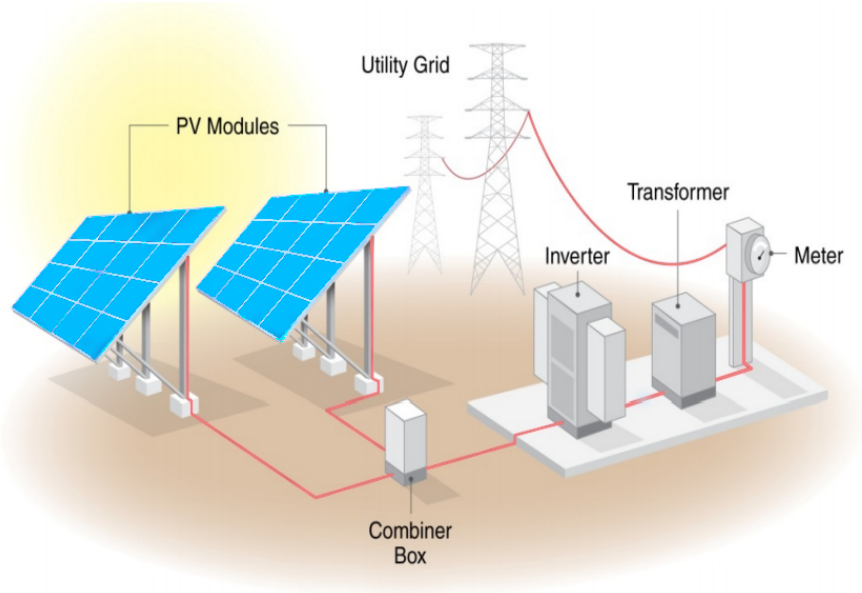

Figure 1.3: Common configuration for large Photovoltaic systems connected to grid [12].

India is at the forefront of expanding its renewable energy capacity in the world. India in 2019 at United Nations climate summit, announced its plan of doubling its renewable energy target of 175 GW by 2022 to 450 GW by the same year. Modern renewable energy sources such as geothermal and tidal are projected to grow massively by that year. This target includes doubling of wind power capacity and increasing installed solar energy capacity by 15 times from its April 2016 figure [13]. Such ambitious targets empowers India to lead the world in renewable energy sources usage and be a central figure in its "sunshine countries" International Solar Alliance project. This project promotes growth and development of the solar energy sources for the 120 countries lying in the equatorial belt of the Earth which receives sun light most of the time of the year.

It is a fact that energy plays a vital role in the growth of any country. India being second in position next to China in terms of population accounts for approximately 18% of total world figure. This increased population and rising standard of living puts India at fourth position globally in terms of energy consumption. As the use of depleting fossil fuel have resulted in great amount of pollution resulting in global warming and climate crisis, Renewable energy presents us with the best alternative. This is due to the fact that energy demand is increasing day by day and proper use of both resources is the solution for the present day.

Indian government's target of installing 20 GW of solar energy by 2022 was completed by January 2018 (4 years ahead of target), through both roof top solar panels and solar parks [13]. After which India sets a new target: 100 GW of solar power, 60 GW of wind power, 10 GW of biomass, and 5 GW of small hydro plants by 2022 [13]. Three of the top Five largest solar parks in the world are in India. The second-largest solar park in the world is situated at Kurnool, Andhra Pradesh, with a capacity of 1 GW.

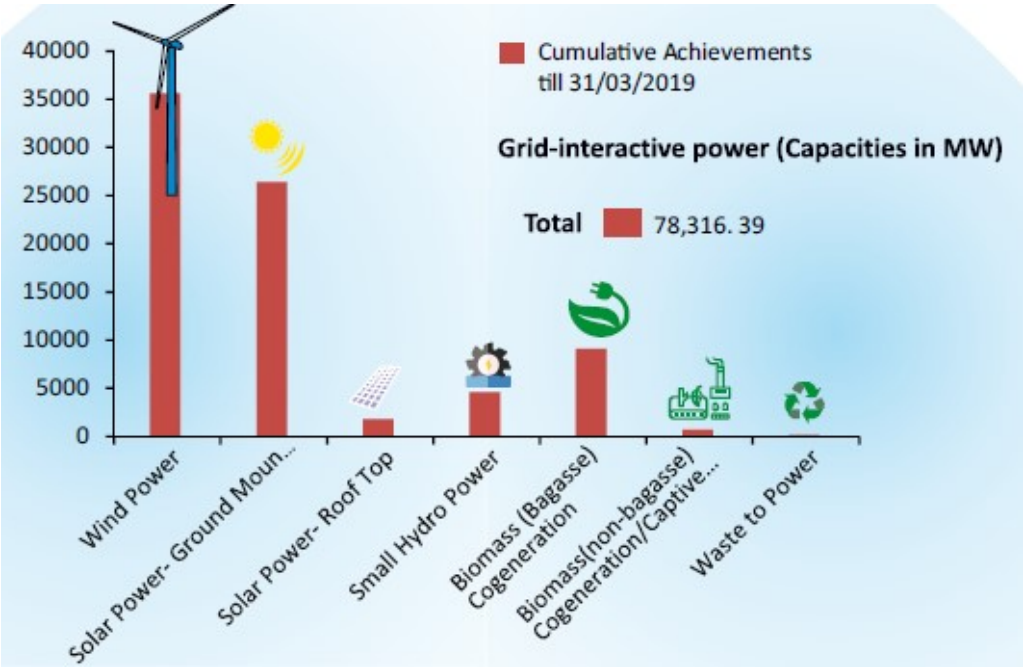

Figure 1.4: Renewable energy in India at a glance [9]

Most of the country do not have electrical grid supply, so the first use of solar energy in such an agriculture country was water pumping and lighting. This is

because a pump was consuming 5 hp (3.5 kW). Some large solar projects have also been proposed, such as one in Thar dessert (an area of 35,000 km^2) is estimated to produce power of 700-2100 GW. The yearly growth rate of solar power in India is around 113% and the energy rate has dropped to Rs 4.34 /kWh. This value is 18% lower than the average cost of electrical energy generated by coal [13].

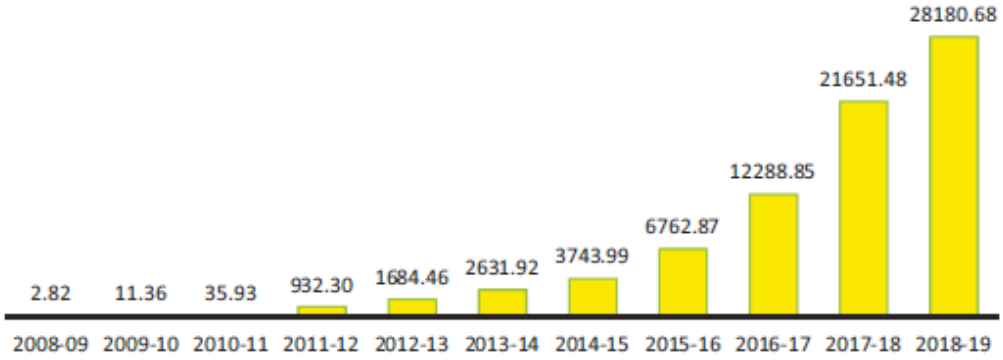

Figure 1.5: Cumulative installed solar power capacity in India in MW, (till March 2019) [9]

The British Petroleum in its Annual Energy Outlook 2019 has projected that renewable energy will become the dominant source of energy by the year 2040. IEA's Annual Energy Outlook 2018 has estimated that cheaper renewable technologies, digitization and increased importance of electricity is a crucial factor for change. The report also predicted that the world is witnessing a major shift in energy demand with demand growing maximum in India.

1.3 Photovoltaic System

1.3.1 Solar cell working principle

Solar cell is the basic component of a solar module. Silicon (Si) is a semi-conductor material primarily used for manufacturing the cell. It is doped with another material to obtain either n type or p type material. Doping Silicon with electron rich atoms (such as phosphorous, arsenic, antimony) produces n-type material, whereas doping it with electron deficient atoms (boron, aluminum, gallium) produces p-type material. The two material thus formed are combined together to form a p-n junction. Solar irradiation on coming in contact with the junction causes current to flow and hence power flow takes place.

On combining the two materials, free holes from p-type diffuses in the n-layer leaving behind negatively charged ions, Similar process happens with the free electrons in n-layer leaving behind positively charged ions. This creates a electric field region in due time between the two layers which stops the charge flow. When sunlight falls on the cell, electron-hole pairs are generated resulting in current flow [14].

The sequence of operation taking place in a solar cell are [15]:

- Photo-generated carriers are produced
- Carriers are collected to generate the current flow

- Potential difference across the solar cell is produced; and
- Output power is dissipated in the load and parasitic impedance

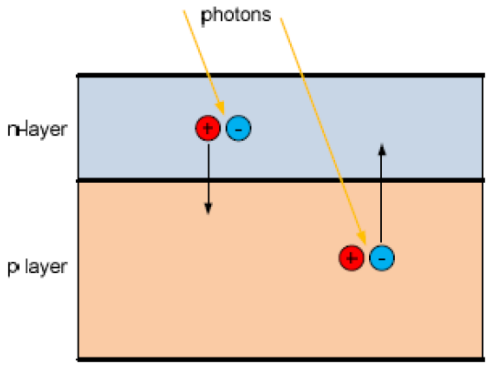

Figure 1.6: Conceptual diagram of a solar cell [16]

1.3.2 Equivalent mathematical circuit

The mathematical model of a solar cell is described in the below Fig. 1.7

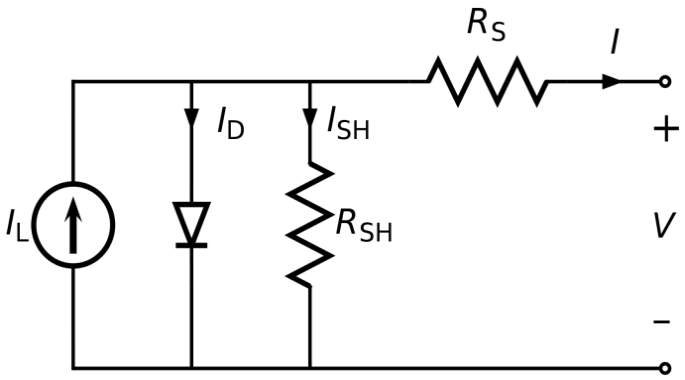

Figure 1.7: Electrical equivalent circuit of a solar cell [16]

Where,

R_S : represents series resistance of the solar cell. It appears due to current flow through the base-emitter junction of the cell and contact resistance between metal and silicon wafer.

R_{SH} : represents shunt resistance of the cell. It is present due to the fact that p-n junction's property is not ideal and there is presence of impurities on the edges that causes short circuit path around the junction. In ideal case, series resistance would be zero and shunt resistance would be infinite [15].

The output current is represented by the following equation:

$$I = I_L - I_D - I_{SH} \tag{1.1}$$

where,

I is solar cell's output current in Ampere,

I_D is the current passing through diode in Ampere
R_{SH} is the current passing through R_{SH} in Ampere
I_L is the current generated due to irradiation in Ampere

From Shockley equation, the diode current I_D is expressed as

$$I_D = I_o(e^{\frac{V+R_sI}{\eta KT}} - 1) \tag{1.2}$$

where,
I_o is the dark current in Ampere (leakage current flowing in the diode in absence of light)
q is the electron charge in Coulomb
η is the diode ideality factor (assumed 1 for Germanium and 2 for Silicon)
K is the Boltzmann's constant in Joule/Kelvin

Using nodal analysis, the shunt resistance current I_{SH} can be found out to be:

$$I_{SH} = \frac{V + R_sI}{R_{SH}} \tag{1.3}$$

Therefore now the output current can be expressed in the form as shown.

$$I = I_L - (I_o(e^{\frac{V+R_sI}{\eta KT}} - 1)) - (\frac{V + R_sI}{R_{SH}}) \tag{1.4}$$

Many such solar cells connected in series or parallel constitutes a PV panel. This is to bring the voltages and currents of the panel equivalent to the utility's parameter values. Now if we consider C be the number of solar cells in series; N_s to be the series connected panels; and N_p to be the parallel connected panels, then the characteristic equation of the array becomes:

$$I = I_LN_p - I_{SH} - I_D \tag{1.5}$$

$$I_L = \frac{I_{SC} + k(T_{OP} - T_{REF})}{1000}\lambda \tag{1.6}$$

$$I_D = I_oN_p[e^{\frac{V+IR_s}{\eta V_tN_sC}} - 1] \tag{1.7}$$

$$I_{SH} = \frac{N_p(V_o + IR_s)}{R_{SH}} \tag{1.8}$$

where,
T_{OP} is the operating temperature of the solar cell in Kelvin,
T_{REF} is the standard operating temperature of the cell in Kelvin
λ is the solar irradiance in Watt/sq. meter

$$V_t = \frac{(T_{OP} \times k)}{q} \tag{1.9}$$

Above equations are capable of capturing the characteristics of the practical solar panel. They can be used in simulation environments (Simulink) to model and test the panel in various conditions. This project utilizes the in built MATLAB/Simulink

block of PV array module which is also based on these equations.

1.3.3 Solar cell parameters

Short circuit current, open circuit voltage, and maximum power point

The three main parameters of a solar cell are short circuit current, open circuit voltage and maximum power point (MPP). Power generated by the cell is zero when it is at short circuit current and open circuit voltage whereas maximum power is achieved when it is at maximum power point. This is shown by the I-V and P-V characteristic curve of the solar cell in Fig. 1.8

Neglecting shunt resistance R_{SH} and keeping output current $I = 0$, the open circuit voltage can be approximated as eqn. 1.10

$$V_{OC} = \frac{\eta kT}{q} \ln(\frac{I_L}{I} + 1) \tag{1.10}$$

whereas the short circuit current is obtained when $V = 0$ and is approximated to be equal to light generated current as shown in eqn (1.11).

$$I_{SC} = I_L \tag{1.11}$$

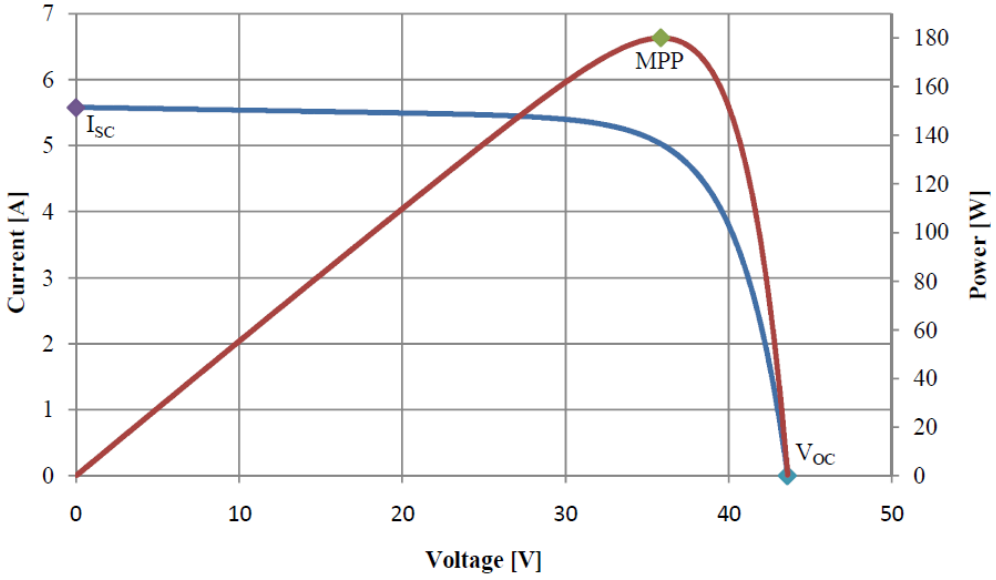

Figure 1.8: Short circuit Current, Open circuit voltage, and MPP points [16]

Fill Factor

It is defined as the ratio of power at the maximum power point to the theoretical power at V_{OC} and I_{SC}.
It is given by:

$$FF = \frac{V_{MPP} \times I_{MPP}}{V_{OC} \times I_{SC}} \tag{1.12}$$

Current and voltage at the maximum power point is always less than the open circuit voltage and short circuit current due to internal resistance of the system. Thus the fill factor can never be more than 1. Typical value of fill factor lie in the range of 0.65-0.75. This ratio signifies the quality of the panel.

1.3.4 Effect of atmospheric variations on PV

Change in irradiance

Variation of irradiance causes changes in almost all parameters such as open circuit voltage, short circuit current and efficiency as well. This is because the photo generated current directly depends on irradiance, and short circuit current depends directly on photo generated current. However the effect of irradiance on open circuit voltage is relatively small. The I-V and P-V characteristic curve is shown in Fig. 1.9, where curve is plotted for four different irradiation values.

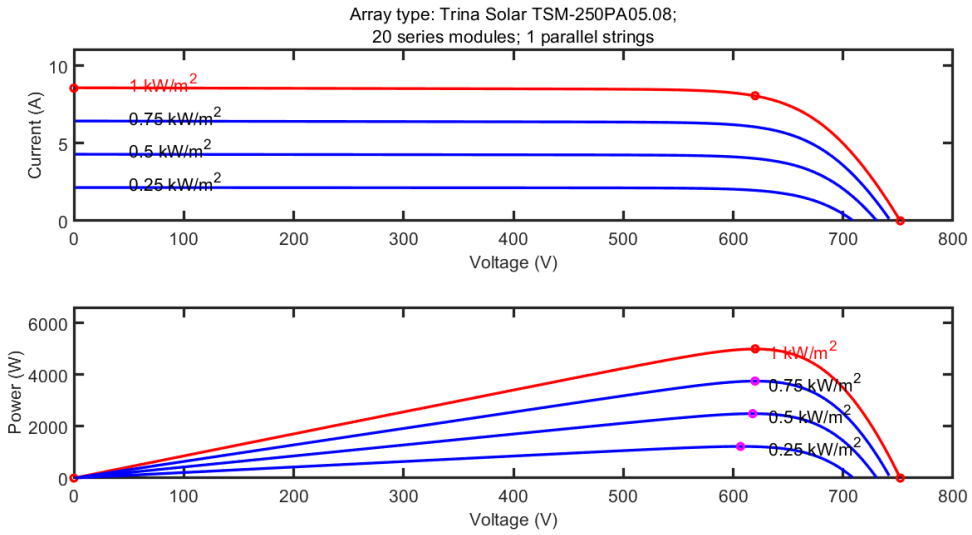

Figure 1.9: I-V & P-V curve of Trina Solar (TSM-250PA05.08) at different irradiance

Change in temperature

Varying the temperature affects the open circuit voltage more than the short circuit current. They both are directly proportional to each other. Whereas the short circuit current is not affected much with respect to changing temperature. With increase in temperature, the power reduces as shown in Fig. 1.10.

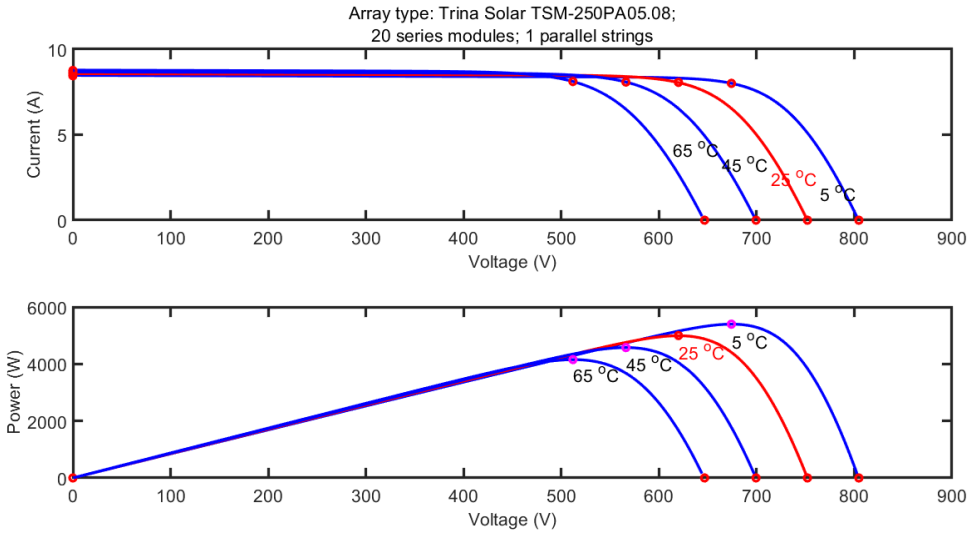

Figure 1.10: I-V & P-V curve of Trina Solar (TSM-250PA05.08) at different temperature

1.3.5 Single PV module parameters

Trina Solar TSM-250PA05.08 parameters are taken from its datasheet present in the MATLAB PV block. The parameters are tabulated below in table 1.1:

Parameters	Value
Maximum power (P_{max})	249.86 W
Voltage at peak power (V_{mpp})	31 V
Current at peak power (I_{mpp})	8.06 A
Cells per module	60
Open circuit voltage (V_{oc})	37.6 V
Short circuit current (I_{sc})	8.55 A
Temperature coefficient of V_{oc}	$-0.35\%/$ °C
Temperature coefficient of I_{sc}	$0.06\%/$ °C

Table 1.1: Simulated single PV module parameters

1.4 Power electronic converters

Power electronics converters are used in various fields of industry, such as renewable energy sector, Power systems, domestic equipment and transportation sector. In Photovoltaic two stage system, the DC/DC converter is used to extract maximum power from the panel. After which the the DC power is converted to the AC power via an inverter so that power can be injected into the power grid. A general scheme of the two stage system is shown in the Fig. 1.11. Power converters employed in the renewable energy sector offers extraction of maximum power, better dynamic control, low current THD injected into the grid and in the case of wind generators, they eliminates the need of a gearbox for regulating turbine speed [17].

In olden days the main focus of design was dynamic performance and stability of system but nowadays the industrial constraints are more strict focusing more on standards, technical specs and codes. Such strict regulations cannot be met by hardware alone and there is a need for a robust control system which can work along to achieve desired output. Thus design of a power electronics converter encompasses an optimization problem and solving many such constraints at once. The main objectives expected from a converter's control system are listed below: [18]:

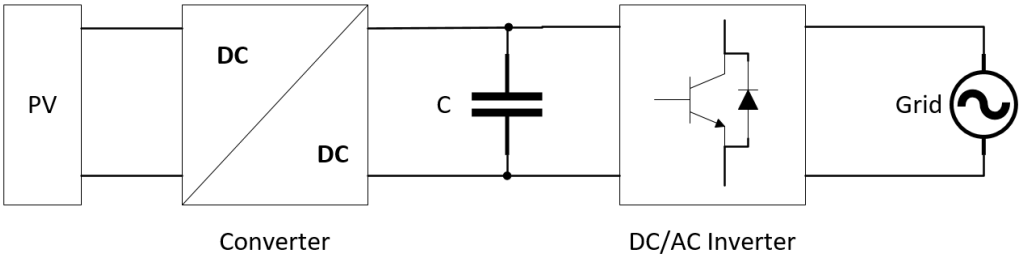

Figure 1.11: General two stage PV system configuration block diagram

- To reduce the switching frequency, leading to decreased switching loss and therefore increasing efficiency and better utilization of semiconductor devices.
- Improvement in the dynamic behavior of the output such that the reference and controlled variable remains as close to each other as possible giving minimum tracking error.
- A challenging task is to have a good performance in case of a non linear system. It should not only operate at specific conditions but it is desirable to have it operate for a wide range of conditions.
- The total harmonic distortion (THD) is another constraint in many applications and which develops in the modulating stage of controller. It is required to be kept as minimum as possible.
- Finally each converter topology has its own limitations and advantages, for example it is not advisable in a three level converter to change the switches state directly from -1 to 1 without having a 0 state in between.

1.5 Control methods

The Fig. 1.12 presents various types of control methods that are generally used in power electronic converters and electrical drives. The gray boxes indicates the control methods specifically used for drive applications and therefore are not discussed in details as they out of the scope of this project. The classification presented consists of classical methods as well as more recent methods that require more computation. The discussion on the aforementioned methods are as follows:

In **hysteresis control** the switching is controlled in such a manner that the measured variable stays inside the hysteresis error boundary and follows the reference signal. The state of the switch is changed as soon as the variable reaches the boundary. The method is quite simple as compared to others and is used for simple

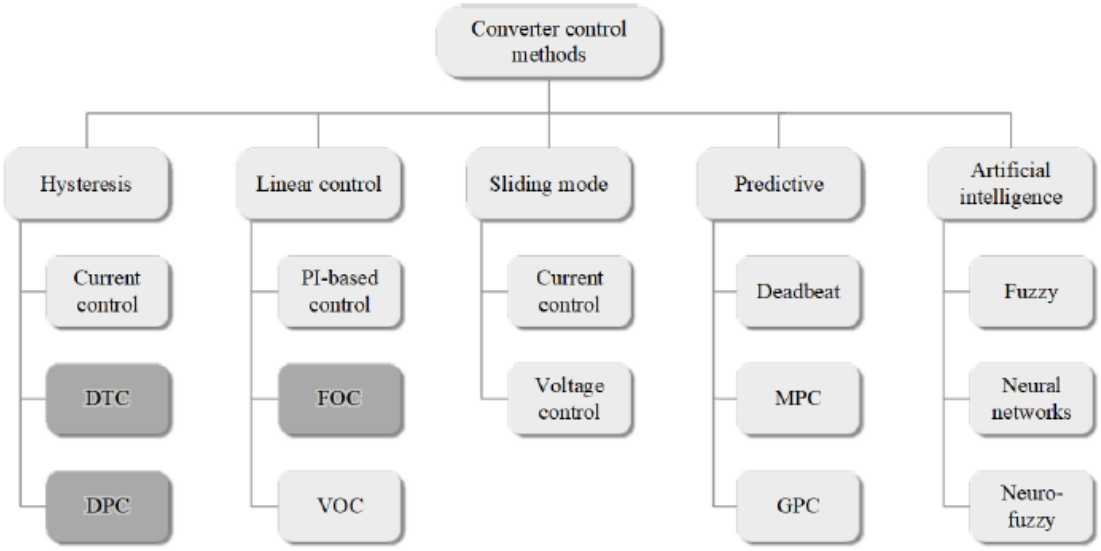

Figure 1.12: General control methods classification for power converters and electrical drives [18]

control such as current control and also in complex situations like Direct torque control (DTC) or Direct power control (DPC). Implementing this control is simple and it does not have complex computation [18].

It is a well known control method which has its root from analog electronics. Though easy to implement in analog domain, it however requires very high sampling frequency in case of digital domain, so as to bound the controlled variable inside the hysteresis band. It is therefore problematic to use hysteresis control in low power applications because there is high switching loss [19]. The method have few drawbacks such as non-linearity, variable switching frequency, dependency on hysteresis width and operating constraints which makes it less desirable from other control methods . Also above technical problems causes resonance and harmonics, which then again requires costly filter circuits [18].

linear controllers can be applied to converters with modulating stage. The job of the modulator is to linearize the converter by generating proper signals for switching devices. Proportional-Integral (PI) control is the most common linear control, whereas Field oriented control (FOC) is specifically used for drives and voltage oriented control (VOC) is the general choice for grid connected converters to control the output current. A mathematical concept of Pulse Width Modulation (PWM) is often usesd along the linear controllers [19]. In this technique, a sinusoidal reference is compared with a triangular carrier wave, thus producing pulses for the switching devices. Like for example, if instantaneous value of sinusoidal signal is more than that of carrier wave then the PWM gives value as 1, otherwise it gives 0 to the switches, thus controlling in such a manner [18].

The limitation of a linear regulator is that it is controlling a non-linear system and hence it is not able to give even performance for a wide dynamic range .With the use of linear controllers it becomes difficult to control certain variable or constraints (like switching frequency, THD, or peak current) directly [18].

Sliding mode control considers the inherent switching charateristics of the converter and provides dynamic stability during different disturbances, however the

algorithm is complex to implement.

Artificial intelligence are techniques that has recently got so much attention. They are generally used in applications where some parameters are missing or undetermined; One such control technique is Fuzzy Logic. Other methods include genetic algorithm, neural network or a combination of them, like neuro-fuzzy technique [20].

Predictive control utilizes the state space model of the converter and predicts the behavior of the controlled variable according to the applied input. In its algorithm, it includes the optimization criteria which will produce the most desirable switching state at that instant. As this method avoids cascaded structures found in linear regulators, the response time of this technique is quite fast [20].

Deadbeat control also uses the mathematical model of the system to find voltage that will eliminate the error in one sampling time, and produces this voltage by means of a modulating stage [20]. MPC is implemented by means of a cost function formed by taking weighted control objectives.Hence this method can also predict the variable many time steps into the future so as to select the most appropriate switching state, but this however requires a lot of computational work [18].

1.6 Objectives of the Present Work

The main focus of the present work is at:

1. To design and simulate a single-stage single-phase PV system consisting of PV array and H-bridge inverter connected to an Electrical grid via a low pass LCL filter.

2. To model and analyze control system which can extract maximum power from the PV system and deliver it to the Electrical grid.

3. To simulate and compare the designed current controllers based on their dynamic response, complexity, and the resultant current THD. The delivered current should not have %THD more than 5% as per IEEE 1547.

4. To introduce hardware implementation of a standalone single phase H-bridge inverter with an LC filter operating in an open loop configuration.

1.7 Outline of the Thesis

There are total six chapters in this dissertation work.

1. **Chapter 1** presents a brief introduction to the conventional and renewable energy resources. It also discusses in detail, the mathematical modeling of a solar cell. Its change in parameters due to the change in atmospheric conditions (i.e. irradiance and temperature) is also discussed, along with the general idea of power electronics converters.

2. **Chapter 2** presents the design of the power circuit of the system. It gives the design process of the LCL filter used for filtering the harmonics of inverter output. Other important design parameters such as DC link capacitor value, required PWM technique, PV parasitic capacitance and different MPPT techniques are also presented in brief.

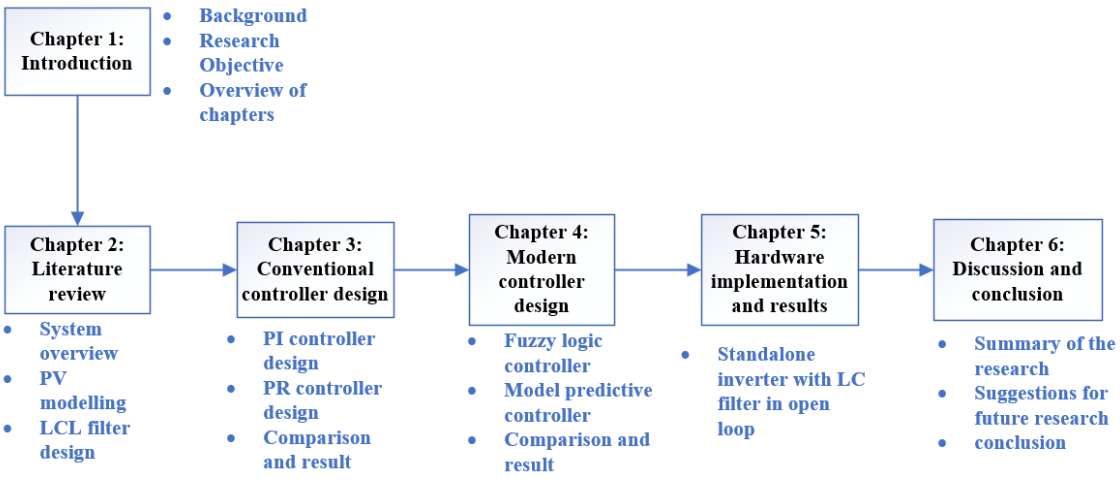

Figure 1.13: Brief overview of the chapters in the thesis

3. **Chapter 3** discusses two of the classical controllers used for inverter current control. The first controller discussed is d-q frame control. It consists of PI controller in synchronous reference frame. The second control system designed is Proportional Resonant controller which is a general case of a PI controller and therefore there is no requirement of converting signals to synchronous reference frame.

4. **Chapter 4** discusses two of the advanced control techniques which are fuzzy logic and model predictive control (MPC). Fuzzy logic control (FLC) is a part of artificial intelligence. whereas MPC controller is based on the finite states of the power converters and how its state can be predicted beforehand. Their characteristics are presented, simulated, and compared.

5. **Chapter 5** explores the hardware implementation of an H-bridge inverter with an LC filter in an open loop configuration. Arduino Uno is used to control the inverter using Unipolar PWM strategy. This chapter discusses all the steps taken to make the setup.

6. **Chapter 6** gives a brief conclusion of the presented work in this dissertation and the future scope of this project.

Chapter 2

POWER CIRCUIT AND ITS DESIGN

2.1 Overview

This chapter presents the design of the power circuit of the simulated system and its component sizing. It describes the design and selection of all the components required for a grid connected inverter. Section 2·2 discusses the different PV system configuration such as single-stage or double-stage structure. Section 2·3 gives a brief account of various MPPT techniques in the literature for extracting maximum power of the panels and why Perturb & Observe is selected for the purpose. The conceptual overview about H-bridge and its merits is described in Section 2·4. Section 2·5 introduces the modulation strategy required in linear controllers, such as Pulse Width Modulation (PWM) and its implication on the PV array ground current. Section 2·6 and 2.7, gives the design procedure for the design of an LCL filter. And the chapter concludes with Section 2·8, that gives the sizing of DC link capacitor and tabulation of all the Power circuit design parameters. The schematic in Fig. 2.1 represents the overall layout of the power circuit, which will be referred in the whole chapter.

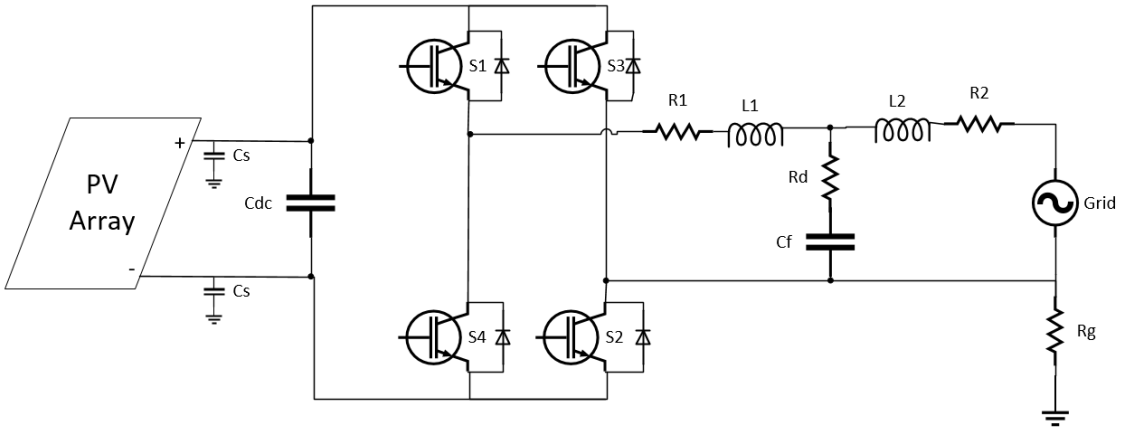

Figure 2.1: Simplified Schematic of the Power circuit

2.2 Configurations of PV system

PV modules or a solar cell in actual produces DC voltage and current. Therefore the natural choice is to use a DC-DC converter for regulating this voltage to a desirable value. After which an inverter is connected to convert the DC voltage to AC voltage so as to supply to electrical loads and utility grid. The type of configuration implemented affects the converter design. Cost and residential environment plays an important role in the selection of the required configuration. Following sub-sections describes four basic solar power configurations.

2.2.1 Single-Stage centralized inverter

This configuration is characterized by solar panels connected in series to form strings, so as to increase the combined voltage. Many such strings are then connected in parallel, along with diodes to stop reverse current flow, to obtain high power. Fig. 2.2 describes the schematic of such connection.

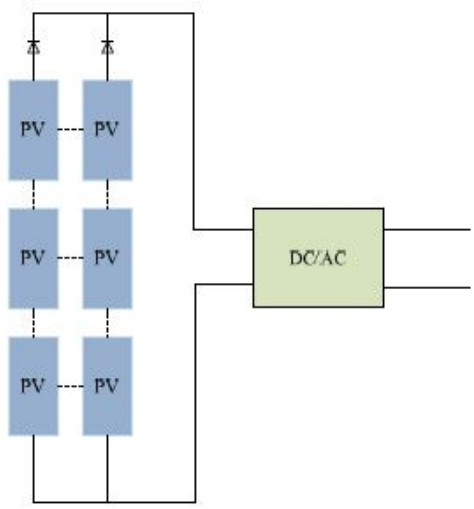

Figure 2.2: Single-stage centralized inverter configuration [21]

It is clearly observable in this configuration that voltage shared by all strings remains always same. So, if there is partial shading or panel mismatch then all strings cannot operate at MPP. This affects the energy harvesting process for low power applications. However, this configuration is beneficial due to its low cost requirement [22]. This configuration is implemented in this project work due to its low cost and its suitability with the residential solar roof top systems. Although it is cost effective in the first stage due to elimination of DC-DC converter, but the size of inverter increases proportionally.

2.2.2 Single-Stage String Inverter

This configuration is described in the Fig. 2.3. This connection overcome the limitations of the centralized inverter as each PV array has individual inverter and therefore achieves MPP. Each inverter control its respective panels and extract maximum power from them. In that sense, this configuration is superior to that of the

previously discussed connection. However, the initial cost shoots up as each PV string requires their own inverter circuit to deliver power [22].

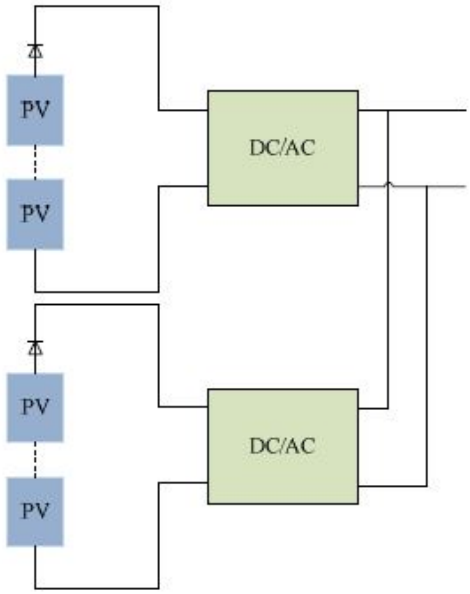

Figure 2.3: Single-stage string inverter [21]

2.2.3 Double-Stage String Inverter

Fig. 2.4 shows the Two-Stage configuration with String Inverter. This cascaded structure is popular due to its modular connection, energy extracting capability and flexibility in design [22]. With the reduction of solar panels in a string, the robustness of the configuration increases. The first stage task is to increase the DC voltage to a higher value so as to reduce current and hence increase efficiency. Also, MPPT algorithm is applied at this stage. The second stage is required to convert DC voltage to AC so that power can be utilized by the loads.

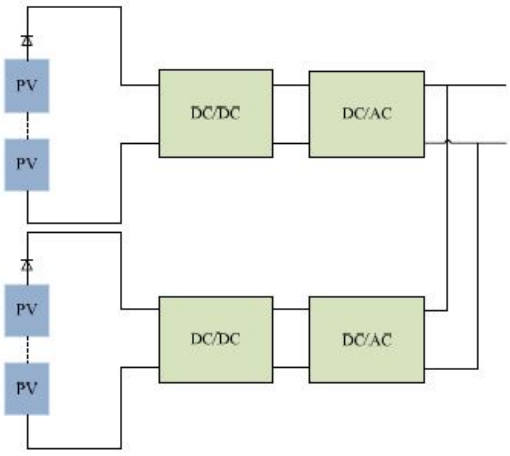

Figure 2.4: Two-stage string inverter [21]

2.2.4 Double-Stage Centralized Inverter

This connection is represented in Fig. 2.5. The first stage is similar to that of previous configuration which is tasked with voltage amplification and performing MPPT control. The second stage is common to all the PV strings and one main inverter is used to convert the voltage cycle.

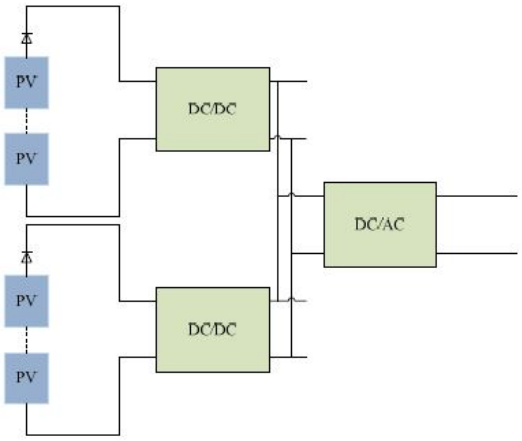

Figure 2.5: Two-stage Centralized inverter [21]

2.3 Maximum Power Point Tracking

The solar cell characteristic changes with respect to changing atmospheric conditions such as irradiance and temperature. Thus it becomes very important to not waste any energy coming from the solar panels and extract maximum power from them at all times.

Hence an MPPT algorithm plays a vital role in getting maximum power out of the PV array. It is a real time control algorithm that tracks the atmospheric conditions and accordingly set the voltage to keep the PV system on MPP. There are MPPT algorithms that are embedded in the converter to achieve the desired result.

A brief description of some of the major algorithms used to achieve MPPT are as follows [23]:-

- **Perturb & Observe**: The algorithm begins with varying voltage in small steps and corresponding power is measured. If measured power is increased, then same control action is applied until the power change becomes negligible. This is the most basic algorithm used, although it produces oscillations about the maximum power point.It is generally termed as hill climbing method because the power versus voltage curve looks like a hill with peak at MPP. The best thing about this method lies in its simplicity and ease of implementation. The method have many variants in the literature which have much more efficiency than normal P&O. Mostly adaptive and predictive hill climbing strategy is applied in such advance variants.[24]

- **Incremental Conductance**: In this control algorithm, an incremental change in PV module voltage and current is measured and then it predicts the effect

of change in voltage. This is method is much better than the Perturb and Observe (P&O) method in terms of dynamic tracking of the MPP. But incremental conductance method, like P&O, produces oscillations at the peak value [25]. Incremental conductance (dI/dV) is used in this method of MPPT to compute the sign change of the change in power with change in voltage (dP/dV). Thus it computes the maximum power by comparing the incremental conductance (I_Δ/V_Δ) with solar panels conductance (I/V). When these both ratios are equal ($I/V = I_\Delta/V_\Delta$), then the controller reaches the MPP. IC maintains that point until change in irradiance or temperature takes place after which the same process repeats.
The mathematical concept behind the incremental conductance is that at the maximum power point, dP/dV = 0, and that P = IV. The PV array current can be expressed as a function of voltage; P = I(v)V. Hence we get, dP/dV = VdI/dV + I(V). Equating the expression to zero gives: dI/dV = -I(V)/V. Therefore, the controller observes maximum power when incremental conductance is equal to negative of the instantaneous conductance.

- **Constant Voltage**: The 'constant voltage' method is defined in two ways by different authors; one in which a constant voltage is kept at the PV array, and in second the the ratio of PV array voltage to the open circuit voltage (V_{oc}) is kept constant. The second method is popularly known as the "Open voltage method" be many experts. In case of first method, the voltage is kept constant at all times and so it is not technically a MPPT algorithm, but it does provides some merits in situations where other methods fail, So in a sense it is usually used as a supplement method. Whereas in open voltage method, the PV array is momentarily disconnected from the load, and open circuit voltage is measured. After measuring the voltage the circuit is again connected and voltage is set to some fix ratio with respect to open circuit voltage V_{oc}.Typically, the ratio is set to 0.76 times that of V_{OC}. This value is generally the point near the maximum power point, calculated either empirically or from mathematical modeling [25].

- **Current Sweep**: In this algorithm, a current sweep waveform is applied to the PV array to obtain the I-V characteristic of the array at fixed intervals of time. Once the I-V curve is known, It is easy to find the maximum power point for that interval. Though slow, this method can also be used for partial shading or panel mismatch situations.

- **Temperature Method**: This is an estimation method, based on estimating the MPP voltage V_{mpp} by measuring the PV array temperature and comparing it against the reference.[26] The idea behind this estimation lies in the relation between MPP voltage and irradiance change. V_{mpp} is negligibly affected due to change in irradiance and therefore the voltage only depends on the temperature and that too linearly.

  Following equation relates the two variable linearly:

$$V_{mpp}(T) = V_{mpp}(T_{ref}) + u_{V\,mpp}(T - T_{ref}) \tag{2.1}$$

  where:

V_{mpp} is the maximum power point voltage at temperature T;

T_{ref} is the reference temperature in Celsius;

T is the measured temperature in Celsius;

u_{Vmpp} is the temperature coefficient V_{mpp} given by manufacturer

Due to its simplicity, accuracy, ease of implementation and low computation requirement, Perturb and Observe (P&O) method is chosen in this project for achieving MPPT.

2.3.1 Perturb And Observe

This algorithm in simple terms is a hill climbing method. The algorithm begins with perturbing the voltage by small amount and then power is measured at that voltage. If this measured power is more than the previous step power, then perturbation is carried in the same direction. However, if power measured decreases then the perturbation is reversed in other direction [24]. This is how maximum power is achieved by this method. Its flowchart is shown in Fig. 2.6

- If dP/dV > 0 : MPP is on the right side
- If dP/dV $= 0$: is the maximum power point
- If dP/dV < 0 : MPP is on the left side

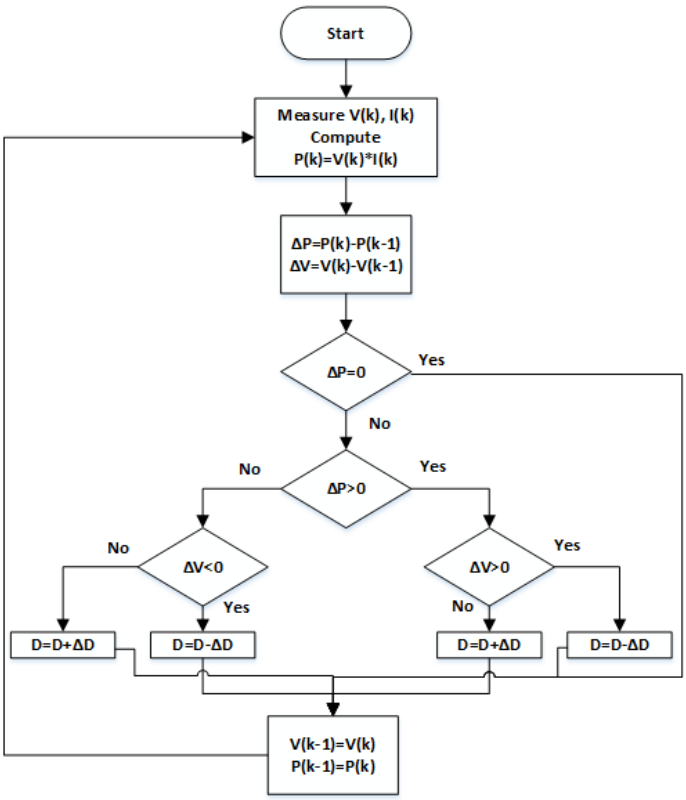

Figure 2.6: Hill climbing P&O method flow diagram [16]

Advantages:

1. A simple method to implement
2. Faster method due to its less calculations
3. Computation is relatively less than other algorithms

Disadvantages:

1. Inherent oscillations about the maximum power point
2. If $V_1 \neq V_2$ but $P_1 = P_2$ then there is problem in the working.

2.4 DC-AC Converter Topology

There are many inverter topologies in the literature. On the basis of number of switch legs, inverters can be broadly classified as either half bridge or full bridge inverter (also known as the H-bridge configuration).On the basis of the type of source, the inverter can be divided into either current source or voltage source inverter. Relating the input voltage magnitude and output peak voltage classifies the inverter into buck inverter, boost inverter, and buck-boost inverter. In this report, an H-bridge inverter is used due to its simple design and good efficiency. The selected inverter topology is that of full bridge buck type voltage source inverter (VSI). Fig. 2.7 shows the schematic of the converter system simulated.

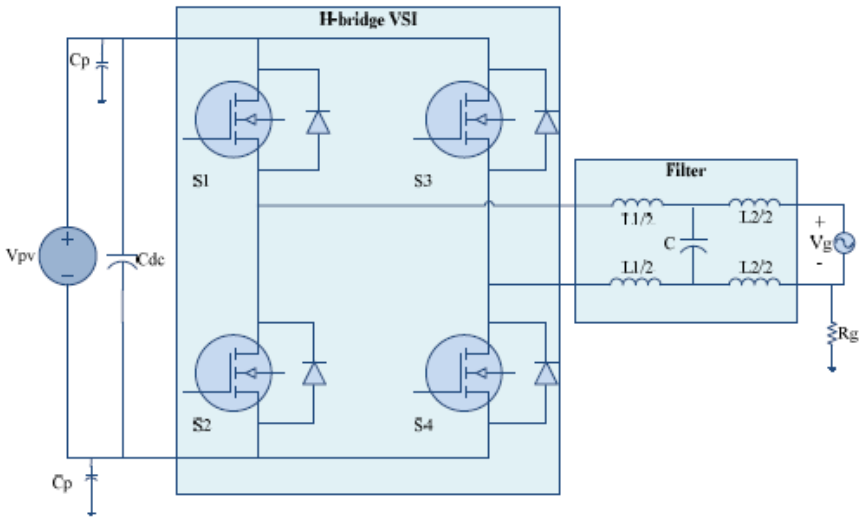

Figure 2.7: Single-phase H-bridge inverter topology [21]

2.5 PWM Techniques

By varying the duty cycle of the PWM signal, it is possible to obtain specific voltage pattern across the electrical load thus getting the AC signal. A low pass filter is required to generate pure sinusoidal wave from the PWM output. A PWM control signal can be produced using either an analog comparator or digital micro-controller.

Both of the methods are equally used in the industry for the purpose of generating sinusoidal PWM signal get sinusoidal inverter output.

The applications of a PWM signal is wide in the field of Power electronics. Following are some of the reasons behind its usage:

- Power loss is considerably reduced - If switches are remaining turned off or turned on for long time then this results into very less conduction power loss across the corresponding switches.
- Generation is easy - PWM signal generation has become very simple, especially in digital domain. Many micro-controllers have inbuilt hardware to handle and produce PWM waves and controller does not have to worry about its generation.
- D/A conversion - The control of the output signal using just the duty cycle greatly enhances this technique, and thus it can be easily used for digital to analog signal conversion. For example, just by controlling the duty cycle, one can control the speed of the analog DC motor.

2.5.1 Unipolar SPWM

This modulation technique usually requires only two sinusoidal waveform that is of amplitude V_m and $-V_m$, Both these waves have same amplitude but are 180 °phase shifted with each other. Above two sinusoidal waves are compared with a triangular carrier waveform V_c thus producing gating signal V_{g1} and V_{g2} for the upper switches of the two legs. It can be directly observed that two upper switches do not get turned on simultaneously, unlike bipolar SPWM where two switches are always turned on at a given time. The output voltage varies between zero and $+V_d$ for the positve half cycle and between zero and $-V_d$ for negative half cycle, and therefore it is named unipolar SPWM. The unipolar PWM inverter offers less electromagnetic interference and switching loss. The efficiency offered by the unipolar switching is more than its counterpart [27].

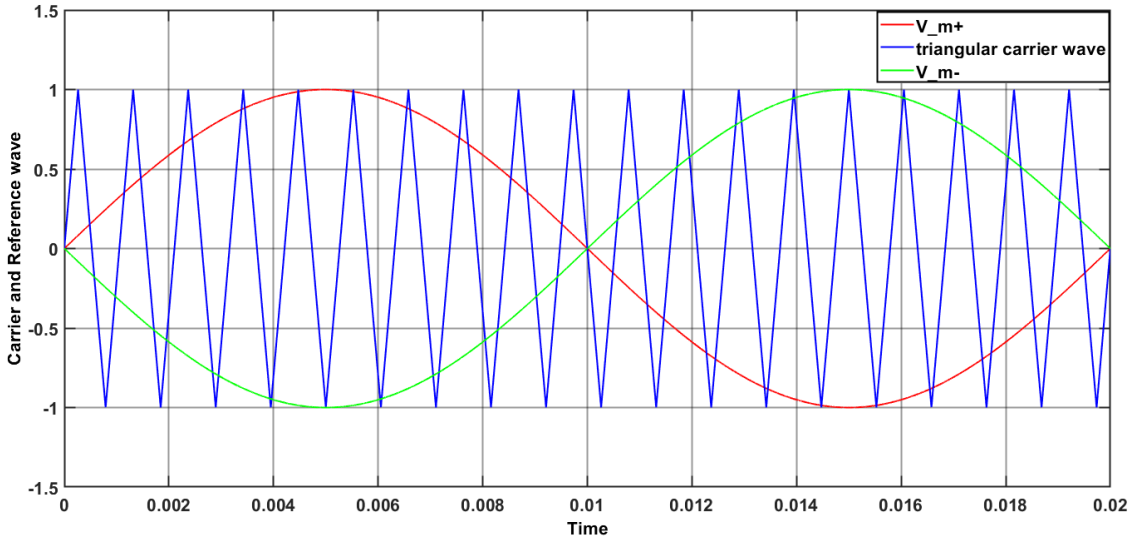

Figure 2.8: Unipolar SPWM waveform

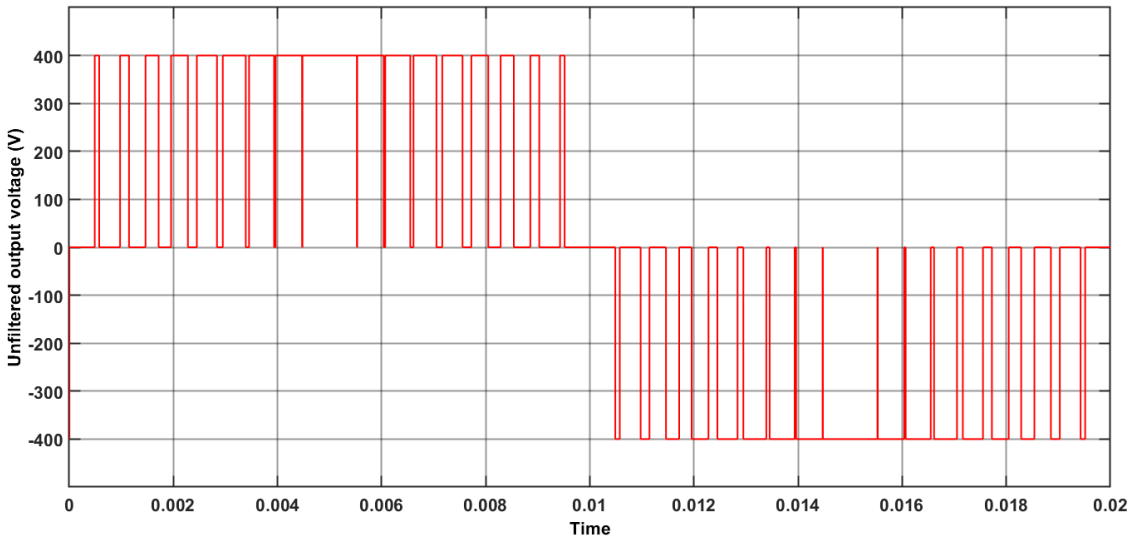

Figure 2.9: Inverter output voltage with Unipolar SPWM

2.5.2 Bipolar SPWM

In this technique, the upper and lower switch of a leg do not switch on and switch off simultaneously, meaning that they switch in a complementary fashion. Therefore one only needs to control two gating signal, namely V_{g1} and V_{g2}. which are generated by comparing one sinusoidal wave V_m and triangular carrier wave V_c. The output voltage of the inverter varies between $+V_d$ and V_d for both the half cycles and thus it is termed as bipolar SPWM [27].

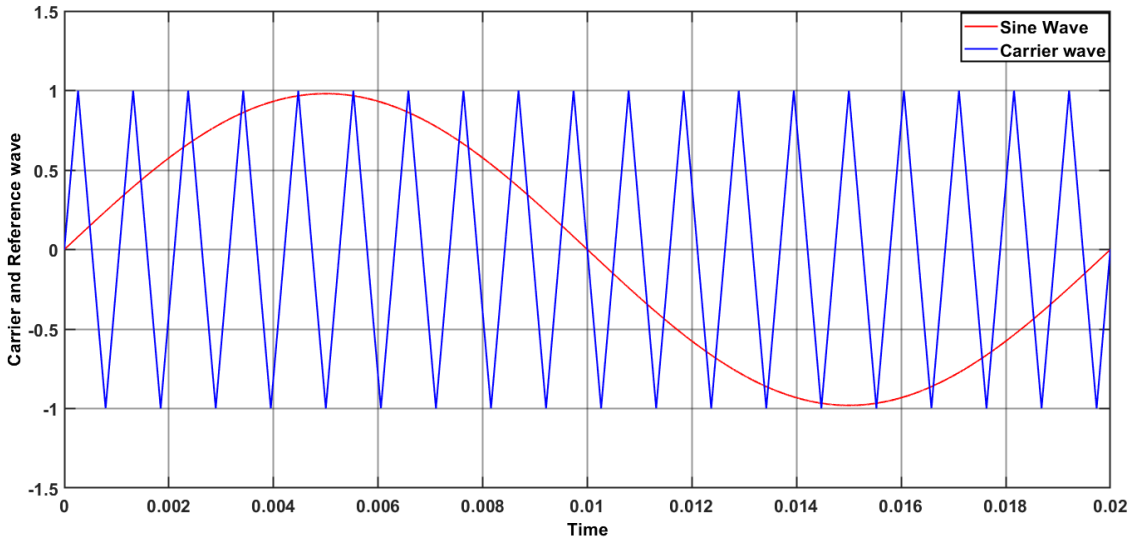

Figure 2.10: Bipolar SPWM waveform

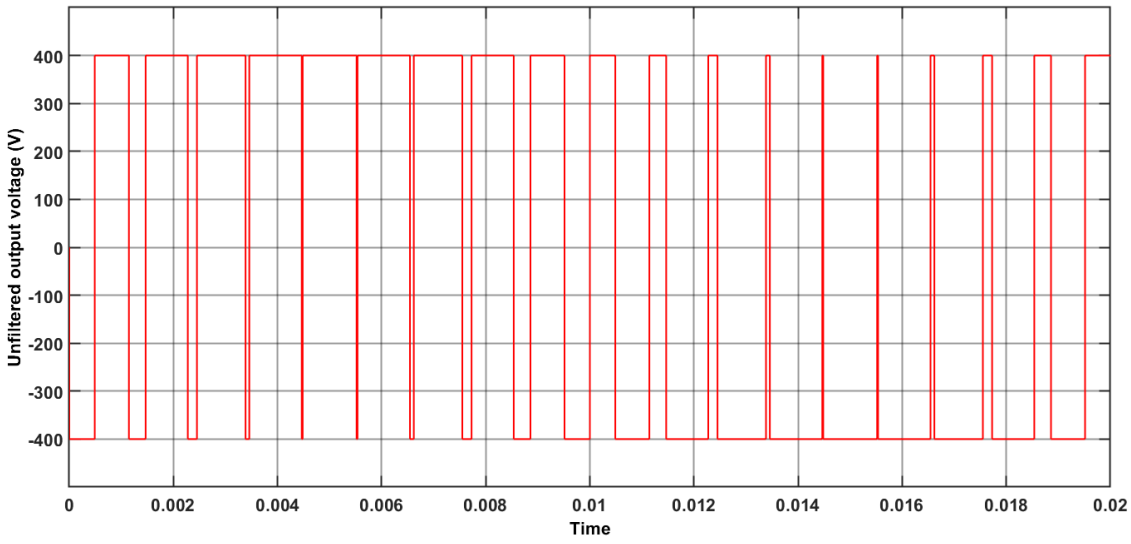

Figure 2.11: Inverter output voltage with Bipolar SPWM

2.5.3 Ground current in a Transformer-less PV system

A single phase power converter can be used for the purpose of low power transfer to grid. In such an application, it is possible to remove the transformer at the inverter's output as it reduces weight, losses and size of the overall setup. But such removal of transformer can result into ground leakage current between the dc source and the utility grid, this is because of the absence of galvanic isolation provided by the transformer and also due to PV parasitic capacitance. These currents are useless in the sense that they increase losses, incur electromagnetic emissions and adds harmonics to the power grid. Factors such as applied PWM strategy, converter topology, and in most cases the resonance formed by the parasitic capacitance, converter, low pass filter and the grid affects the magnitude and phase of the the leakage current[28]. In this project, the ground leakage current is observed under different PWM techniques for a 5kW PV system. The setup includes a series string of PV panels (20 in number), a full bridge inverter and an LCL low pass filter connected to the grid.

The fundamental reason for appearance of the leakage current is the elimination of the transformer from the design as it galvanic isolation between the two sources. The problems associated with it includes safety issues, EM compatibility impairment and unnecessary losses in the system. Therefore it becomes important to have a limitation on the ground current and there are many standards regarding it. For example, in Germany, it is compulsory to install a residual current monitoring unit (RCMU) to measure the leakage current and if it is found to be more than 300mA, then the PV system must be disconnected within 0.3 s [28].

The ground current tends to superimpose with the grid current and thus increasing the harmonic content as compared to when they are absent. As apparent in the shown in Fig. 2.12, a resonant circuit is formed when the dc source is grounded. This circuit comprises of the converter switching, low pass filter, dc source parasitic capacitance, and the utility grid impedance. Based on the environmental conditions and the type of source, magnitude of the leakage current is affected. In the specific case of the PV panels; the ground capacitance values are very high. This is due to

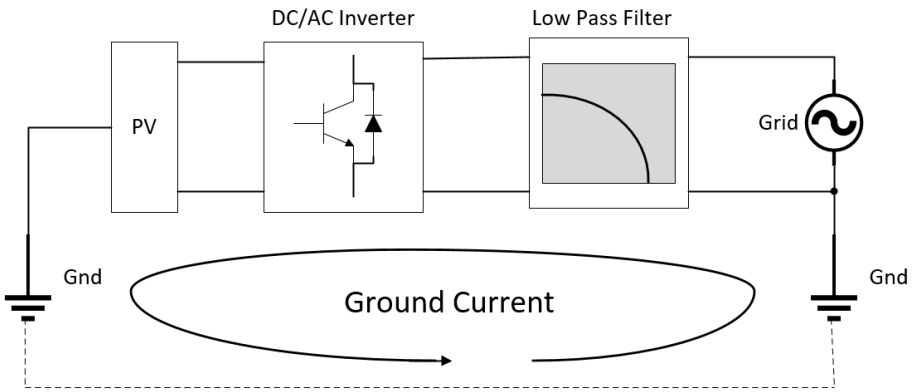

Figure 2.12: Ground current in a PV transformer-less inverter connected to the grid.

the fact that PV panels form a sort of huge capacitor where one plate is formed by the solar cell and other plate by the ground, thus the value varies from nanofarads to micro-farads. And for this reason, they become an important design parameter for PV transformer-less system as their values can go very high.

PWM technique not only affects ground currents but also the design of the filter. Unipolar SPWM is much more efficient and more sinusoidal. Also the equivalent switching frequency in case of Unipolar SPWM is double that of Bipolar SPWM, keeping the carrier frequency same [29]. This leads to small filter size for Unipolar SPWM. But the advantage of using Bipolar SPWM is that the ground currents are negligible when there is no transformer [21]. According to the setup shown in Fig. 2.7 ($R_g = 0.4\Omega$, $C_p = 5nF$), a comparison is done between the two strategies, keeping the same carrier frequency. The Fig. 2.13 represents the ground leakge current in the system due to unipolar SPWM, whereas Fig. 2.14 represents negligible leakage current in case of Bipolar SPWM. In this project, Bipolar SPWM is chosen as the PWM technique for operating inverter, as the power circuit comprises of no galvanic isolation component.

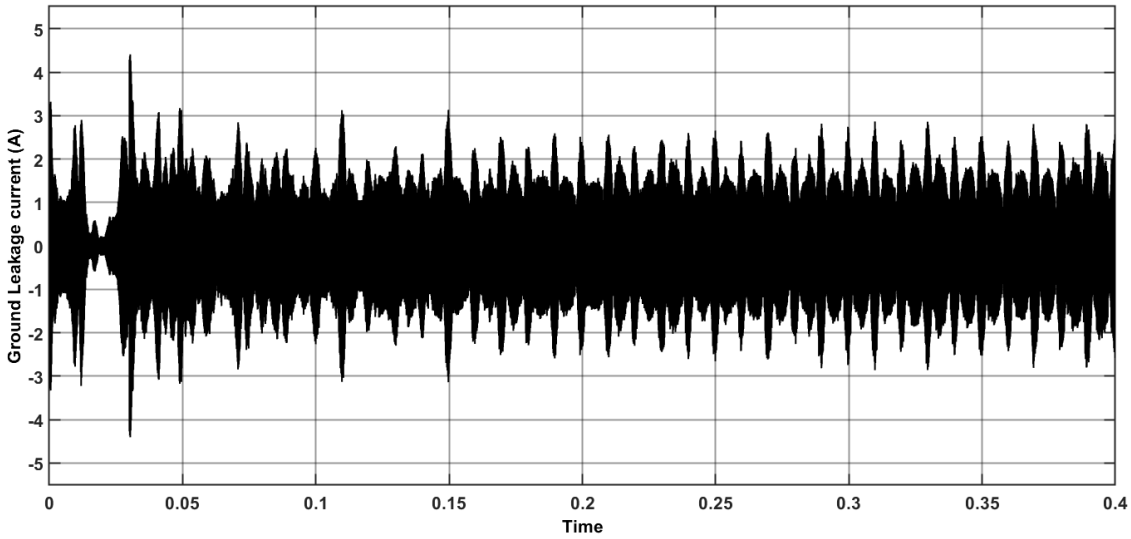

Figure 2.13: Effect of Unipolar SPWM on ground leakage current

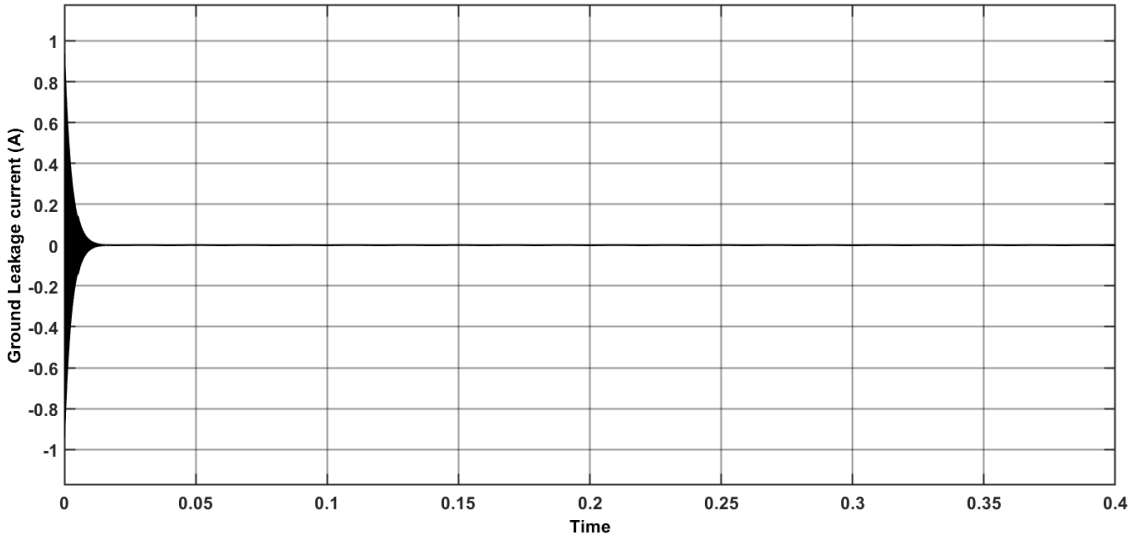

Figure 2.14: Effect of Bipolar SPWM on ground leakage current

2.6 Inverter AC Filter Topologies

For any inverter topology, there is a need of a low pass filter at its output, to get the power frequency out. There are four common low pass filters that are usually used along with H-bridge inverter, they are: L type, LC type, LCL type, and LLCL type filter.

The L-type filter consists of only a single series inductor as shown in Fi. 2.15. It have an attenuation of -20 dB/dec over the entire frequency range. Usually a high value inductance is needed to eliminate the high frequency harmonics. And a large value means large size, high cost, also the voltage drop across it increases, which adversely affects the inverter dynamics.

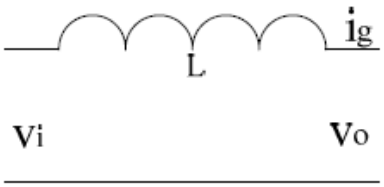

Figure 2.15: Schematic of L filter

The LC filter being a second order system gives an attenuation of -40dB/dec. Its schematic is shown in the Fig. 2.16. Designing the filter is relatively simple. The working concept is that filtering is shared by both, thus reducing inductor cost. However, if a high value of capacitance is selected then it absorbs high reactive current and load the inverter. One other limitation of this filter topology is that its resonant frequency becomes dependent on the grid impedance when connected to the utility grid [30]. The filter is mostly used in standalone situations due to its compact size and good attenuation.

Fig. 2.17 shows the schematic of an LCL filter, which is very popular with grid connected inverters due to its good attenuation beyond resonant frequency. This is

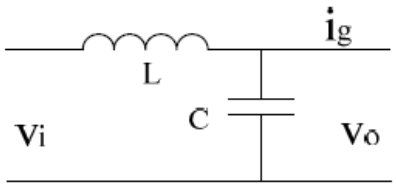

Figure 2.16: Schematic of LC filter

also preferred because it decouples grid impedance from the filter circuit [31]. The design of an LCL filter is not that all simple as one needs to consider the inherent resonance and current ripple limit through the inductor. A detailed procedure of designing the filter component values is presented in the following section.

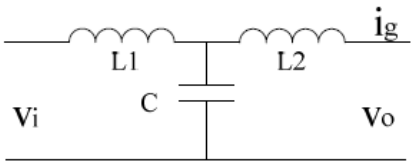

Figure 2.17: Schematic of LCL filter

Fig. 2.18 shows the bode plot of three filters, as discussed above, namely L, LC, and LCL filter. From the graph, it is observed that frequency response is same for L type and LCL type filter at low frequency. The inherent resonant peak in the LCL filter is clearly seen at the resonant frequency, which is dependent on the value of capacitor and inductors.

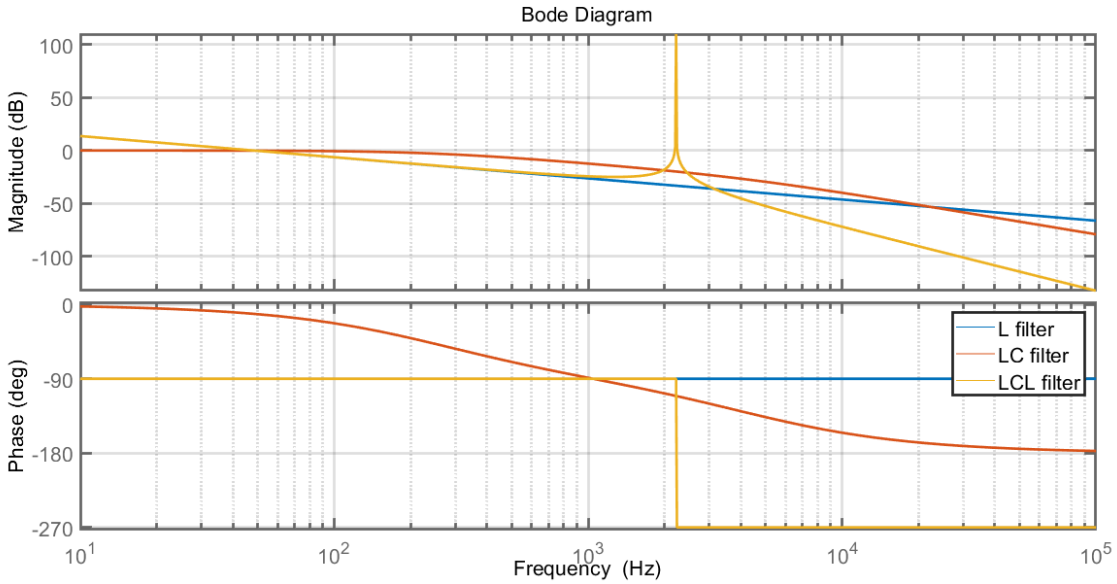

Figure 2.18: Bode plot of different filter types

2.7 Design of LCL low pass filter

With reference to the previous discussion, an LCL filter is selected because it provides good performance and relative simple design. Typically, the filter design criteria for standalone inverter system is less stringent than that of grid connected inverter. Therefore, the filter designed on the basis of grid connected system always satisfy the standards of standalone PV system. The inverter side inductance value is calculated on the basis of maximum allowable ripple current and the amount of attenuation of the unnecessary harmonics. Whereas the filter capacitance is selected solely on the basis of amount of reactive power absorbed by it.

There are generally some guidelines for the design of the said filter [21]. The total inductance of the two inductors (i.e. $L_1 + L_2$) should be less than 10% of the system base impedance so as to avoid large voltage drop across them, as that would affect the inverter's dynamics [30]. The current ripple should not be more than 20% of the peak rated current. In case of capacitance selection, it should not be very less or very high. Too low a value diminishes the impact of the filter, whereas a high value capacitance absorbs large amount of reactive power [30]. The inherent resonance frequency should possibly lie in the range shown by the equation (2.2). Where, f_s denotes the sampling frequency and f_g denotes fundamental power frequency. To have a good system stability, the grid side inductance L_2 should be a fraction of the inverter side inductance L_1. Finally, the grid current THD should not exceed the value of 5% as per IEEE 519-1992.

$$10f_g < f_{res} < 0.5f_s \tag{2.2}$$

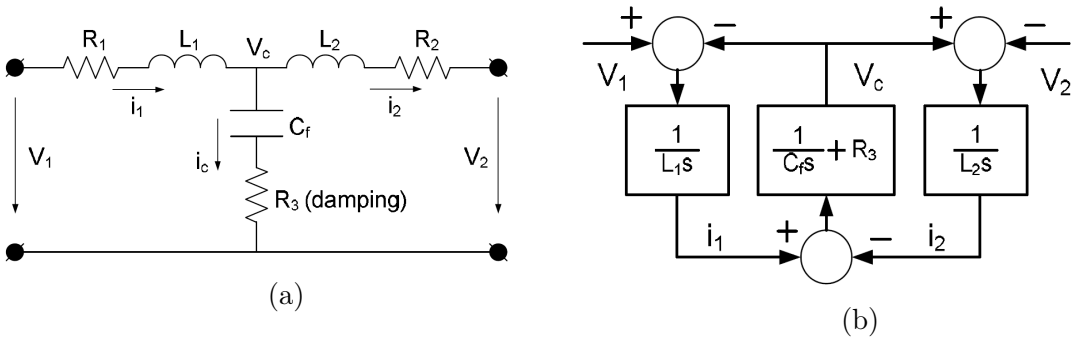

Figure 2.19: (a) Equivalent circuit diagram and (b) model of LCL-filter [31]

The Fig. 2.19a represents the schematic of the LCL filter and Fig. 2.19b represents the equicalent model of the filter. Where the terms have their usual meaning with the addition of R_d representing the damping resistance in series with the filer capacitance C_f.

Bases on the Fig. 2.19b, reprsenting the equivalent model, a transfer function can easily be derived. The transfer function shown by the eqn. (2.3) neglects the inductors series resistances, thus simplifying the equation:

$$G(s) = \frac{i_2(s)}{v_1(s)} = \frac{R_d C s + 1}{L_1 L_2 C s^3 + (L_1 + L_2) R_d C s^2 + (L_1 + L_2) s} \tag{2.3}$$

$$f_{res} = \frac{1}{2\pi}\sqrt{\frac{L_1 + L_2}{L_1 L_2 C}} \tag{2.4}$$

2.7.1 Filter Inductance Calculation

The formula for calculating minimum value of total inductance required for the filter is described in the eqn. (2.5), according to [32].

$$L > \frac{\epsilon V_{dc}}{4 f_{sw} I_{rated} \xi} \tag{2.5}$$

where, ϵ denotes the type of SPWM used, its value is 1 for Unipolar SPWM and 2 for Bipolar SPWM. V_{dc} is the optimum dc link capacitor voltage, I_{rated} is the rated current of the inverter, f_{sw} represents the switching frequency of the PWM, and finally the symbol ξ represents the maximum current ripple percentage. The value of ξ is chosen to be 20% of the I_{rated} in this project.

As discussed in previous section, the total inductance (i.e. $L_1 + L_2$) should not exceed 10% of the rated current I_{rated}, as beyond this the voltage drop increases significantly and thus affecting the inverter operation. Total inductance should satisfy both the equations (2.5) and (2.6). In eqn. (2.6), V_{rated} is the rated grid rms voltage; f_o is the fundamental power frequency; and S_{rated} is the rated apparent power of the system. Based on both the equations of total inductance, the value L_1 should be at least 2.4mH and the total inductance L should not exceed the value of 3.7mH. The grid side inductance value is found using eqn. (2.8), where, γ is chosen to be 2.

$$L_1 + L_2 < 0.1\frac{V_{rated}^2}{2\pi f_o S_{rated}} \tag{2.6}$$

$$L_1 + L_2 = L \tag{2.7}$$

$$L_1 = \gamma L_2 \tag{2.8}$$

2.7.2 Filter Capacitance Calculation

For sizing the filter capacitance, the idea is to calculate the reactive power absorbed by it. Eqn. (2.9) shows the design formula for filter capacitance [31]:

$$C = \frac{Q_{re}}{w_o V_{rated}^2} = \frac{\alpha P_{rated}}{w_o V_{rated}^2} \tag{2.9}$$

where, Q_{re} is the reactive power absorbed by the capacitor at power frequency and P_{rated} is the rated power of the inverter. α is the power ratio ($< 5\%$); w_o is grid frequency; and V_{rated} is the rated grid voltage.

The value of α greater than 5% can lead to more reactive power demand by the capacitor, which in turn increases current through the inverter side inductor, which ultimately leads to loading of the inverter and reduction of efficiency. Whereas, α taken too much less also means neglecting the capacitance and the size of inductor increases giving rise to virtual L filter.

2.7.3 Filter Damping

Active and Passive damping

For the PWM control method of the system represented in Fig. 2.1, there is a possibility of resonance at the resonant frequency because of the presence of LCL filter [33]. The resonance frequency calculation is as per the eqn. (2.4) [34].

Due to the inherent resonance problem of the LCL filter. A vecctor control technique can not be applied directly. There is a need of damping the resonance using either a passive or active device/circuit. A simple yet robust passive damping method involves connecting a small resistance in series with the filter capacitor [35]. An active damping method involves either adding a notch filter (with cut off frequency at the resonance frequency) or using capacitor current feedback, but this adds a current sensor leading to increased cost [36].

The problem with Passive damping methods are that they decrease the overall efficiency. whereas active damping methods are sensitive to parameter variations and may become unstable. In addition to it, the controller bandwidth limits the functioning of active damping stability [37].

In this thesis, passive damping is the chosen method of damping. A small resistance R_d is added in series with filter capacitor. It is given by the following equation:

$$R_d = \frac{1}{3w_{res}C_f} \tag{2.10}$$

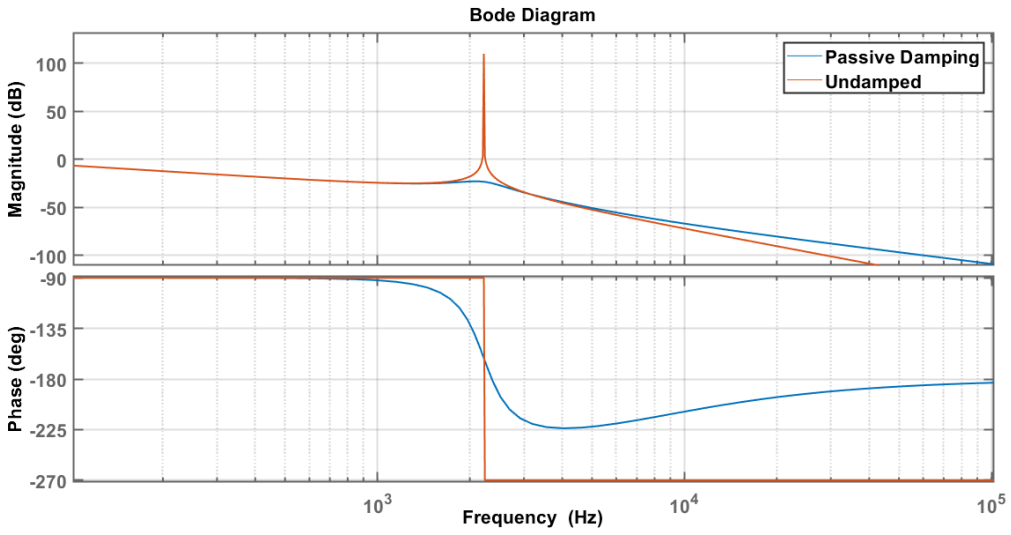

Figure 2.20: Bode plot of LCL filter with and without passive damping

2.8 Sizing of DC link capacitor

Let inverter output voltage and current be,

$$v_o(t) = \sqrt{2}V_{o-rms}sin(w_o t) \tag{2.11}$$

$$i_o(t) = \sqrt{2}I_{o-rms}sin(w_o t + \varphi) \tag{2.12}$$

Thus, the inverter instantaneous output power is,

$$p_{out}(t) = v_o(t) \times i_o(t) = V_{o-rms} I_{o-rms} \cos\varphi - V_{o-rms} I_{o-rms} \cos(2w_o t + \varphi) \quad (2.13)$$

There is a second harmonic component ($2w_o$) in the output power equation of the inverter as shown in the eqn. (2.13). this double frequency term also gets reflected on the inverter's input.Therefore, the job of DC link capacitor is also to limit this double line frequency term to exceed particular value. The sizing of the capacitor should be done in such a way that the voltage fluctuations are as small as possible. However, a large size capacitor value is also undesirable, this is because it increases the cost and makes the system very sluggish. The design procedure for DC link capacitor is as follows:

Rewriting the output power yields,

$$p_{out}(t) = S_{rated} \cos\varphi - V_{rated} \cos(2w_o t + \varphi) \quad (2.14)$$

The inverter power on the input side is as shown,

$$p_{in}(t) \cong V_{dc} \times [I_{dc} + i_r(t)] = V_{dc} I_{dc} + V_{dc} i_r(t) \quad (2.15)$$

If we neglect the power loss and assume the inverter to be ideal. we get,

$$p_{in}(t) = p_{out}(t) \quad (2.16)$$

Since a capacitor filters out high frequency component, therefore the double line frequency component is represented as,

$$V_{dc} i_r(t) = S_{rated} \cos(2w_o t + \varphi) \quad (2.17)$$

Thus, the double line frequency current on the dc side is:

$$i_r(t) = \frac{S_{rated}}{V_{dc}} \cos(2w_o t + \varphi) = I_r \cos(2w_o t + \varphi) \quad (2.18)$$

In this project, the maximum ripple voltage is set to 2.5% of the rated DC voltage. The calculated dc link capacitor value is derived by using,

$$C_{dc} = I_r / 2w_o V_{rmax} = S_{rated} / 4\pi f_o V_{dc} V_{rmax} \quad (2.19)$$

2.9 Simulation Parameters and Results

The design parameters assumed and derived is given in the table 2.1. The simulations conducted in the this and the following chapters are based on the values of this parameter table.

Parameter	Value	Parameter	Value
Modules in series (N_s)	20	Filter Capacitance (C_f)	7uF
Modules in parallel (N_p)	1	Damping resistance (R_d)	3.43Ω
Rated Power (P_{rated})	5kVA	DC link capacitance (C_{dc})	2.1mF
Rated grid voltage (V_{rated})	$240V_{rms}$	PV stray capacitance (C_{stray})	5nF
Power frequency (f_o)	50Hz	Grid side gnd resistance (R_g)	0.4Ω
switching frequency (f_{sw})	19950Hz	Resonance frequency (f_{res})	2.2kHz
Inverter side inductance (L_1)	2.4mH	Sampling frequency (f_{samp})	160kHz
Grid side inductance (L_2)	1.2mH	DC link capacitor vtg (V_{dc})	600V

Table 2.1: Parameter values chosen for the purpose of simulation

The simulation of the whole power circuit is represented in the Fig. 2.21. The system is simulated using the chosen value as discussed in the previous section. Two green blocks is shown in the diagram are controller and measurement block. The red block represents the load connected to the inverter. Fig 2.23 and Fig 2.22 represents the DC link capacitor voltage and grid current %THD respectively, when the system is simulated in open loop configuration and with $MI = 0.6$ and $MI = 0.9$

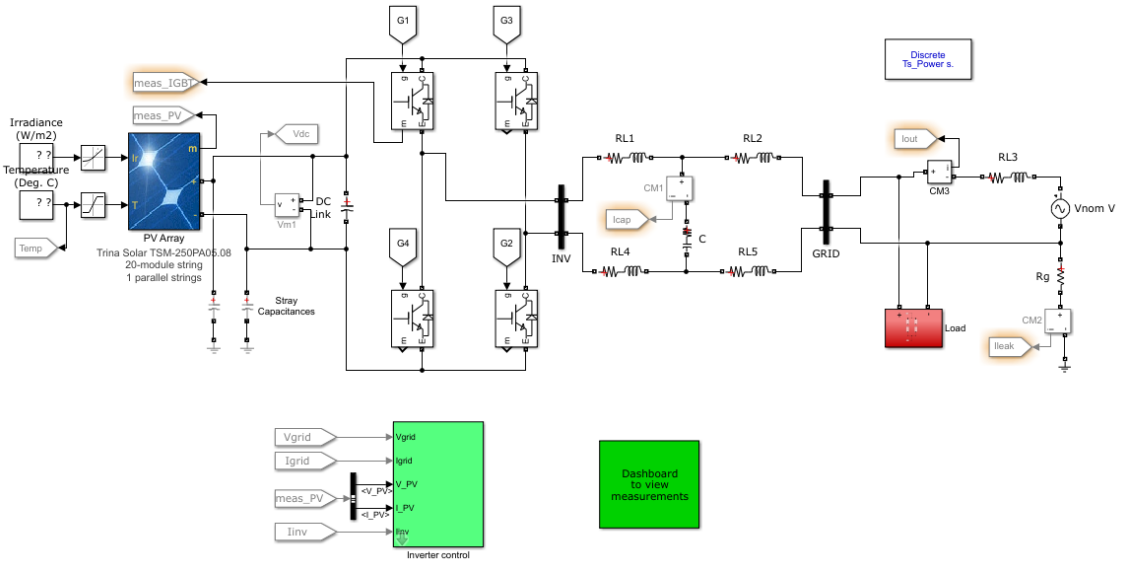

Figure 2.21: SIMULINK model of the entire simulated system

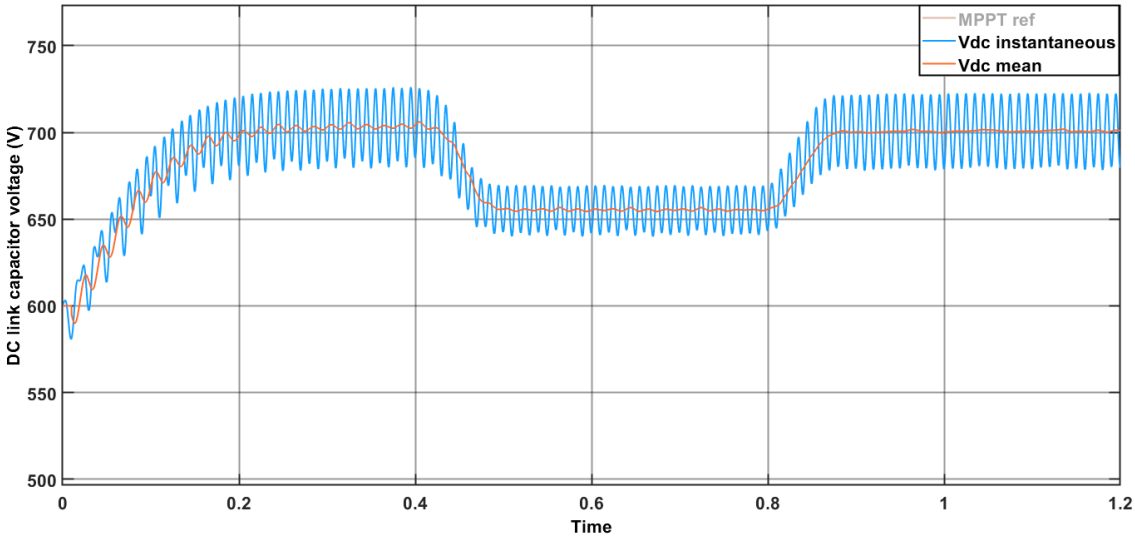

Figure 2.22: DC link capacitor voltage graph for MI=0.6, in open loop operation

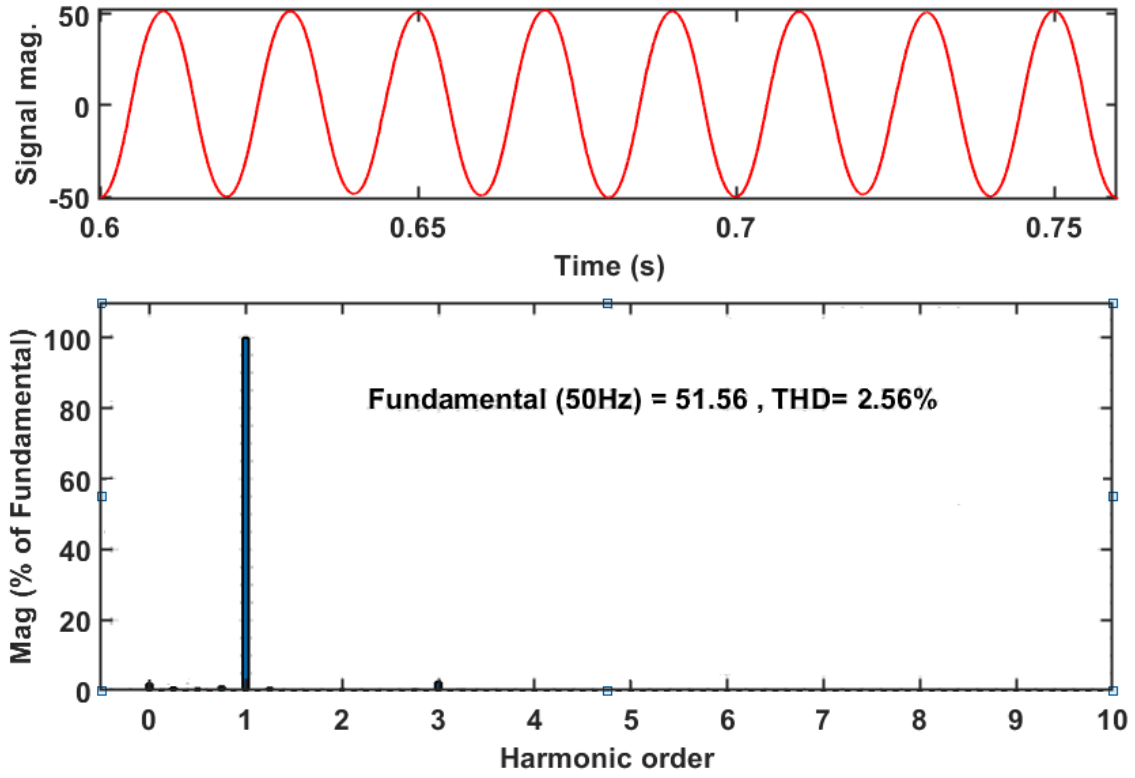

Figure 2.23: %THD of the grid current for MI=0.6, in open loop operation

2.10 Conclusion

The following conclusion can be drawn from the given chapter of the thesis:

- The ground leakage current of the PV system configuration is significantly reduced by using Bipolar SPWM. This is important as otherwise it injects high frequency current in the Grid.
- The designed filter inductance and capacitance value of the LCL filter is according to the required constraints. Also the passive damping method (R_d) in series with (C_f) attenuates the inherent resonance of the filter configuration.
- The open loop operation of the designed power circuit is successfully simulated. The %THD and DC link capacitor voltage ripples are within the required limits with Modulation Index (MI) taken as 0.6.

Chapter 3

DESIGN OF CLASSICAL CONTROLLERS

3.1 Overview

This chapter is an introduction to the design of two classical control methods. Classical controllers are linear regulators which utilizes a modulating stage for the controlling switches. The modulating scheme selected for this purpose is Bipolar SPWM explained in previous chapter. Section 3·2 discusses the synchronous reference frame theory for three phase systems and how to implement it in single phase inverter system. Similarly Section 3·3 describes the design of the Proportional resonant controller for controlling current in stationary frame.this sections also derives the difference between the fundamental PI and PR controller. Section 3.4 gives the simulation results for both the control systems performed in MATLAB SIMULINK. The graphs such as PV array extracted power, DC link capacitor voltage and grid current's percent THD are presented which can be compared to get the difference between the two methods. Fig. 3.1 presents a general current control block diagram for the PV-inverter system with LCL filter.

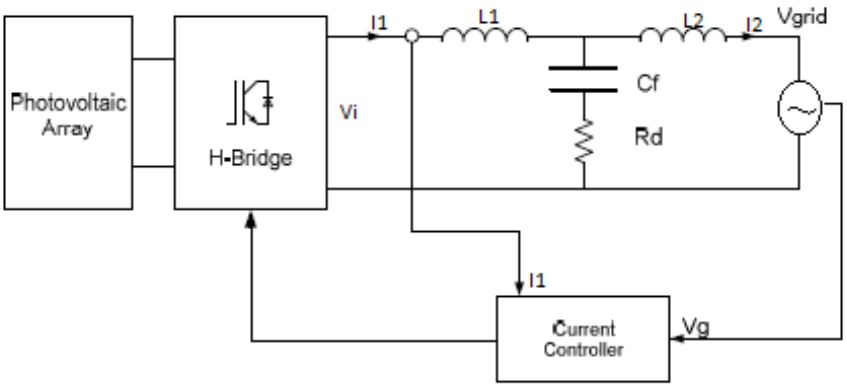

Figure 3.1: Generic Block diagram for current controlled inverter

3.2 d-q controller design

3.2.1 Synchronous Reference Frame theory

This subsection begins with a explanation of the stationary frame of reference, the synchronous frame of reference, and the transformations that occurs between these frames in a three-phase system. The Clarke transform is used to transform parameters of the circuits to a two-dimensional stationary reference frame. This conversion is generally used to convert balanced three-phase vectors into an orthogonal two-dimensional reference frame, and is therefore sometimes known as a 3-2 transform in its transforms, for example three phase currents into two internal variables. The Park transform is generally used in three-phase electric machine models. It generally eliminates the time varying parameters in two dimensional stationary frame by converting them to rotating reference frame parameters, making them time invariant. The Park transform is a 2-2 transform that also have a reference angle input. If the reference angle is rotating at the same speed as a frequency component of the two-dimensional input to the Park transform, the output of the latter corresponding to this frequency component will be stationary.

In the 1920's, R. H. Park [38] revolutionized analysis of electric machines. He formulated changing of quantities; by replacing the quantities (flux, currents, and voltages) referred to the stator side into the quantities referred to rotor side. In other words, he used projection and two-axis equations in order to transform the stator variables to a reference frame fixed in the rotor. The park transform has the property to eliminate fundamental frequency time variant quantities from the equations in the synchronous machine, appearing due to:

- Relative motion of electric circuits with each other.
- Sinusoidal magnetic reluctance of the electric circuits.

The transformation of the three-phase system from the stationary reference frame to the synchronous rotating reference frame can be easily done by the following procedure:

1. Resolving the three-phases into two phases by the use of the Clarke transformation as in (3.1). That is, the three-phase stationary reference frame components are projected onto two orthogonal axes (X_α and X_β) appropriately fixed in the same stationary reference frame, as shown in Fig. 3.2.

$$\begin{bmatrix} X_\alpha \\ X_\beta \end{bmatrix} = \begin{bmatrix} 1 & -\frac{1}{2} & -\frac{1}{2} \\ 0 & \frac{\sqrt{3}}{2} & -\frac{\sqrt{3}}{2} \end{bmatrix} \begin{bmatrix} U \\ V \\ W \end{bmatrix} \tag{3.1}$$

   where U, V, and W represent three-phase stationary-frame balanced components, and the projected orthogonal axis is represented by the X_α and X_β.

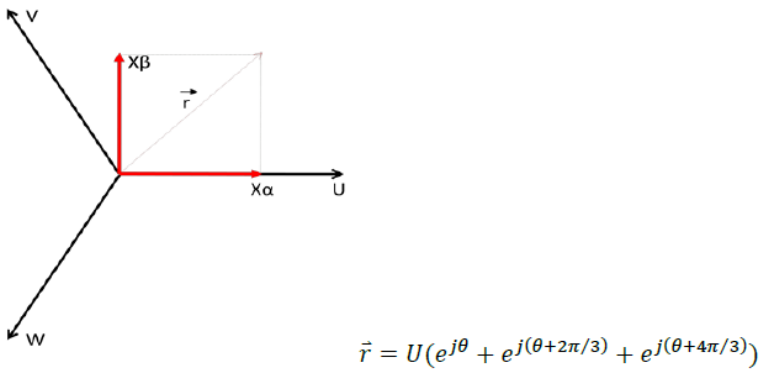

Figure 3.2: Clarke Transformation Vector

2. Transforming the two phase quantities (X_α and X_β) from the stationary reference frame to the synchronous rotating frame (with the corresponding d-q axis) which rotates at the angular speed of ω along with the rotor of the synchronous machine. This transformation equates synchronous reference frame with stationary frame of reference rotating woth angular velocity ω. Equation (3.2) is termed as park transformation, which is used to convert stationary frame to rotating frame (X_d and X_q), presented in Fig. 3.3.

$$\begin{bmatrix} X_d \\ X_q \end{bmatrix} = \begin{bmatrix} \cos\omega t & \sin\omega t \\ -\sin\omega t & \cos\omega t \end{bmatrix} \begin{bmatrix} X_\alpha \\ X_\beta \end{bmatrix} \tag{3.2}$$

However, note that the Park transformation matrix is an orthogonal non-singular matrix ($T \cdot T^{-1} = 1$). It simply represents the relationship between the stationary and the rotating frame components.

These mathematical transformations lead to the new frame components becoming time invariant in the rotating reference frame with respect to angular velocity ω, Fig. 3.3.

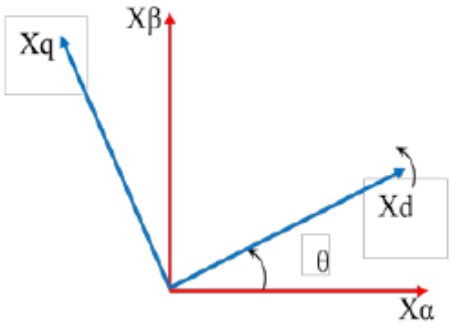

Figure 3.3: Park Transformation

These transformations and reference frame theory has recently received renewed interest in control system strategies as a result of the following factors :

- The time-invariant quantities (of the fundamental frequency) have advantages over time-variant quantities in the feedback control when compensated by PI

controllers. Simply put, the PI controllers are unable to eliminate the steady state amplitude and phase error in case of AC quantities.

- Use of solid-state device inverters for AC machine drives applications, in which the transformation theory is already used for control purpose.
- Digital controllers have become powerful, practical, and cheap. They are also popular in industry.
- The design of voltage-source inverter for three phase switching strategies is most effectively done by using space vector pulse width modulation (SVPWM).

3.2.2 Use of imaginary phase for single phase inverter

Present application of the park transformation needs minimum of 2 independent phase quantities of the system. Thus single phase systems cannot use the transformation directly to convert the reference frame to rotating reference frame.

In the following subsection, the mathematical model of the power stage in the d-q frame is derived. The derivation follows the construction of the imaginary circuit, transforming the overall circuit into stationary frame, and finally by using park transformation, converting the stationary frame to rotating frame of reference.

The aim of this solution is to build a single-phase inverter controller operating in the synchronous frame of reference which can produce high dynamic performance by reducing the fundamental frequency error component, and therefore improve the electrical power quality generated by the single-phase single stage PV system.

To create the imaginary orthogonal phasors of current and voltages, three method are mentioned that can be utilized to produce the required state variables, as represented in the Fig. 3.4. The methods are:

- By differentiating the inductor current and grid voltage [39]. As the said quantities are sinusoidal in nature, their differentiation also yield sinusoidal quantities orthogonal to the original. However, differentiation is sensitive to noise and therefore affects the controller dynamics. The inverter feedback controller is significantly affected by error in the stationary orthogonal phases. Also, the differentiation calculations require significant micro controller computation.
- Some work such as [39] proposes using an observer to construct the β-axis component. This approach can achieve a good result, but is very complex in terms of software and hardware processing requirements to design and implement.
- A more common and simple method to produce an imaginary signal is by using a quarter delay. The delay output should lag the input signal by 90 thus generating β axis component with much less computation. The demerit of this method is that the controller will not able to work for quarter time period.

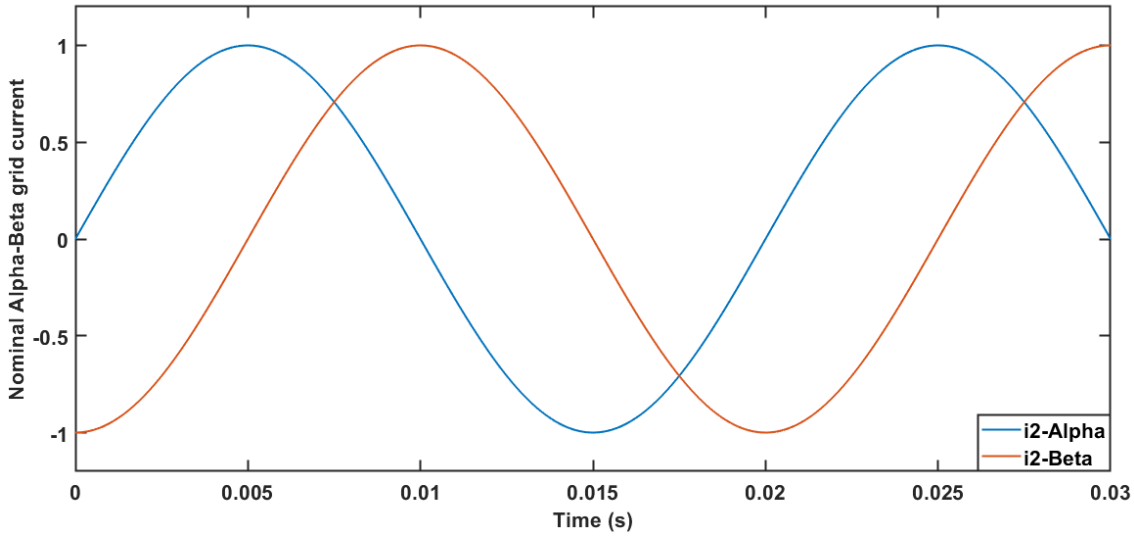

Figure 3.4: Grid currents in alpha-beta coordinates using a quarter delay

3.2.3 Mathematical modeling of inverter in d-q frame

The schematic of a grid connected single phase inverter with an LCL filter is shown in the Fig. 3.5. The low pass filter is connected between the VSI and the utility grid. The LCL filter is usually the choice for grid connected inverter due to its good attenuation and decouple nature. It filters out high frequency content and supply quality current to the grid.

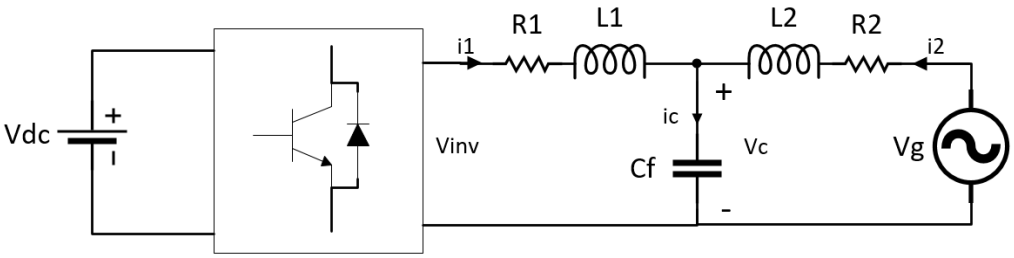

Figure 3.5: Schematic diagram of single phase inverter connected to grid via LCL filter

The single phase inverter with LCL filter can be mathematically described by the differential equations (3.3)(3.5)(3.5) [40], The conventions used is that of the used in motors:

$$L_1 \frac{di_1}{dt} + R_1 i_1 = v_c - v_{inv} \tag{3.3}$$

$$L_2 \frac{di_2}{dt} + R_2 i_2 = v_g - v_c \tag{3.4}$$

$$C_f \frac{dv_c}{dt} = i_2 - i_1 \tag{3.5}$$

where:
L_1 and L_2 represents inverter side and grid side inductance;

R_1 and R_2 represents the ESR of respective inductance;
i_1 and i_2 denotes the inverter side and grid side fundamental current;
v_c denotes the voltage across the filter capacitor;
v_{inv} is the output voltage of the inverter;
v_g is the constant grid voltage.
Whereas, the concept of imaginary orthogonal phasor is shown in the fig. 3.6 [40]. This circuit has all the components similar to that of the real circuit, except for the voltages and currents, which are 90 apart from the real quantities.

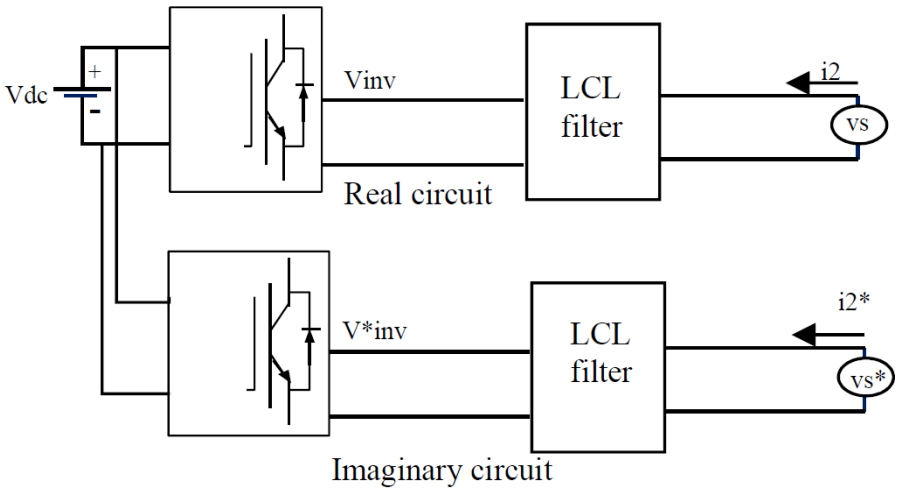

Figure 3.6: imaginary orthogonal circuit for applying d-q transform [40]

Eqns. (3.6)(3.7)(3.8) refers to the imaginary circuit mathematical differential equations. They are:

$$L_1 \frac{di_1^*}{dt} + R_1 i_1^* = v_c^* - v_{inv}^* \tag{3.6}$$

$$L_2 \frac{di_2^*}{dt} + R_2 i_2^* = v_g^* - v_c^* \tag{3.7}$$

$$C_f \frac{dv_c^*}{dt} = i_2^* - i_1^* \tag{3.8}$$

where:
i_1^* and i_2^* represents the fundamental component of inverter side and grid side current;
v_c^* denotes the voltage across the imaginary filter capacitor;
v_{inv}^* is the imaginary inverter's output voltage;
v_g^* is the imaginary Grid voltage.
where:
$v_g^* = v_g e^{-\pi/2}; i_1^* = i_1 e^{-\pi/2}; i_2^* = i_2 e^{-\pi/2}; v_c^* = v_c e^{-\pi/2}$
The real and imaginary circuit represents the $X_\alpha and X_\beta$ stationary frame of reference. This is converter to d-q reference fame using the expression shown by (3.9) [40].

$$T = \begin{bmatrix} \cos\omega t & \sin\omega t \\ -\sin\omega t & \cos\omega t \end{bmatrix} \tag{3.9}$$

The inverse transformation matrix is given by the following matrix equation:

$$T_{inv} = T^t = \begin{bmatrix} \cos\omega t & \sin\omega t \\ -\sin\omega t & \cos\omega t \end{bmatrix} \tag{3.10}$$

The (3.11) represents average state space model of the inverter in d-q frame by linearizing of the eqn. (3.3) through (3.8) around the stable operating point.

$$\frac{dx}{dt} = A.x + B.u \tag{3.11}$$

where:
$x = [i_{2d}\ i_{2q}\ i_{1d}\ i_{1q}\ v_{cd}\ v_{cq}]^T$, $u = [v_{gd}\ v_{gq}\ v_{id}\ v_{iq}]^T$

Therefore, the state space mathematical model of the LCL-GCC system is described by the matrix eqn. (3.12) [41],

$$\begin{aligned} \frac{d}{dt}\begin{bmatrix} i_{2d} \\ i_{2q} \\ i_{1d} \\ i_{1q} \\ v_{cd} \\ v_{cq} \end{bmatrix} &= \begin{bmatrix} -\frac{R_2}{L_2} & \omega_o & 0 & 0 & -\frac{1}{L_2} & 0 \\ -\omega_o & -\frac{R_2}{L_2} & 0 & 0 & 0 & -\frac{1}{L_2} \\ 0 & 0 & -\frac{R_1}{L_1} & \omega_o & -\frac{1}{L_1} & 0 \\ 0 & 0 & \omega_o & -\frac{R_1}{L_1} & 0 & -\frac{1}{L_1} \\ \frac{1}{C_f} & 0 & -\frac{1}{C_f} & 0 & 0 & \omega_o \\ 0 & \frac{1}{C_f} & 0 & -\frac{1}{C_f} & -\omega_o & 0 \end{bmatrix} \begin{bmatrix} i_{2d} \\ i_{2q} \\ i_{1d} \\ i_{1q} \\ v_{cd} \\ v_{cq} \end{bmatrix} \\ &+ \begin{bmatrix} \frac{1}{L_2} & 0 & 0 & 0 & 0 & 0 & 0 \\ 0 & \frac{1}{L_2} & 0 & 0 & 0 & 0 & 0 \\ 0 & 0 & -\frac{1}{L_1} & 0 & 0 & 0 & 0 \\ 0 & 0 & 0 & 0 & -\frac{1}{L_1} & 0 & 0 \\ 0 & 0 & 0 & 0 & 0 & 0 & 0 \\ 0 & 0 & 0 & 0 & 0 & 0 & 0 \end{bmatrix} \begin{bmatrix} v_{gd} \\ v_{gq} \\ v_{id} \\ v_{iq} \\ 0 \\ 0 \end{bmatrix} \end{aligned} \tag{3.12}$$

where ω_o is the fundamental angular frequency of the utility voltage, and other symbols in the above eqn. (3.12) are in accordance to the referred Fig. 3.5, e.g. $i_{2\alpha}, i_{2\beta} \leftrightarrow i_d, i_q$, $i_{1\alpha}, i_{1\beta} \leftrightarrow i_{d1}, i_{q1}$; $v_{c\alpha}, v_{c\beta} \leftrightarrow v_{cd}, v_{cq}$; $v_{g\alpha}, v_{g\beta} \leftrightarrow v_d, v_q$, and $v_{i\alpha}, v_{i\beta} \leftrightarrow v_{d1}, v_{q1}$.

The major hurdle in deriving the vector control is to decouple the state variable of LCL-GCC in eqn. (3.12). To solve the issue and simplify calculations, [42] proposed a strategy to neglect the filter capacitor and thus observing as if only an L filter is connected. Thus neglecting the capacitance in the eqn. (3.12) really simplifies the complexity giving the eqn. (3.13):

$$\frac{d}{dt}\begin{bmatrix} i_{2d} \\ i_{2q} \end{bmatrix} = -\begin{bmatrix} -\frac{R_2+R_1}{L_2+L_1} & -\omega_o \\ \omega_o & -\frac{R_2+R_1}{L_2+L_1} \end{bmatrix} \begin{bmatrix} i_{2d} \\ i_{2q} \end{bmatrix} - \frac{1}{L_2+L_1}\begin{bmatrix} v_{id} - v_{gd} \\ v_{iq} - v_{gq} \end{bmatrix} \tag{3.13}$$

By simplifying the above eqn. (3.13), the state equations are as follows [42]:

$$v_{id} = -(R_2 + R_1)i_{2d} + (L_2 + L_1)\frac{di_{2d}}{dt} + \omega_o(L_2 + L_1)i_{2q} + v_{gd} \tag{3.14}$$

$$v_{iq} = -(R_2 + R_1)i_{2q} + (L_2 + L_1)\frac{di_{2q}}{dt} - \omega_o(L_2 + L_1)i_{2d} + v_{gq} \tag{3.15}$$

where in the symbols v_d' and v_q' denotes the state equations that relates input voltage to output current for the current loop of the d-q frame control. The rest of the parameters are for compensation sake. Therefore for designing the current loop, the corresponding transfer function $1/[(R_2 + R_1) + (L_2 + L_1)s]$ is utilized [42].

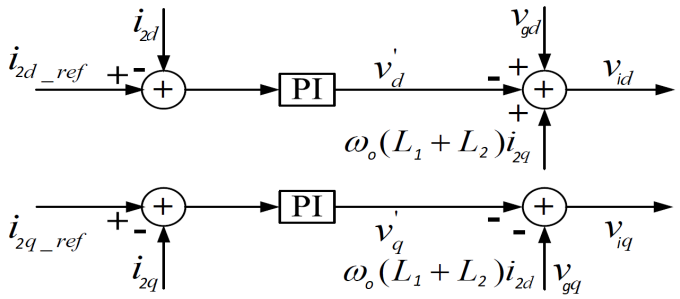

Figure 3.7: current control block diagram for LCL-GCC system

Thus Fig. 3.7 represents the decoupled form of current control in an LCL-GCC system, formed by the eqns. (3.14) and (3.15), Which is nothing but similar to that of an L-GCC system. The d-q frame gate control signal v_{id} and v_{iq} consists of output from PI controllers and corresponding decoupling terms.

3.2.4 Proposed d-q controller structure

The single-phase inverter model in this thesis developed in the previous section is used in developing a suitable controller in the d-q synchronous reference frame.

The single-phase inverter model was derived in the previous section using a synchronous rotating reference frame. Consequently, the controller should also operate in the d-q frame of reference. The current controller consists of 2 channels (one each for d and q axis) where as both are driven by single outer voltage control loop.

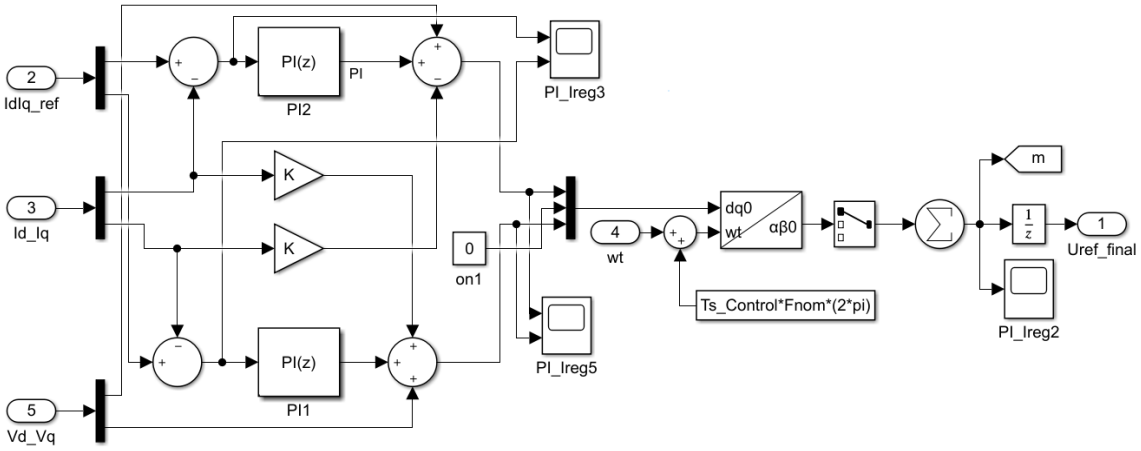

Figure 3.8: Simulated proposed dq controller structure

The control system is configured as in Fig. 3.9. The diagram shows the voltage-source inverter, the orthogonal signal extraction and Park transformation blocks ($\alpha - \beta$ to dq), controller structure and the SPWM block. The grid voltage and current are sampled and two orthogonal stationary reference frames are generated using quarter delay function. The transformation into rotating reference frame from

stationary reference frame is achieved by using Park transform. The controller controls the active current in the d channel and reactive current in the q channel respectively. The outer voltage loop consists of a MPPT block and a PI controller. The output from this PI controller acts as the reference for the current control loop. This is followed by the last step in the controller structure: to produce switching gate signals for the IGBT by inverse transforming the the controller output back to $\alpha - \beta$ frame. Output from only α is used to generate the PWM signals.

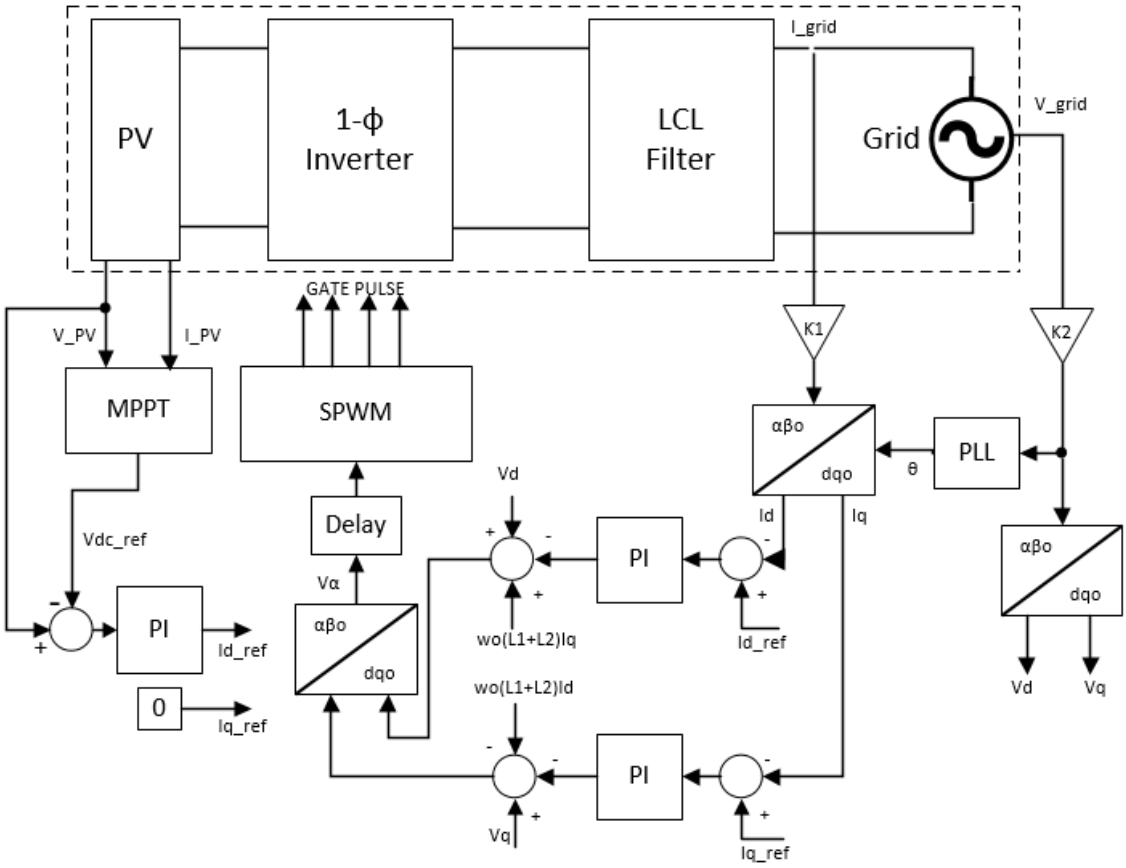

Figure 3.9: d-q reference frame control block diagram

The PI controller settings of the outer voltage loop is selected based on Nichols-Zieglar method. That is, $K_p^v = 12$ and $K_i^v = 200$ is the approximate solution obtained from the method. The PI parameters of the d-q current controller is derived from hit & try method. Thus, they are taken as, $K_p^{dq} = 0.15$ and $K_i^{dq} = 6.6$ in the simulation model.

Phase Locked Loop

A PLL is a system that generates output signal with fix phase angle related to the input signal. There are many methods of implementing PLL: one of the easiest way is to have phase detector and variable frequency oscillator in a negative feedback loop. The oscillator produces a periodic signal, and phase detector compares that signal and input signal and output the phase difference between them and the oscillator then minimizes this phase difference.

Maintaining the phase in lock also implicitly implies keeping frequency the same. As a result, the PLL can not only maintain an input frequency but also track and

synchronize with it, also it can be used to generate frequency that is multiple of the input frequency. These properties of it are exploited in clock synchronization, synthesis of high frequency signals, and demodulation.

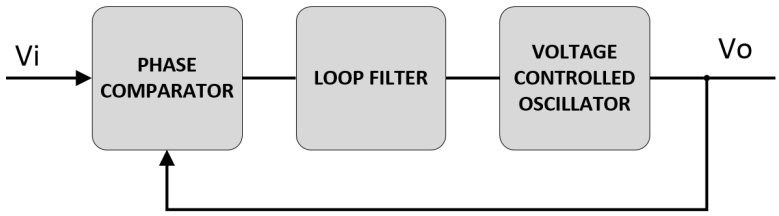

Figure 3.10: Block diagram of simplest analog phase locked loop

The PLL block of MATLAB is a closed loop system, where it tracks the phase difference and frequency of the applied sinusoidal signal by using variable frequency oscillator. The PID controller in the system adjust the frequency so as to maintain zero phase difference. The internal block diagram of the SRF-PLL is shown in the Fig. 3.11

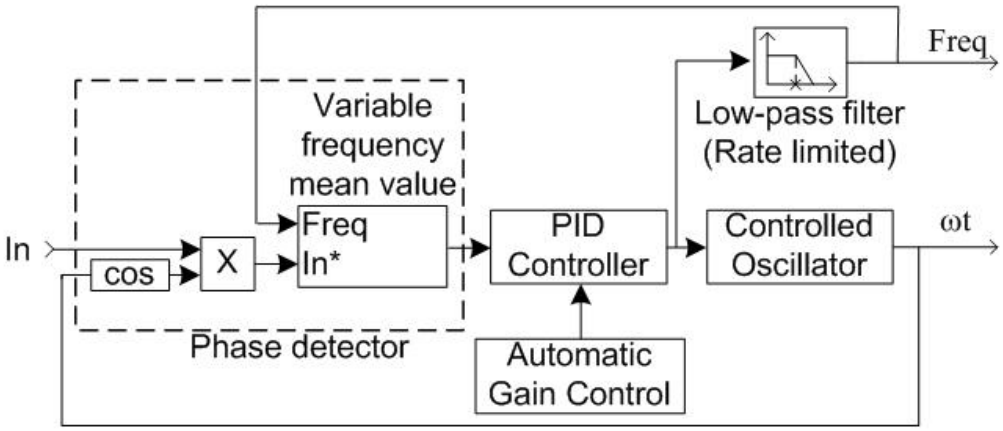

Figure 3.11: Block diagram of PLL subsystem [43]

The input signal is superimposed with the oscillator's signal. The DC component of this mixed signal is then applied to variable frequency mean value so as to extract the phase difference between the two signals. A PID controller then tracks the phase difference and makes it 0 by controlling the oscillator. In between, the output from PID (angular velocity) is given to a low pass filter. The filter's output is in hertz and it is used by the mean value [43].

3.3 P-R controller design

3.3.1 Comparison of PI and PR controller

Ideal and non-ideal PI controller

Eqn. (3.16) defines the transfer function of an ideal PI controller. It is transformed into eqn. (3.17) if a first order low pass filter is used in the synchronous reference

frame. Thus, the eqn. (3.17) can not only be seen as a non ideal form of PI controller but it can also be used to derive non ideal PR controller [44].

$$G_I(s) = K_p + \frac{K_I}{s} = \frac{K_p s + K_I}{s} = K_p(1 + \frac{1}{T_i s}) \tag{3.16}$$

$$G_I(s) = K_p + \frac{K_i w_c}{s + w_c} \tag{3.17}$$

where K_p, K_i and $T_i = \frac{K_p}{K_i}$ are the controller's proportional gain, integral gain and integral time constant, whereas the angular frequency is given by the term w_c .

Nichols-Zieglar method can be used to find the proportional and integral gains of the PI controller. For quite large number of plants, the methods gives fast and non-oscillatory response for the closed loop system. The fig. 3.12 shows the bode plot of PI controller following the eqn. (3.16).

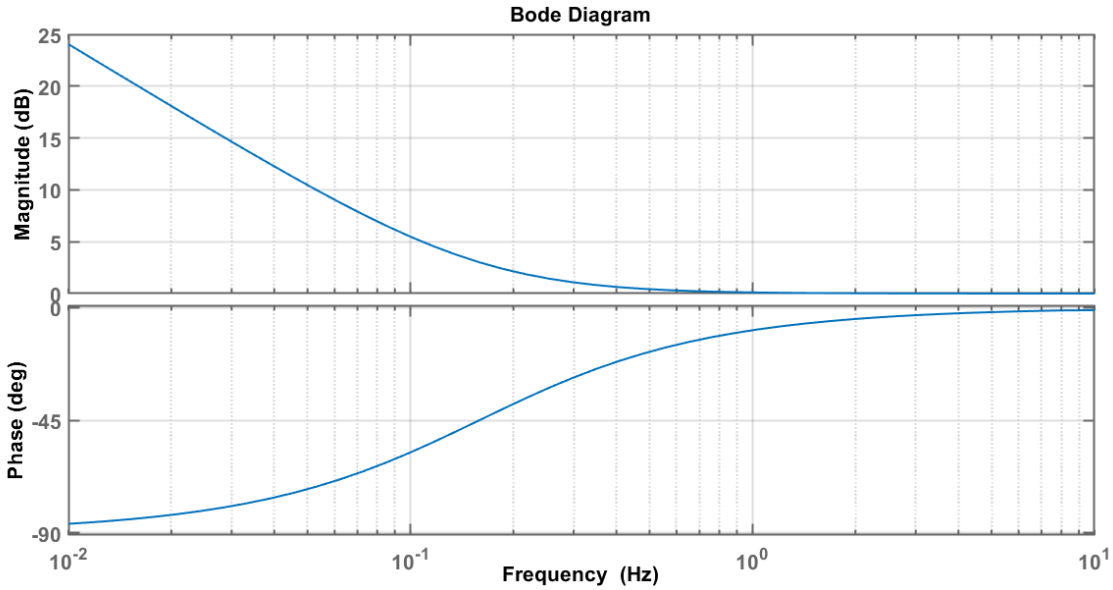

Figure 3.12: PI transfer function bode plot with $K_p = 1$ and $K_i = 1$

Implementation in digital domain

The equation of a PI controller in time domain is given by [45]:

$$u(t) = K_p e(t) + K_i \int_0^t e(t)dt \tag{3.18}$$

where $u(t)$ is the controller output and $e(t)$ is the error input signal applied to the controller in the time domain.

The eqn. (3.18) can be used to obtain discrete form by taking the sampling time T_s:

$$u(k) = K_p e(k) + K_i T_s \sum_k e(k) \tag{3.19}$$

And for the sampling time at $(k-1)$:

$$u(k-1) = K_p e(k-1) + K_i T_s \sum_{k-1} e(k) \tag{3.20}$$

Subtract (3.19) to (3.20), we can get

$$u(k) = u(k-1) + K_p[e(k) - e(k-1)] + K_i T_s e(k) \tag{3.21}$$

The discrete form of the PI controller in digital domain is represented by the eqn. (3.21).

Ideal and non-ideal PR controller

The park transformation (synchronous reference frame control) can not be applied directly to single phase inverters due to absence of two independent phasors. Thus, a frequency modulated method can be alternatively approached for the sake of transforming the controller parameters into dc quantities. The process is shown as follows: [45][46]:

$$G_R(s) = G_I^{ac}(s) = \frac{1}{2}[G_I(s + jw_o) + G_I(s - jw_o)] \tag{3.22}$$

where w_o represents the fundamental angular frequency.

In the eqn. (3.22), the transfer function $G_I(s)$ is that of a low pass filter. This equation is used for frequency shifting transformation. This is can be accomplished by either a first order low pass filter or a PI controller in synchronous frame of reference rotating at an angular frequency of w_o, After which we get (3.23):

$$\begin{aligned} G_R(s) = G_I^{ac}(s) &= \frac{1}{2}[K_p + K_i\frac{1}{s + jw_o} + K_p + K_i\frac{1}{s - jw_o}] \\ &= K_p + K_i\frac{s}{s^2 + w_o^2} \end{aligned} \tag{3.23}$$

Equation (3.23) describes the ideal transfer function of a PR controller, that has infinite gain at an angular frequency of w_o.

To overcome the resonance issue of the ideal PR controller, an approximate transfer function is used which is known as non ideal PR controller. This is achieved by substituting non ideal PI controller transfer function from (3.17) into (3.22). It is like adding a high gain low pass filter [46]. Thus the approximate form of a PR controller follows:

$$G_R(s) = K_p + K_i\frac{(w_c s) + w_c^2}{s^2 + 2w_c s + w_c^2 + w_o^2} \tag{3.24}$$

Assuming $w_c \ll w_o$ a simpler approximation is:

$$G_R(s) = K_p + K_i\frac{K_i w_c s}{s^2 + 2w_c s + w_o^2} \tag{3.25}$$

The gains of the non ideal PR controller can be changed such that it eliminates the voltage tracking error. The gain values can be designed by a step by step pro-

cedure described in [47]. The bode plot of Proportional Resonant transfer function is shown in Fig. 3.13.

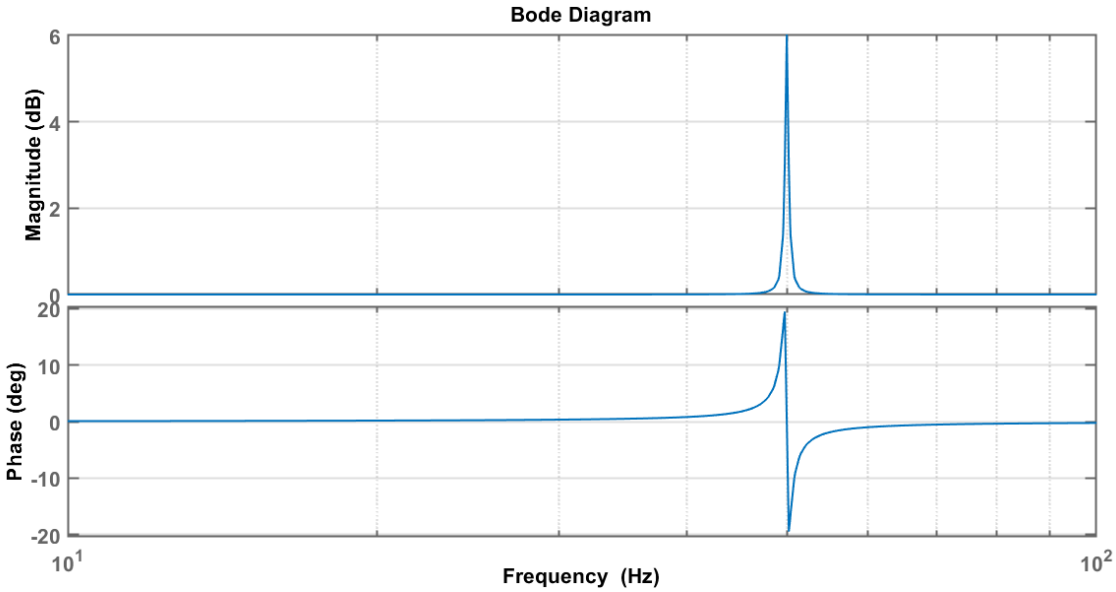

Figure 3.13: PR transfer function bode plot Kp=1, Kr=1 and wo=314.18

Digital implementation

By substituting $s = \frac{2}{T_s}\frac{1-z^{-1}}{1+z^{-1}}$(Bi-linear transform) into eqn. (3.25), the transfer function of the PR controller in the discrete form is given by:

$$G_R(z) = \frac{n_0 + n_1 z^{-1} + n_2 z^{-1}}{1 + d_1 z^{-1} + d_2 z^{-1}} \tag{3.26}$$

where T_s is the sampling time and

$$n_0 = \frac{(4 + 4T_s w_c + w_o^2 T_s^2)K_p + 4K_i T_s w_c}{4 + 4T_s w_c + w_o^2 T_s^2} \tag{3.27}$$

$$n_1 = \frac{(-8 + 2w_o^2 T_s^2)k_p}{4 + 4T_s w_c + w_o^2 T_s^2} \tag{3.28}$$

$$n_2 = \frac{(4 - 4T_s w_c + w_o^2 T_s^2)K_p - 4K_i T_s w_c}{4 + 4T_s w_c + w_o^2 T_s^2} \tag{3.29}$$

$$d_1 = \frac{-8 + 2w_o^2 T_s^2}{4 + 4T_s w_c + w_o^2 T_s^2} \tag{3.30}$$

$$d_2 = \frac{4 - 4T_s w_c + w_o^2 T_s^2}{4 + 4T_s w_c + w_o^2 T_s^2} \tag{3.31}$$

In simplified form, the eqn. (3.26) can be represented as:

$$y(k) = n_0 u(k) + n_1 u(k-1) + n_2 u(k-2) - d_1 u(k-1) - d_2 u(k-2) \tag{3.32}$$

where, similar to discrete form of PI controller, $u(k)$ is the input error and $y(k)$

is the controller's output.

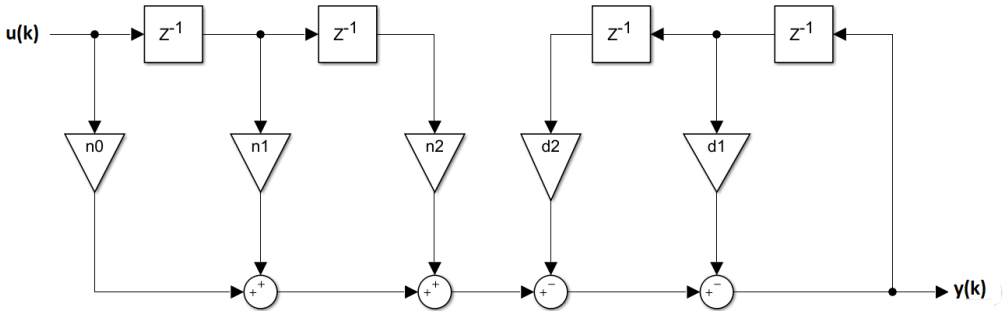

Figure 3.14: Discrete PR controller

3.3.2 Proposed PR controller structure

The grid frequency does not always remain constant, because of grid faults and varying load demand. When the grid frequency changes more than the range set by the PR controller, the gain reduces. this results into increase in error. To ensure that this never happens, the eqn. (3.33) is used such that controller can have wider frequency range.

$$G_i(s) = K_p + \frac{K_r \omega_i s}{s^2 + 2\omega_i s + \omega_o^2} \tag{3.33}$$

A PR transfer function (3.33) has a wider frequency band around the resonance. Where, w_i represents the cut off frequency of the resonant peak (-3 dB from the peak); K_p denotes the proportional gain of the controller; K_r denotes the resonant gain of the controller, and $\omega_o = 2\pi f_o$ describes the power angular frequency. By increasing the value of w_i, the resonant frequency band increases, thus allocating varying grid frequency.

Following enumerations presents the influence of the PR controller parameters, such as K_p, K_r, and w_i on the performance of the controller [48]:

1. $K_p = 1$ and K_r is varied:

   It is seen from the Fig. 3.16 that when K_p is kept constant and K_r is increased, the resonant peak of the controller increases. Whereas the bandwidth remains approximately same.

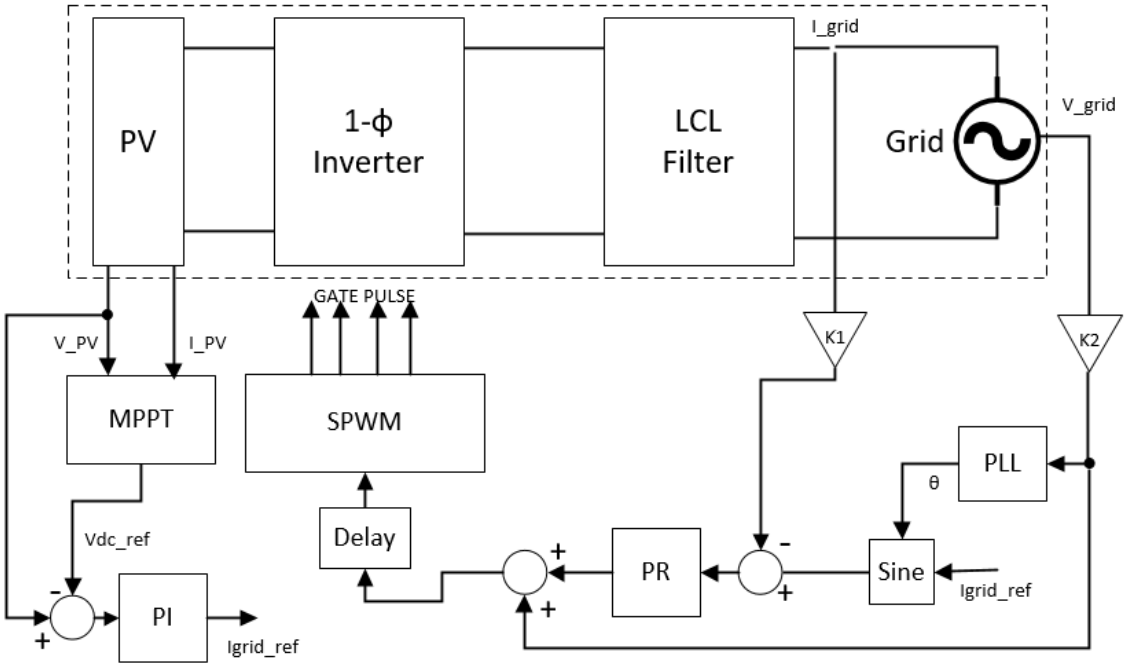

Figure 3.15: P-R controller block diagram

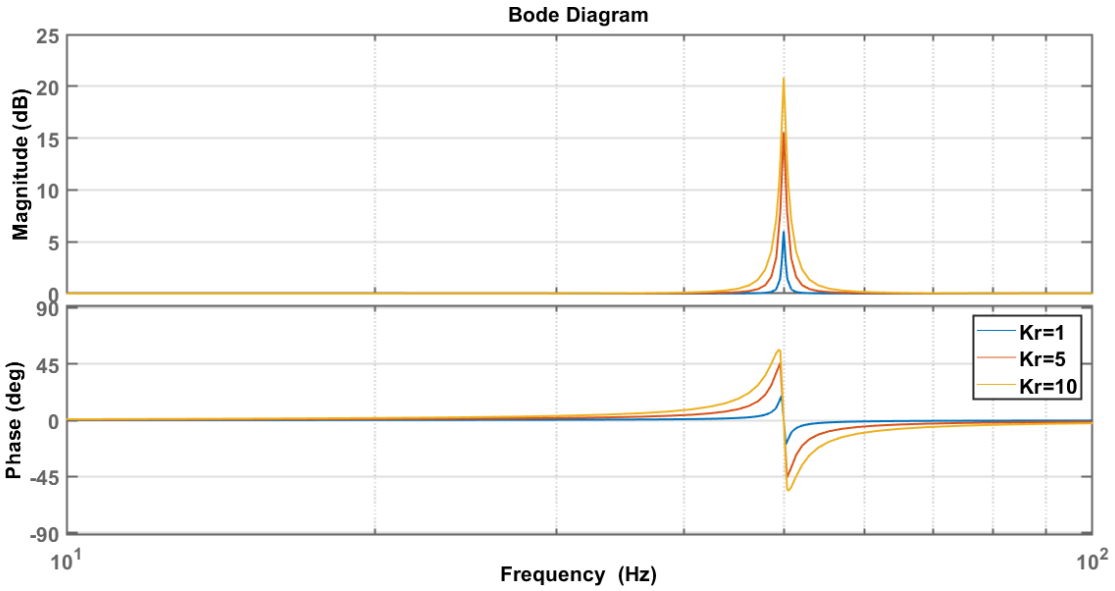

Figure 3.16: Bode plot; Kr=1, wi=1, and Kp changes

2. $K_r = 1$ is kept same, K_p is varied:

   With reference to the Fig. 3.17, The value of K_p is increased keeping the K_r constant. The gain of the controller is increased but the resonant peak is reduced a little bit.

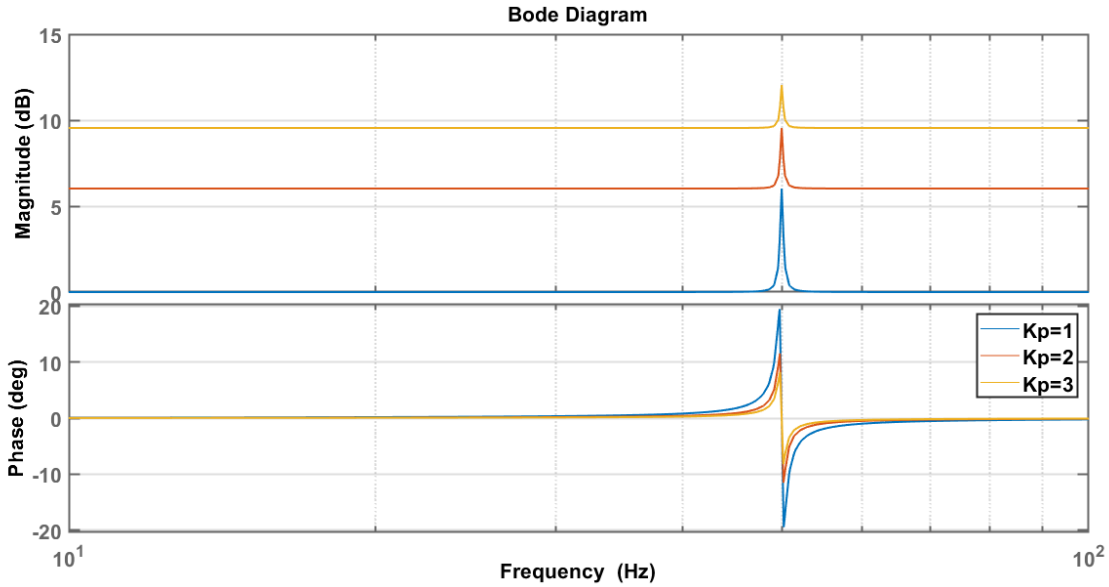

Figure 3.17: Bode plot; Kp=1, wi=1, and Kr changes

3. $K_r = 1$ and $K_p = 1$ stays same, $w_i$changes:

   Increasing the value of w_i causes the gain of the controller to remain same but the bandwidth of the controller increases. The parameter should compensate the change in the grid frequency. Fig. 3.18 shows the diagram of discussed variations in w_i.

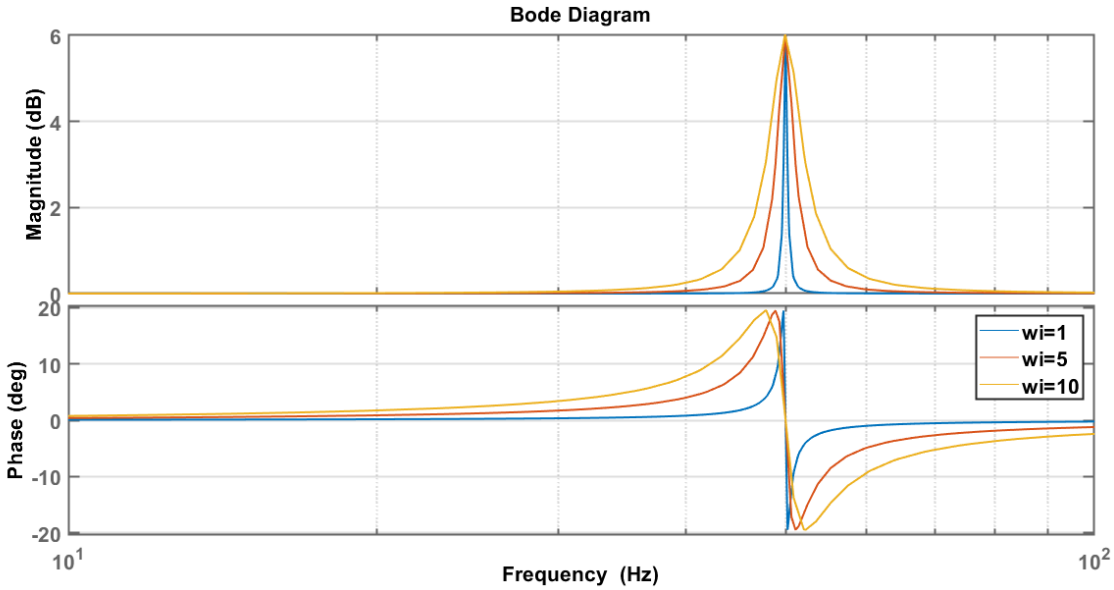

Figure 3.18: Bode plot; Kr=1, Kp=1, and wi changes

The two constant parameters of the PR controller (K_p^{pr} and K_r^{pr}) are selected to be same as that of the d-q controller. That is, $K_p^{pr} = 0.15$ and $K_r^{pr} = 6.6$ are the values taken for the simulation model. Whereas $w_i = 2$ is taken so as to incorporate small changes in grid frequency.

3.4 Simulation Results

The simulation results obtained are shown in the following figures. The simulation time is set to 1.2 seconds. Initially the irradiance is $300W/m^2$ and the temperature is set to 25 ℃. There are 2 disturbances injected into the system at different interval of time and the performance of the controller is noted from the graphs.

1. First, at 0.4 second, the irradiance is increased to $1000W/m^2$, and temperature is increased to 55 ℃.

2. then, at 0.8 second, the irradiance is reduced to $400W/m^2$, and the temperature is reduced to 30 ℃

The results of both the controllers are plotted in the following subsections.

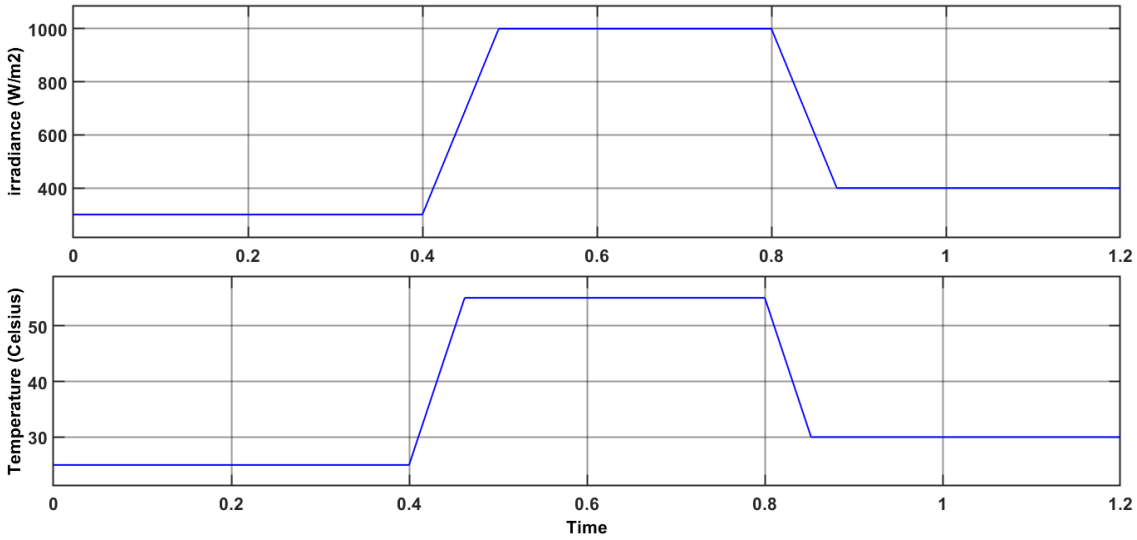

Figure 3.19: Irradiance and temperature change for the give simulation

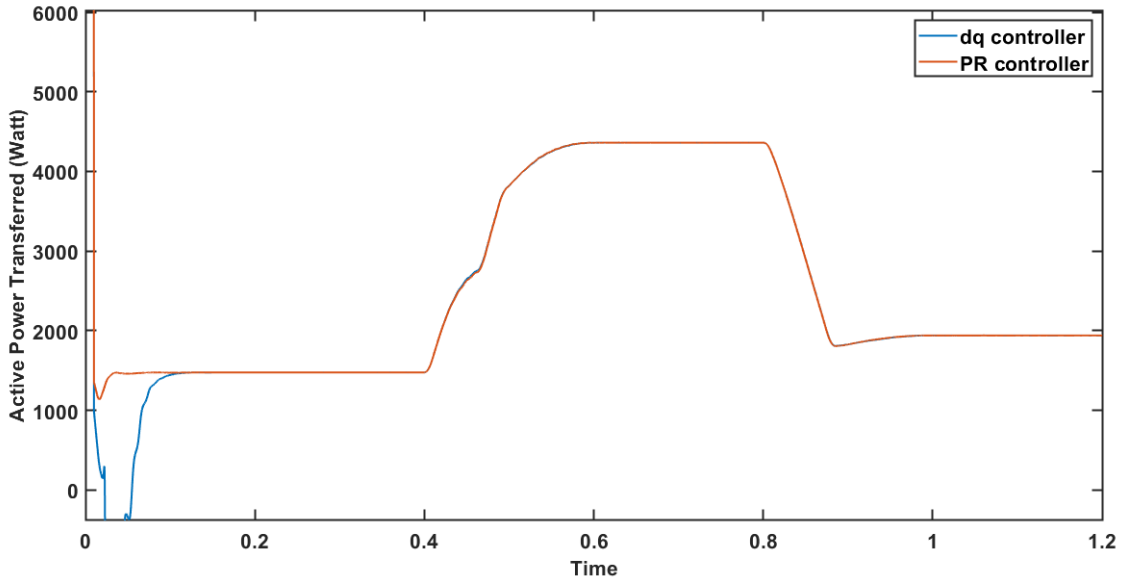

Figure 3.20: MPPT plot for d-q and PR controller

3.4.1 dq controller results

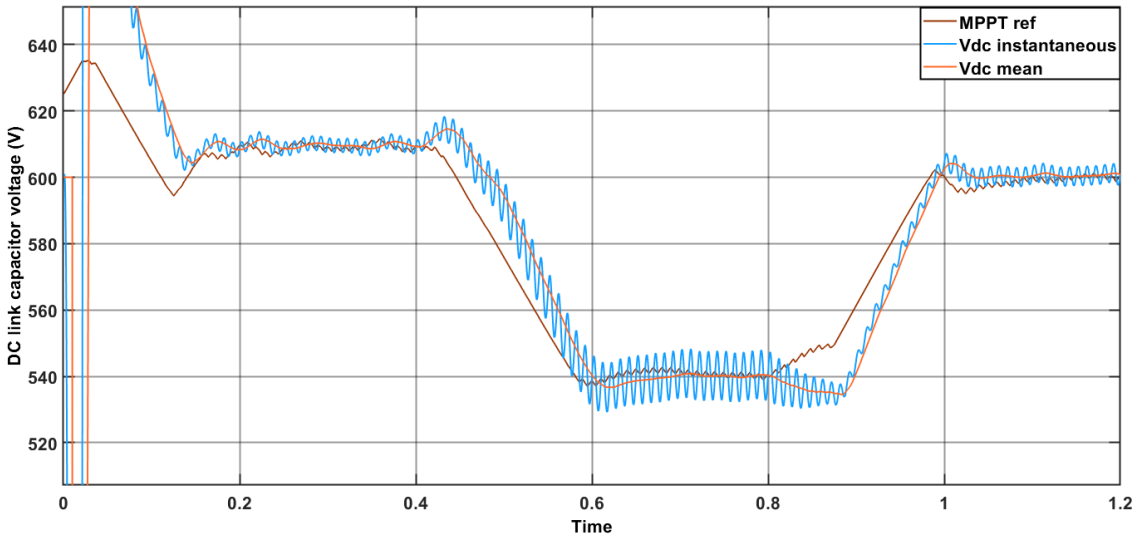

Figure 3.21: DC link capacitor voltage

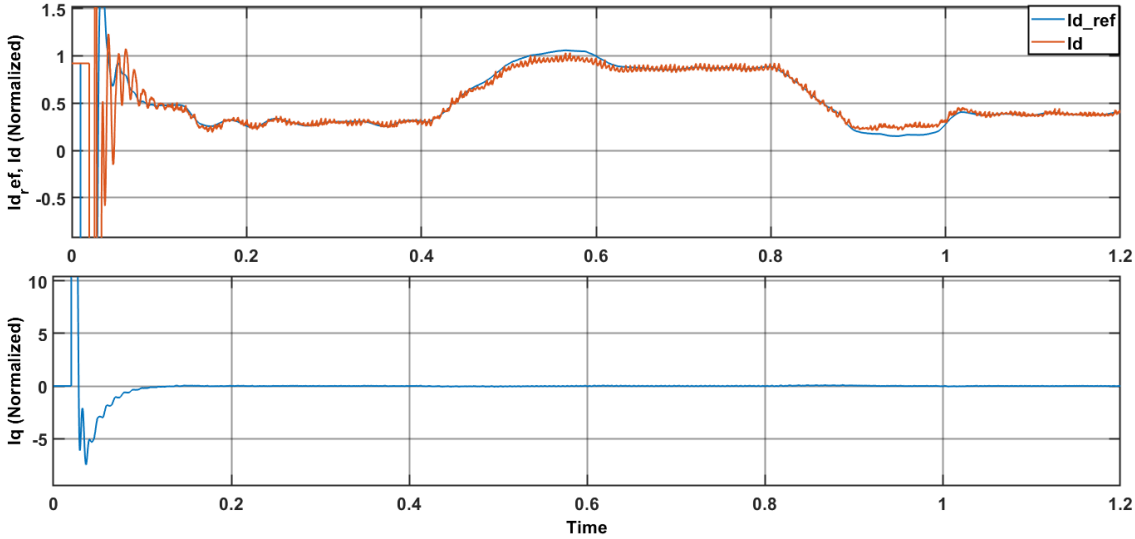

Figure 3.22: Plot of Id and Iq nominal currents

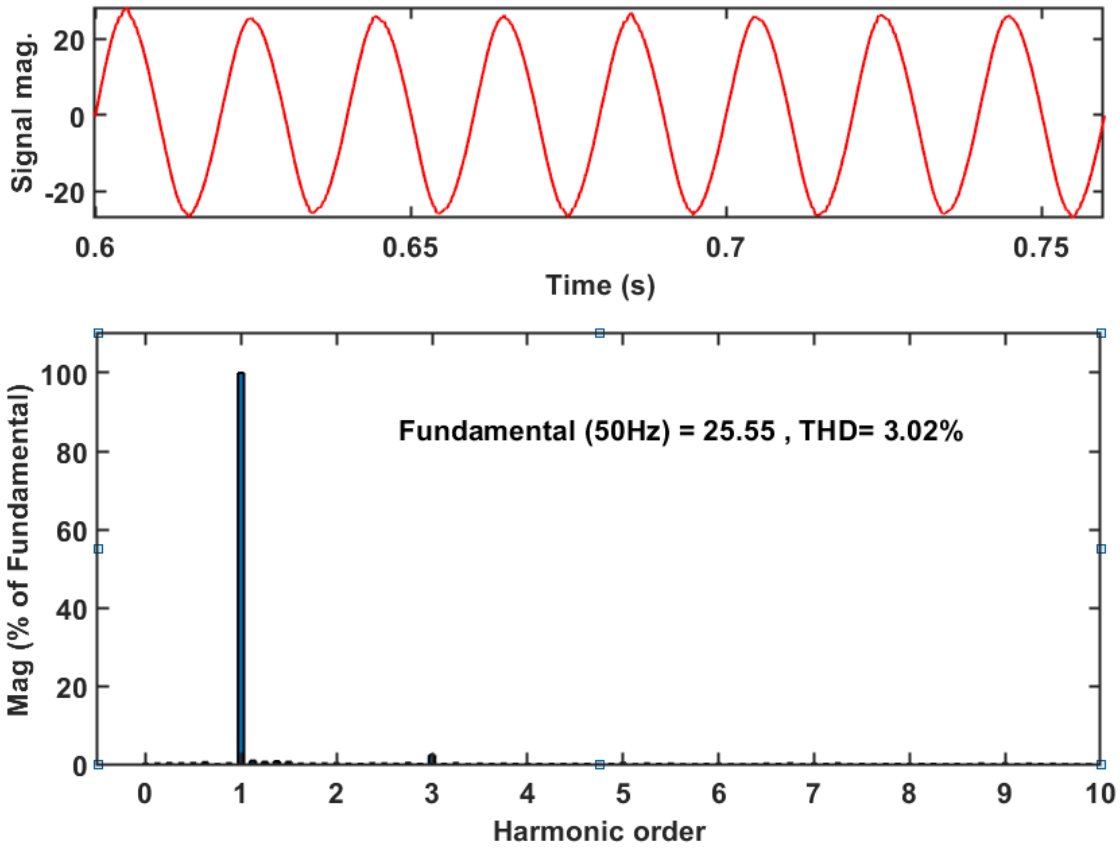

Figure 3.23: Grid current % THD (dq controller)

3.4.2 PR controller results

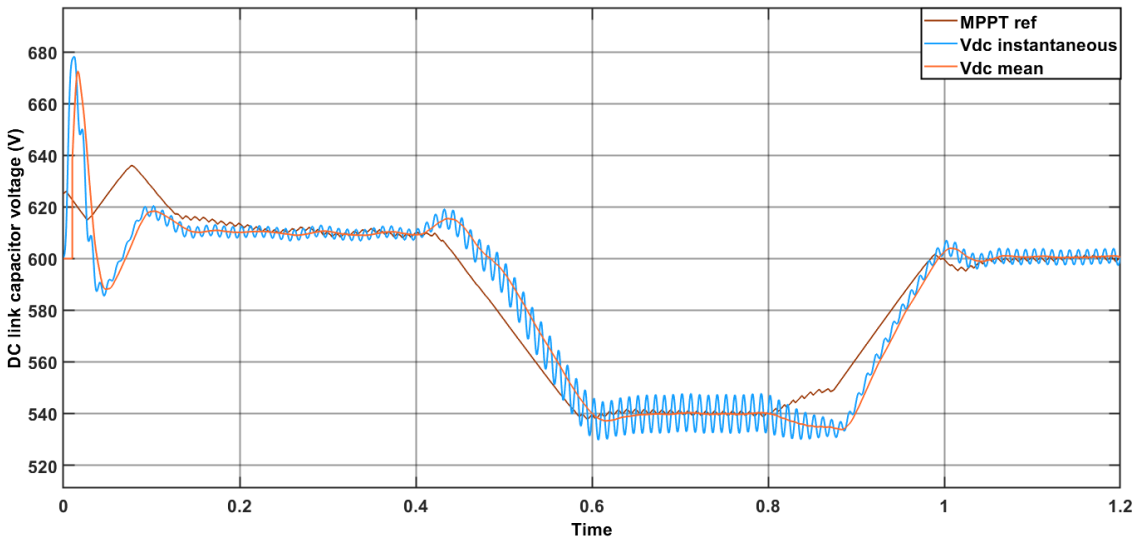

Figure 3.24: DC link capacitor voltage for PR controller

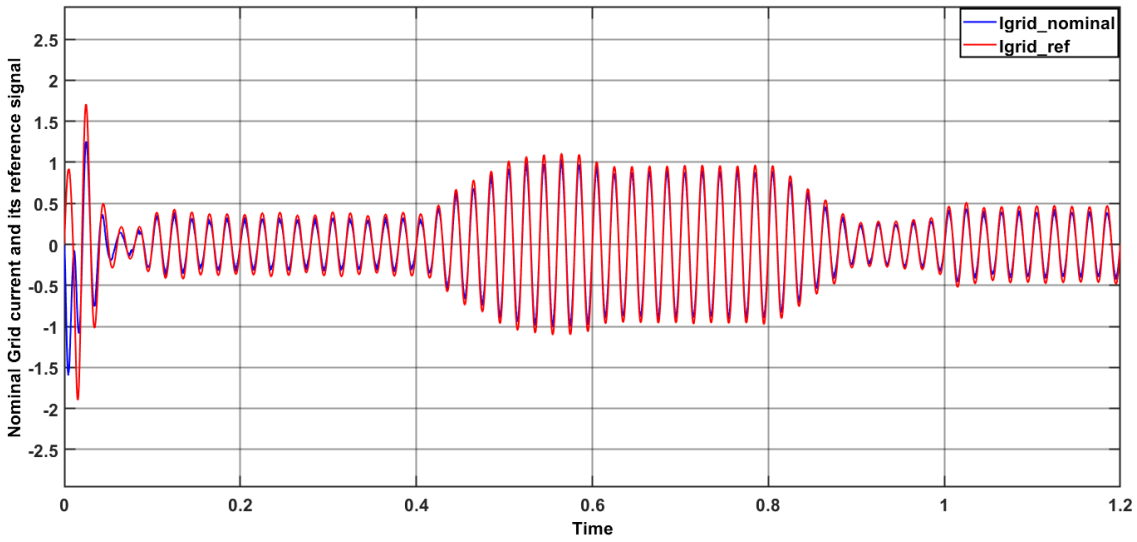

Figure 3.25: Nominal grid current and its reference signal in case of PR controller

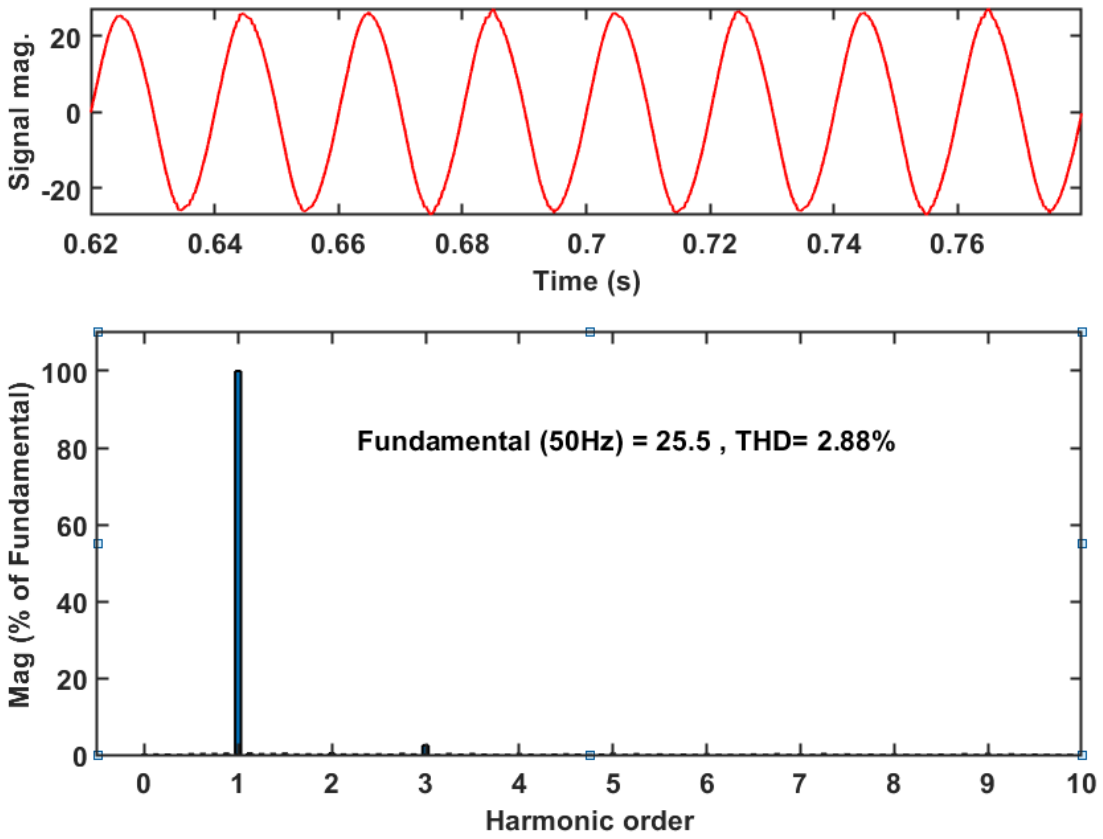

Figure 3.26: Grid current % THD (PR Controller)

3.5 Conclusion

To summarize this chapter it is necessary to comment on the results presented in the previous section. The graphs represents different aspect of the controller working. The comparison of the two controllers is shown in the table 3.1:

Parameters	**d-q controller**	**PR controller**
Initial Overshoot	High	Medium
Settling time	High	Medium
Computational complexity	Medium	Low
Grid current %THD	High (3.08%)	Medium (2.88%)

Table 3.1: Classical controllers performance

- The initial overshoot is very high in case of d-q controller. This is also the synchronization phase of the system. The PR controller performs better in the initial phase with peak value below 2 times that of the steady state nominal grid current. This is shown in the Fig. 3.25
- The DC link capacitor voltage gets stabilized much faster in the case of PR controller (Fig. 3.24) as opposed to the d-q controller (Fig. 3.21). It relates to the controller's settling time.
- The FFT analysis graphs are shown in the Fig. 3.23 and Fig. 3.26. The %THD due to the PR controller is less than the one due to the PI controller. However, the difference is not very large.
- Considering the computational complexity, the d-q controller requires more computation due to the needed conversion to synchronous reference frame. This is absent in case of PR controller. It is observed with the help of the time MATLAB takes to run the complete simulation.
- It is very reasonable to say that among the two conventional controllers, the PR controller provides better performance characteristics than the d-q controller.

Chapter 4

DESIGN OF MODERN CONTROLLERS

4.1 Overview

The Chapter discusses in detail regarding two modern control techniques. These methods are different from linear controllers described in the previous chapter in the sense that these are able to handle the non-linearity nature of the power converter and does not require any linearization stage. It begins with Section 2.2 which answers the question, "What is Fuzzy Logic" and what are its founding principle. The heart of the Fuzzy logic control (FLC) is Fuzzy inference process. It is explained in the subsection 2.2.4. The section ends with the implementation of simple FLC controller, simulated in MATLAB. The section 2.3 describes the concept of Model Predictive Control (MPC). Its basic principles, mathematical modeling and proposed controller are discussed in details. A comparison of the performances of the two controllers is made in section 2.4 from the simulation results obtained, and the chapter ends with a conclusion within section 2.5.

4.2 Fuzzy Logic Controller

4.2.1 What is Fuzzy Logic

This subsection is devoted to the the discussion of fuzzy logic controller for a single phase grid connected PV inverter, so as to address the non-linear and non-ideal nature of Photovoltaic (PV) system and power converter. To optimize the modulation index (MI) of the inverter and minimize the harmonic content in the inverter's output current, fuzzy algorithm ca be easily employed. The algorithm is simulated and analysed in the Simulink environment of MATLAB. The designed fuzzy controller will be validated with other current control methods based on its performance (i.e. response time, Output current THD, and sensitivity to disturbances).

One must first try to understand the word "Fuzzy logic" before going deeper into its concepts as it is has grown very much.

It can be defined in two different ways. In a layman's term, it is seen to be an extension of multi-valued logic. However, in technical terms it can be observed to be synonymous to fuzzy logic set. A theory in which sets does not have concrete boundaries and the relations between the sets is a matter of degree. In this light

of truth, a fuzzy logic is seen as a small part of fuzzy logic sets. And therefore, even in its narrowest understanding, it fundamentally differs from the mathematical concept of multi-valued logic [49].

The fuzzy logic therefore, is just a small portion of multi-valued logic, where the variable's truth value may range from 0 to 1 (inclusive). It is applicable in situations where there is no certainty about true or false. It is in s sense deals with partial truth conditions [50]. Oppose to that, Boolean logic can only take two values, namely true or false.

It can be also imagined that fuzzy logic mimics humans decision making capability. Humans doesn't always analyze in a binary way or with numeric data. Thus fuzzy models is a way of expressing partial and vague information in mathematics terms. These models of fuzzy set are capable of interpreting, recognizing and manipulating the data which is imprecise and lack certainty.[51]

4.2.2 Why Use Fuzzy Logic?

Following are the general features of the Fuzzy logic [49]:

- **simple to understand** : It is easy to understand the concept of the fuzzy theory. Also, the mathematics involved is not very complex to comprehend.
- **Provides flexibility**: It is not necessary to start from scratch, as it is flexible to addition of new functionality with least effort.
- **Imprecise data handling**: If one takes a closer look at the nature, it is full of imprecise data. Fuzzy logic is based on this imprecision, by processing it rather than leaving it as it is.
- **Complex non-linear functions can be modeled**: Any input-output data can be matched using fuzzy logic. Methods such as Adaptive Neuro-Fuzzy Inference Systems (ANFIS) makes this task much more simple.
- **Classical control techniques friendly**: Conventional controllers need not be replaced by the fuzzy systems. In fact, they can be augmented so as to simplify overall implementation.

4.2.3 Foundations of Fuzzy Logic

The basic concept of fuzzy logic involves mapping the input data set with output data set, and it is achieved by the if-then rule based system. The order in which rules are applied is not important and they all are checked simultaneously. The rules are independently important because they relate variables with their adjectives that describes them. Before starting interpretation of the corresponding rules, it is required to define all the necessary variables and adjectives. For example, to say water is hot, one must define the range of temperature change allowed and the meaning of the word hot.

In summary, the fuzzy inference process can be thought of to be a system which interprets input data set, and using defined set of rules, assigns values to output data set.

Fuzzy Sets

Fuzzy set theory is the starting concept of fuzzy logic. It is a set that comprises of blur boundaries and non-crisp values. It can have elements which do not have complete membership but only a partial degree of it.

To understand the basics of the fuzzy set, it is necessary to learn the classical set theory. An element can be either inside the set or outside it. For example, in the Fig. 4.1, a classical set of the weeks undoubtedly includes Monday, Saturday, and Thursday. At the same time, it unquestionably excludes the other elements such as liberty, Butter, etc.

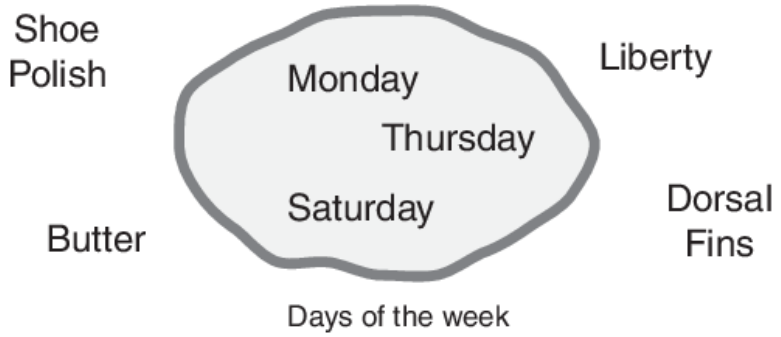

Figure 4.1: Example of a classical set [49]

This type of classification is termed as a classical set as it has been around for very long. The idea was first postulated by Aristotle (Exclude Middle), in which an element X must either be in set Y or set $Y^{'}$ (not Y). The law can be stated as follows:

"Of any subject, one thing must be either asserted or denied."

Restating the above stated law: "Of the subject (say Thursday), one thing (a day of the week) must either be assertive or denied (I assert that Thursday is a day of the week)" This law ascertain that everything should either fall into this set or the not set. It impossible for a day to be day of the week and not a day of the week at the same time.

For another example, let's consider days of the weekend. The fig. 4.2 shows one of the ways in which classification can be achieved.

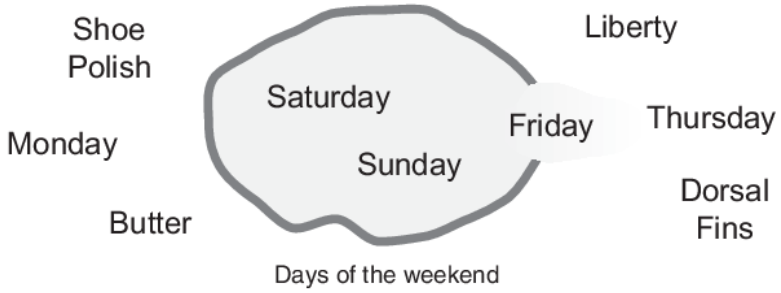

Figure 4.2: Example of a Fuzzy set [49]

It is obvious that Saturday and Sunday should be a part of this set, but what about Friday? It is those situations where one is not ascertain, as Friday is considered a partial weekend most of the time. Therefore, in the above fig. 4.2 Friday make

an attempt to stay at the boundary. This would have been technically wrong as far as classical set classification is considered. It should either stay inside the boundary or outside it. But this situation is close to human experience where such blur boundaries exist.

Membership Functions

The curve which maps the input data vector at each point with a membership value, which ranges from 0 to 1, is defined as the Membership Function (MF). The input vector space is technically called as "universe of discourse".

Let us consider a simple and most commonly referred example of tall people. The universe of discourse (input vector space) is taken to be the potential heights between the range of 3 feet to 9 feet, and the word tall refers to the curve that defines the degree to which any person is tall. If for case, we consider the classical sets and define that a person is tall if his height is greater than 6 feet, and not tall otherwise. This is an absurd way of classification as height cannot be demarcated at 6 feet. This is because in real life situations, it is unreasonable to classify a person short and other person as tall when their height differs not more than width of a hair.

If the above mentioned way is kind of illogical, then what is a better way to do the classification? This can be handled similarly, like the case of weekend. The output value on the right hand sight (μ) is known as the membership value. This curve is termed as membership function and usually denoted by the symbol μ. Such smooth transition classify people not only into short and tall people, but also into other categories such as not so tall, not so short, neither short nor tall, etc.

Logical Operations

Now that we have understood the membership functions, then lets see how it connects with the logical operations of Fuzzy inference.

As it is evident that fuzzy logic set is a super set of Boolean logic set. In short, if we keep the fuzzy values at their extreme points, that is either 1 (complete truth) or 0 (complete false), then standard Boolean operation would hold. As an example, let the Boolean logical operation (AND, OR, and NOT) be shown in the fig. 4.3.

A	B	A and B
0	0	0
0	1	0
1	0	0
1	1	1

AND

A	B	A or B
0	0	0
0	1	1
1	0	1
1	1	1

OR

A	not A
0	1
1	0

NOT

Figure 4.3: Truth Table of Boolean logical operators

Now, can these logical operation table be altered in case of fuzzy set?, as truth is a matter of degree as per Fuzzy reasoning. The input vector space range is the same, that is between 0 and 1. The question is that which operator preserves the

result of AND operation as well as extend to all other real numbers between 0 and 1.

The solution for AND operation is the minimum operator. This is to say that, for input A and B, the AND operation can be obtained by using the function min(A,B). Similarly for the case of OR operation, it is the max(A,B) operator that is used. At last, the NOT A is transformed into the operation (1-A).

If-Then Rules

Like in English grammar there are subject and verb, similarly logical operators and fuzzy set are verb and subject of fuzzy logic reasoning. Therefore the if-then rules are the conditional statement used in decision making.

Suppose a single rule is given by "if x is A, then y is B". Here A and B are the adjectives describing the variable x and y (universe of discourse). The rule presented is divided into two parts. The "if x is A" part is known as antecedent or premise, whereas the second part, "then y is B" is known as consequent or conclusion. An example is discussed in the following paragraph.

"If service is good then tip is average"

There is a value assigned to the word "good", which varies from 0 to 1, and so antecedent is a number expressing the word good. On the other hand, "average" is described as a fuzzy set, and the conclusion is a process that assigns the entire fuzzy set B to output variable y. Therefore, the meaning of the whole rule changes if the antecedent and consequent are interchanged. In programming terminology, this difference is analogous to relational operator "==" and assignment operator "=". Thus following line can be programmed as a fuzzy rule

"If service == good, then tip = average"

4.2.4 Fuzzy Inference system

The process of mapping the input vector space to that of output vector space by using Fuzzy Logic is termed as Fuzzy inference. Such a mapping provides the base for formulating the if-then rules and thereby take decision. All of the above pieces discussed such as Membership functions, Logical operations, and if-then rules forms the essential part of Fuzzy inference process.

Some characteristics of the Fuzzy inference system (FIS) are as follows:-

- The output of FIS is always a fuzzy set, irrespective whether input is crisp or fuzzy.
- When it is used as a controller, then it becomes essential to have output as fuzzy set.
- Ultimately the output fuzzy value from FIS is converter to crisp variables using Defuzzification.

FIS Functional Block diagram

Construction of the FIS can be easily understood by the five functional blocks. They are shown in the Fig. 4.4. They are described as follows [52]:-

- Rule Base: IF-THEN rules are contained in it.
- Database: Membership functions are defined upon which the rules apply.
- Decision making Unit: Rules operation is performed.
- Fuzzification : Conversion of Crisp values into Fuzzy values.
- Defuzzification : Conversion of Fuzzy values into crisp values.

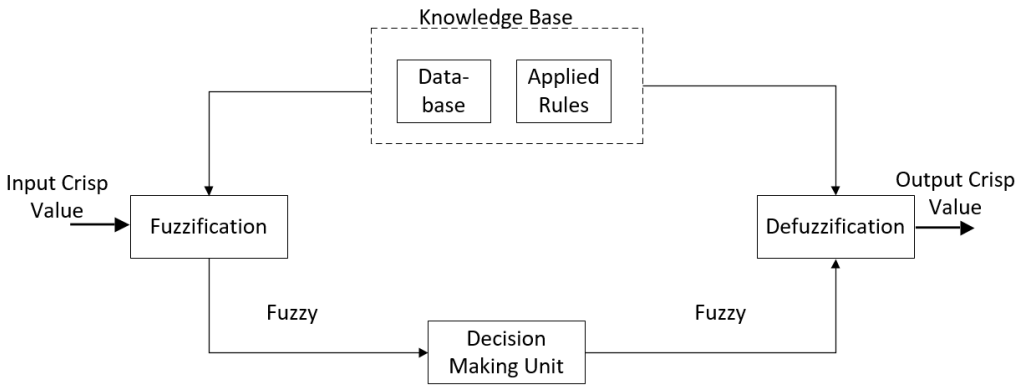

Figure 4.4: block diagram of fuzzy interference system

Types of FIS

FIS can be broadly divided into methods. They have different conclusion of fuzzy rules:-

1. Mamdani Fuzzy Inference System
2. Takagi-Sugeno Fuzzy Model (TS Method)

Mamdani Fuzzy Model

Ebhasim Mamdani proposed this model in the year 1975. It was actually formulated for steam engine and boiler combination by producing the fuzzy set rules obtained from the people working on the train system.

FIS output can be computed by following the steps given in [52]. They are:-

- **Step 1** - Determine the fuzzy rule set.
- **Step 2** - Input variable is made fuzzy by using membership functions.
- **Step 3** - Rule strength is established by combining the fuzzified input in accordance to fuzzy rules .

- **Step 4** - Combine rule strength and output membership function to determine conclusion of rule.
- **Step 5** - All consequents ar combined to get output distribution.
- **Step 6** - A defuzzified output distribution is achieved.

4.2.5 Proposed Fuzzy control strategy

There is need to control output current of the PV inverter due to power fluctuations on the input side. This issue can be easily solved by using an inverter current control using fuzzy logic controller (FLC). This section deal with designing such a control system by deciding proper input variables, membership functions, and output variables. The architecture of FLC have two inputs in discrete times, that is the error signal (e(k)), and rate of change of error (de(k)/dt). The fuzzy control output variable is denoted by u(k). An error is calculated by subtracting measured current from the reference current . The inverter output current is the output control variable. In steady state operation, the output current and the desired current should be as close as possible.

Rule-Based Fuzzy Decision

In this project, a single output and double input is considered to construct the overall structure. The input and output variable are normalized between the values -1 and +1, and this is done due to the AC signals present in the system. For all variables, there are five triangular and two trapezoidal membership functions, as shown in the Fig. 4.5. The seven fuzzy sets are Positive Big (PB), Positve Medium (PM), Positive Small (PS), Zero (ZE), Negative Small (NS), Negative Medium (NM), and Negative Big (NB), assigned for all the three variables [53][54].

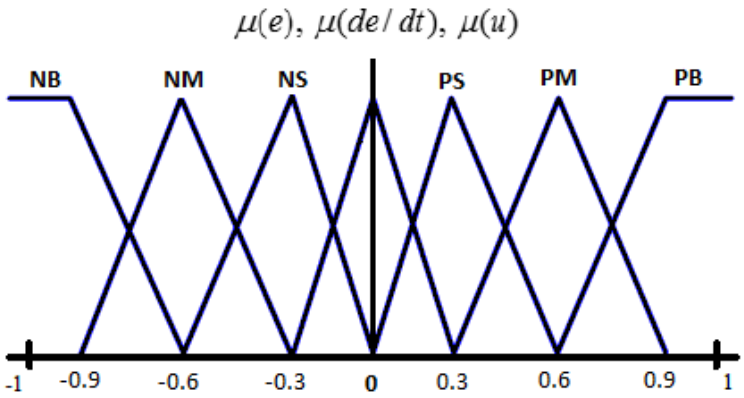

Figure 4.5: Membership function for both the input variables and output variable

For each input variable, there can be 49 rules applied due to presence of seven membership functions (Fuzzy sets). For an easy design, the rules have been presented in a tabular form given in Table 4.1

Error/change in error	PB	PM	PS	ZE	NS	NM	NB
PB	PB	PB	PM	PM	PS	PS	ZE
PM	PB	PM	PM	PS	PS	ZE	NS
PS	PM	PM	PS	PS	ZE	NS	NS
ZE	PM	PS	PS	ZE	NS	NS	NM
NS	PS	PS	ZE	NS	NS	NM	NM
NM	PS	ZE	NS	NS	NM	NM	NB
NB	ZE	NS	NS	NM	NM	NB	NB

Table 4.1: Rules of the proposed FLC system

The above fuzzy rules dictates the decision of the controller. Following are the rules generated as per the table 4.1:

Rule 1: IF error is PB AND Δ error is PB THEN Δu is PB

Rule 2: IF error is PM AND Δ error is PB THEN Δu is PB

Rule 3: IF error is PS AND Δ error is PB THEN Δu is PM

.

.

.

Rule 49: IF error is NB AND Δ error is NB THEN Δu is NB

The 49 rules are manually written in the fuzzy rules editor one by one. The discrete time output of the fuzzy controller $u(k+1)T_s$ varies in accordance with T_s till it reaches the desired output and stabilizes there. The expression is shown in (4.1) [55].

$$u(k+1)T_s = u(kT_s) + \Delta u(kT_s) \tag{4.1}$$

where $\Delta u(kT_s)$ represents the present step value of the output variable at time $t = kT_s$ and k represents an integer value 0, 1, 2, 3,.....

At the final stage, a Defuzzification process is applied to obtain crisp output (non fuzzy output) from the FLC output fuzzy set [56]. It converts the numerical data from the fuzzy controller into a usable variable which is able to drive the control signals. There are many method but most popular method of Defuzzification is by using Center of Gravity (COG) method. The COG of the aggregate output membership function is performed using the eqn. (4.2) [57]. It basically calculates the balance point in the fuzzy output region [55].

$$COG = \frac{\sum_k \mu_k(u_k) \times u_k}{\sum_k \mu_k u_k} \tag{4.2}$$

where u_k denotes the output fuzzy value, whereas $\mu_k(u_k)$ denotes the output membership function value. The simulated Fuzzy controller is shown in the Fig. 4.6

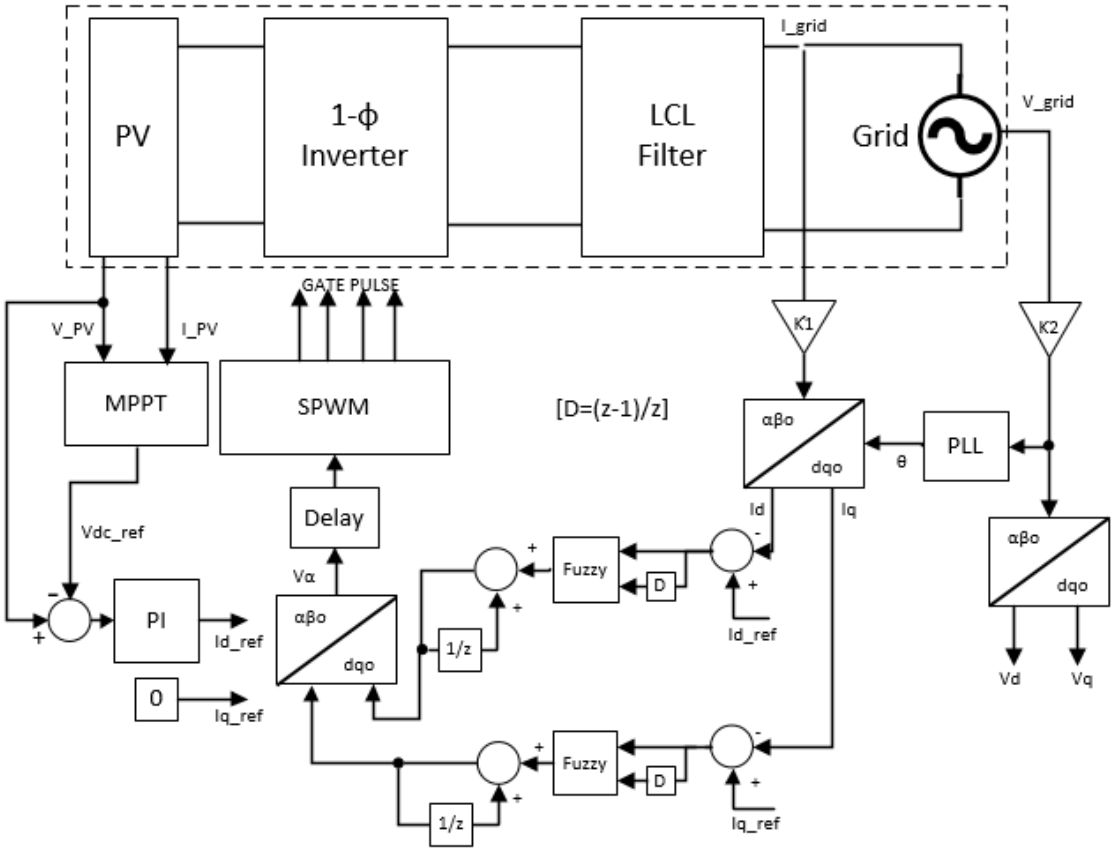

Figure 4.6: Block diagram of the Proposed Fuzzy controller for inverter current control

4.3 Model Predictive Control

4.3.1 Predictive Control types for Power Converters

Basically predictive control contains a wide variety of controllers and it has only recently found its applications in power electronics converters. Fig. 4.7 depicts the classification of different predictive control methods present in the literature [20].

The optimization function required for a hysteresis type predictive control method is to keep the controlled variable withing the hysteresis band [58], whereas in trajectory predictive control, the variable is forced to follow a predefined path [59]. The control in a deadbeat predictive method tries to make the error zero in the next sampling time itself [60]. The model predictive control however uses a more flexible criteria known as cost function, used to minimize the error [61].

One fairly common advantage of predictive control method lies in the absence of a cascaded structure, quite common in linear controller. This increases the transient response of the control system. Speed control of motor using trajectory based predictive control is one such example shown in [58].

There is no need to linearize the given system, as model predictive can handle non-linear nature. This is because it models the converter in state space, thus it is stable for a wide range of conditions. In addition to that, there can be constraints put on some variables in the optimization criteria. These merits are more pronounced

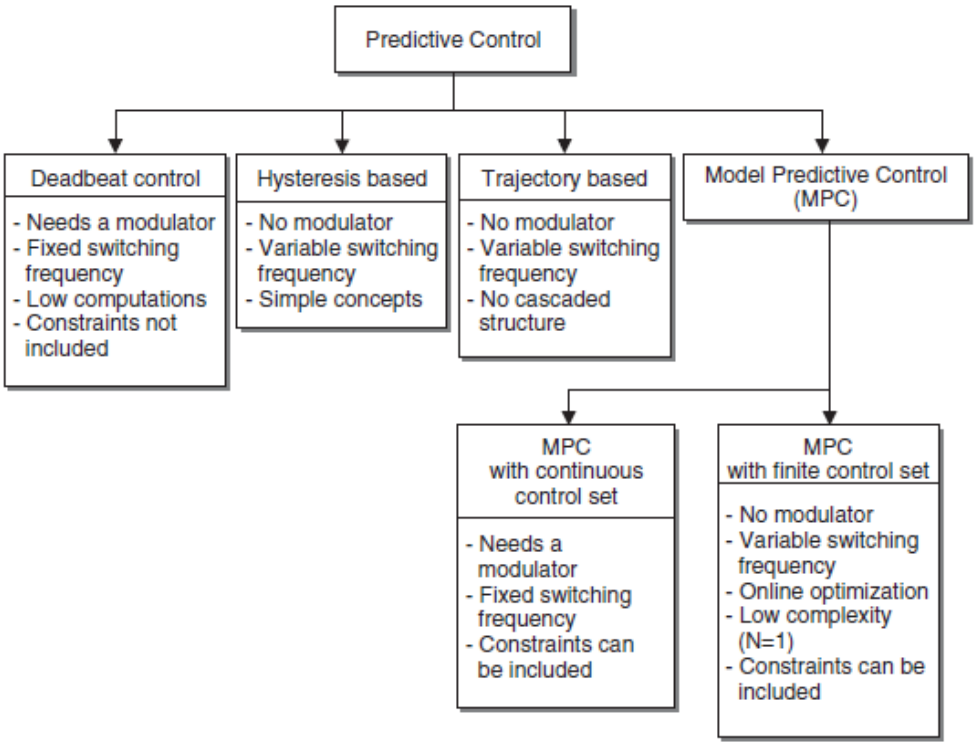

Figure 4.7: Predictive control method classification in Power converters [20]

in case of MPC, rather than the deadbeat controller, where it is not so explicitly controlled.

4.3.2 MPC working principle

MPC is among the top of the advance control techniques used in the industrial process today, advanced as in better than the standard PID controllers. The idea of MPC technique as an optimal control theory was developed way in the 1960s, but it got the attention of the industry a decade later in 1970s. Since then, MPC has been applied in the chemical process industry as the time constant are very large in such process and all calculation cal easily be performed. The entry of MPC in the field of power electronics took place in 1980s, in power system converters with low switching frequency [58]. It could not be used in high switching frequency applications due to high calculation required per cycle. This limitation has been eliminated with the advent of advanced micro-controllers and microprocessors with very high operating frequency.

MPC undertakes many controller strategies, not just one or two . The common Sequence of Operation (SOP) consists of modeling of the system, using the model to predict the future value of the controlled variable until a predefined horizon in time, choosing the most optimal solution of the cost function. Such a SOP has many merits. They are:

- Easy and intuitive concepts.
- Many systems can apply this concept.
- can easily handle multi-variable objective function.

- Compensation of the dead time can be incorporated.

To mention some of the disadvantages, MPC requires a rather large number of calculations than classic controllers. The model of the system also affects the design, and if parameters of the system changes with time, then some adaptive or intelligent algorithms are required to compensate changed parameter. In short, the basic idea of MPC are as follows:

- Use state space model to predict the future value of the controlled variable until a horizon in time.
- An optimization criteria in the form of cost function is defined.
- The optima value is obtained by minimizing the cost function.

To model the system in a micro-controller, a discrete time model of the system is required. The state space model is given by eqn. (4.3) (4.4):

$$x(k+1) = Ax(k) + Bu(k) \tag{4.3}$$

$$y(k) = Cx(k) + Du(k) \tag{4.4}$$

A cost function representing the desired condition is to be defined. It considers all three quantities namely, reference signal, future value, and future control signal [62]:

$$J = f(x(k), u(k), ..., u(k+N)) \tag{4.5}$$

Therefore, MPC consists of an optimization problem with cost function, which is to be minimized at each interval, for a horizon time of N, owing to system model and other system restrictions. This results into sequence of N optimal solutions, and the controller applies only the first element in this sequence

$$u(k) = [1\,0.....0]argmin_u J \tag{4.6}$$

Where the problem is solved at each sampling step, using the new reference and future value, and finding the new sequence of solution. Receding horizon strategy is termed for such design method.

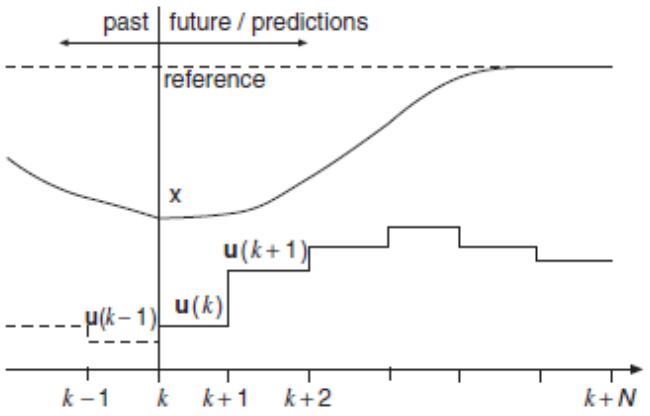

Figure 4.8: MPC working diagram [63]

The basic working principle of the MPC is shown in Fig. 4.8. The future value of the control state is found out for the horizon in time (k+N), using the state space model and information measured till time k. Thereafter, the sequence of optimal solution is calculated by minimization of the cost function, and the first element of the sequence is chosen. A general schematic for MPC is shown in Fig. 4.9, which is used in power electronic converters and drives as in [62].

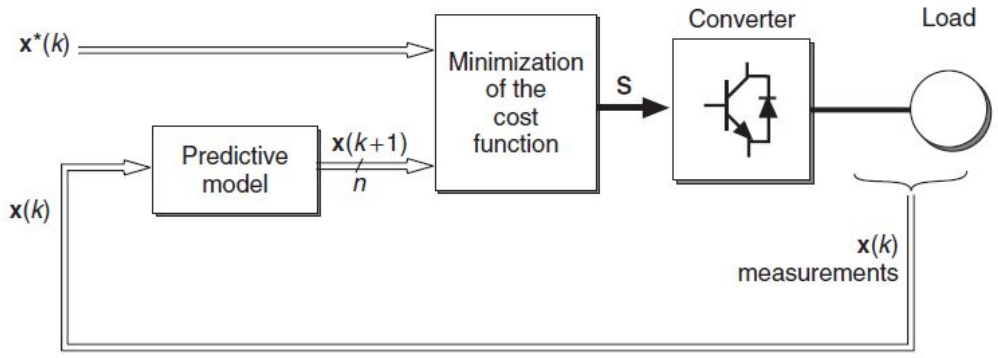

Figure 4.9: General MPC scheme for power converters [63]

4.3.3 Current control using MPC

The control strategy employed is based on the fact that power converters have finite states, and that the system model can be used to predict the the future behavior of the controlled variable for each sampling state. A selection criteria is required to select the desired switching state at that sampling time. The cost function is the criterion that is evaluated to get the predicted value of the controlled variable. Prediction of the future value is calculated for each switching state, and which ever makes the cost function minimum is the required switching state in that time instant.

It is summarized into following points [20]:

- A cost function 'g' is defined.
- Form the state space model of the system and its total finite switching states.
- Select the optimum state using cost function for prediction of current.

Cost Function

The difference between reference current and measured current represents the optimization criteria of the controller. It is mathematically termed as Cost Function. It is represented as shown in (4.7), that is the error between reference current and predictive value of the measured current:

$$g = |i^*(k) - i(k+1)| \tag{4.7}$$

Where i is the predicted inverter output current, for a given voltage vector. The predicted value is found out from the state space model of the converter. The i^* denotes the reference current from the outer voltage loop. For simple calculation, an assumption is made that the reference current remains the same in one sampling

interval, i.e. $i^*(k+1) = i^*(k)$. If a high sampling frequency is considered, then this one sample delay does not introduce much error.

Model of single phase inverter

For an H-bridge single phase inverter, with four switches, as in Fig. 2.1. It is known that the two switches in a leg operates in a complimentary fashion, so as to avoid short circuit. The switching states of the two legs can be described by (4.8) and (4.9) [61]:

$$S_a = \begin{cases} 1, & \text{if } S_1 \text{ is ON and } S_4 \text{ is OFF.} \\ 0, & \text{if } S_4 \text{ is ON and } S_1 \text{ is OFF.} \end{cases} \tag{4.8}$$

$$S_b = \begin{cases} 1, & \text{if } S_3 \text{ is ON and } S_2 \text{ is OFF.} \\ 0, & \text{if } S_2 \text{ is ON and } S_3 \text{ is OFF.} \end{cases} \tag{4.9}$$

The switching state decides the output voltage vector. Such as

$$v_{an} = S_a(V_{dc}) \tag{4.10}$$

$$v_{bn} = S_b(V_{dc}) \tag{4.11}$$

Where V_{dc} represents the DC link voltage. The output voltage is therefore,

$$v = V_{dc}S \tag{4.12}$$

The S is a vector given by (4.13)

$$S = 1.(S_a + aS_b) \tag{4.13}$$

where, $a = e^{j\pi} = -1$;

Value	Process
1.	The reference current $i^*(k)$ is measured from the outer voltage loop and the inverter output current $i(k)$ is measured.
2.	The inverter current is predicted for the next interval $i(k+1)$ using the state space model of the converter
3.	The error between reference current and predicted current in the next interval is evaluated in the cost function G
4.	The switching state that minimizes the cost function value is selected and corresponding voltage is generated.

Table 4.2: MPC algorithm for current control

Considering the gating possibilities of the single phase inverter, four voltage vectors can be generated, as presented in the Table 4.3. Out of these, two voltage vectors corresponds to zero vector.

It is important to note that a complex model can also be formulated, if high switching frequency is taken into account. For example, dead time, IGBT saturation voltage, and diode forward voltage drop can also be included at high frequency

model. But, a simple model of the single phase inverter is emphasized in this thesis, to highlight the fact that a simple MPC controller is still a better control system than a classical controller [64].

S_a	S_b	vector v
0	0	0
0	1	-V_{dc}
1	1	0
1	0	+V_{dc}

Table 4.3: H-bridge inverter switching states

Discrete time model conversion

Taking into account the Equivalent Series Resistance (ESR) of the filter inductance, the inverter output voltage can written in the form, as shown in (4.14). [65]

$$v = e + R_1 L_1 + L_1 \frac{di_1}{dt} + R_2 L_2 + L_2 \frac{di_2}{dt} \tag{4.14}$$

Where, v denotes the inverter output voltage vector; e is the grid voltage; L_1 and L_2 are the LCL filter inductances, whereas R_1 and R_2 are corresponding ESR of the inductances, respectively.

The equation (4.14) is transformed into discrete time domain model with sampling time T_s. This model is used to predict the inverter output current value, by using the voltages and currents at the k^{th} instant. There are good number of methods to convert a continuous equation into a discrete form. Due to the simple first order differential equation, a simple approximation of the derivative can be used to discretized the above equation. However, a more precise conversion is required for system involving higher order differential equations, as the error introduced by this approximation increases significantly.

The inverter output current derivative ($\frac{di}{dt}$) is approximated using forward Euler method. It is depicted in (4.15) from [20]:

$$\frac{di}{dt} \approx \left\{ \frac{i(k+1) - i(k)}{T_s} \right\} \tag{4.15}$$

Equation (4.15) is substituted in (4.14) to obtain the discrete time state space model to calculate the future value of inverter current, for each of the two voltage vectors $v(k)$ at each interval. There after, it is expressed as

$$i(k+1) = (1 - \frac{(R_1 + R_2)T_s}{(L_1 + L_2)})i(k) + \frac{T_s}{(L_1 + L_2)}(v(k) - e(k)) \tag{4.16}$$

where, $e(k)$ is the grid voltage vector.

Equation (4.16) is evaluated for four states, giving three predicted value. The predicted value which is closer to the reference current value is chosen, and in the next sampling time, the corresponding voltage vector is applied. It means that the predicted valued which gives the minimum value of the quality function is the one selected to be applied to the switches.

The MPC method can be designed using the flowchart shown in the Fig. 4.11. As presented in the program flowchart, the switching state corresponding to the predicted output current is selected based on which of them minimizes the cost function for that interval [65].

4.3.4 Proposed MPC Strategy

Figure 4.10 represents the block diagram of the overall control system. The outer voltage loop is controlled by a PI controller which produces the current reference signal. The reference current is converted to sinusoidal signal by synchronizing it with grid voltage via Phase Locked Loop (PLL). The gains K_1 and K_2 are used to normalize the grid voltage and inverter current to unity.

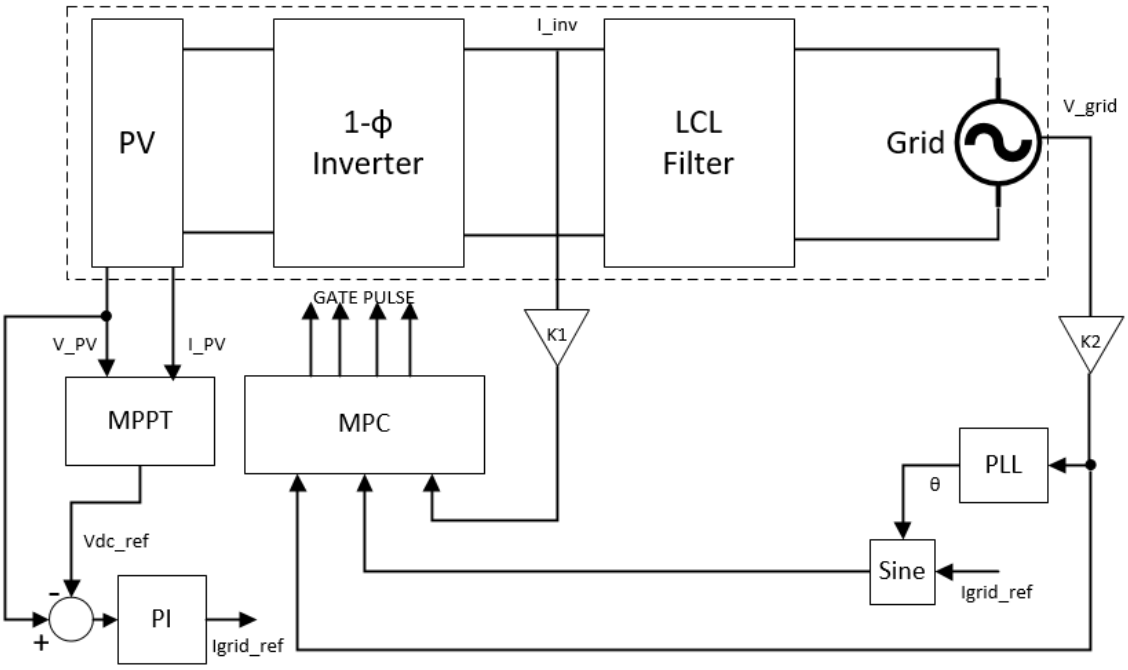

Figure 4.10: Block diagram of the proposed MPC current controller

All the three state variable i_1, i_2, and v_c needs to be controlled in a traditional MPC control system. But the proposed method only sense the inverter output current as shown in the Fig. 4.10. The grid side current reference is generated by the outer voltage loop. That same reference is supplied to the MPC block. This is because the filter capacitance is neglected and both inverter output current and grid current are assumed to be equal [66].

The program flow chart for the proposed model predictive control method is shown in the Fig. **??**. As presented in the program flowchart, the switching state corresponding to the predicted output current is selected based on which of them minimizes the cost function for that interval.

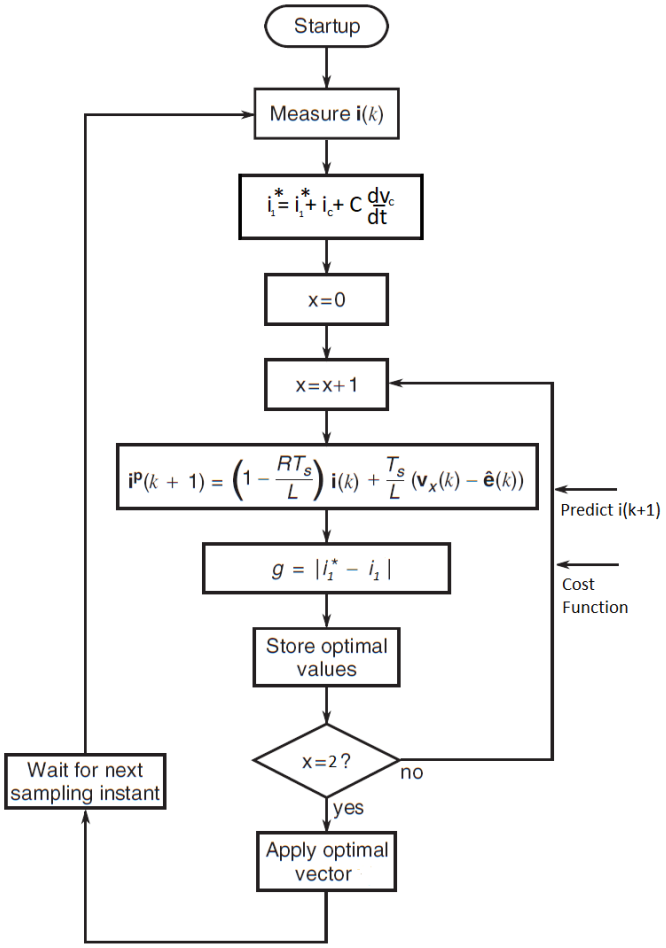

Figure 4.11: MPC program flowchart

Instead of using the three reference and three sensor signal, there is a simple way to track the grid current. The design of MPC controller for an inverter with LCL filter is fairly complex due to the presence of three state variables (i_{L1}, i_{L2}, and v_C) [62]. The proposed control scheme neglects the filter capacitance and the design develops into that of the system with only L filter. The two inductor currents are also assumed to be same and thus obtaining only one state variable, namely i_L. The error introduced is fairly low as compared to the computation reduction, and therefore implementing it becomes simple.

4.4 Simulation Results

The simulation settings is same as that in the previous chapter. It is once again written for easy reference. It is again shown by the fig. 4.12.

1. Initially the irradiance is $300W/m^2$ and the temperature is set to 25 ℃.
2. At 0.4 second, the irradiance is increased to $1000W/m^2$, and temperature is increased to 55 ℃.
3. Lastly, at 0.8 second, the irradiance is reduced to $400W/m^2$, and the temperature is reduced to 30 ℃

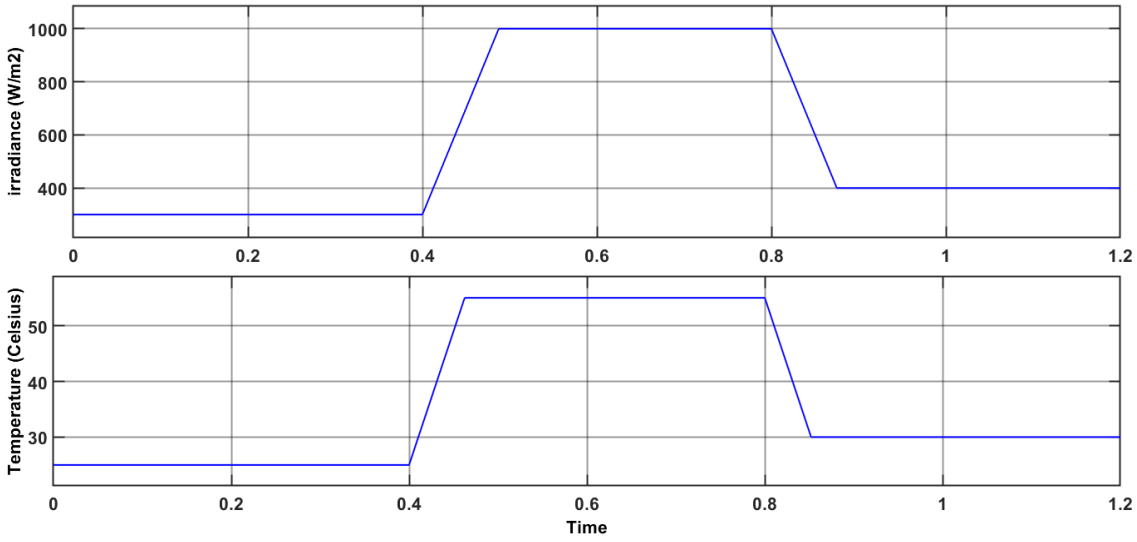

Figure 4.12: Irradiance and temperature change for the give simulation

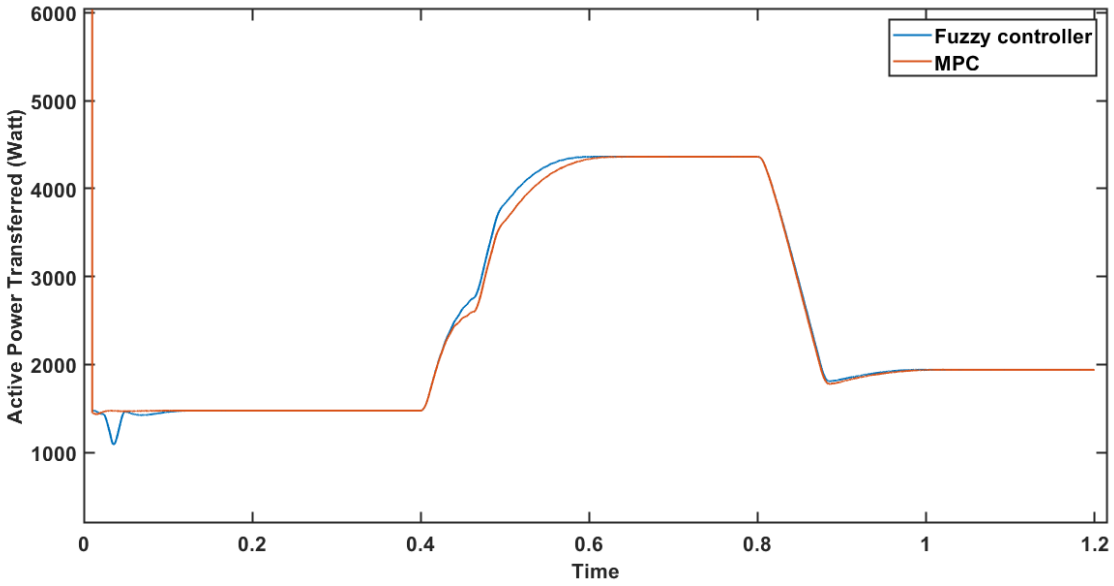

Figure 4.13: MPPT plot for FLC and MPC

4.4.1 Fuzzy Logic Controller

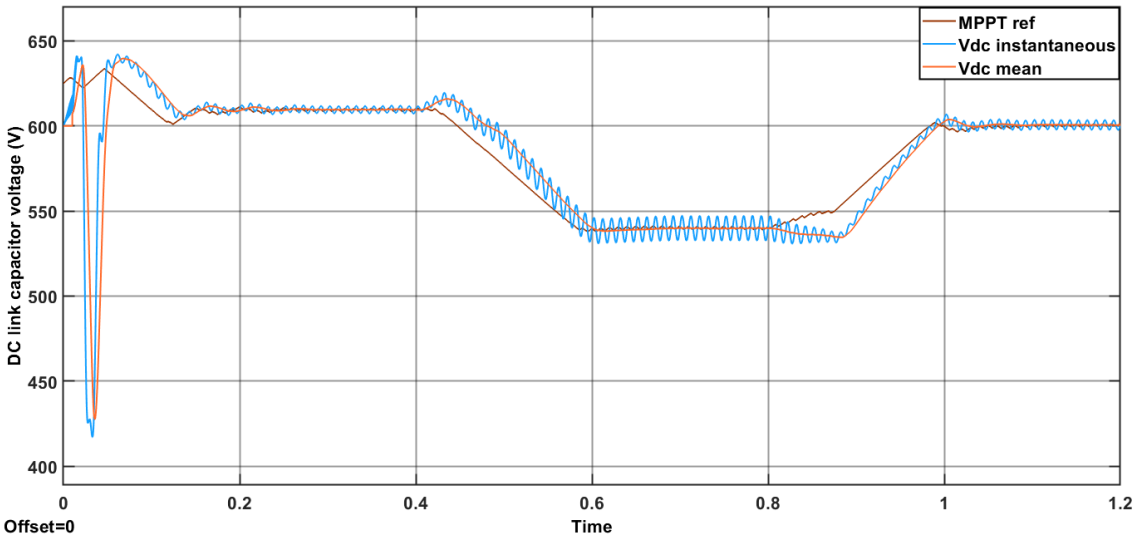

Figure 4.14: DC link capacitor voltage variation (FLC)

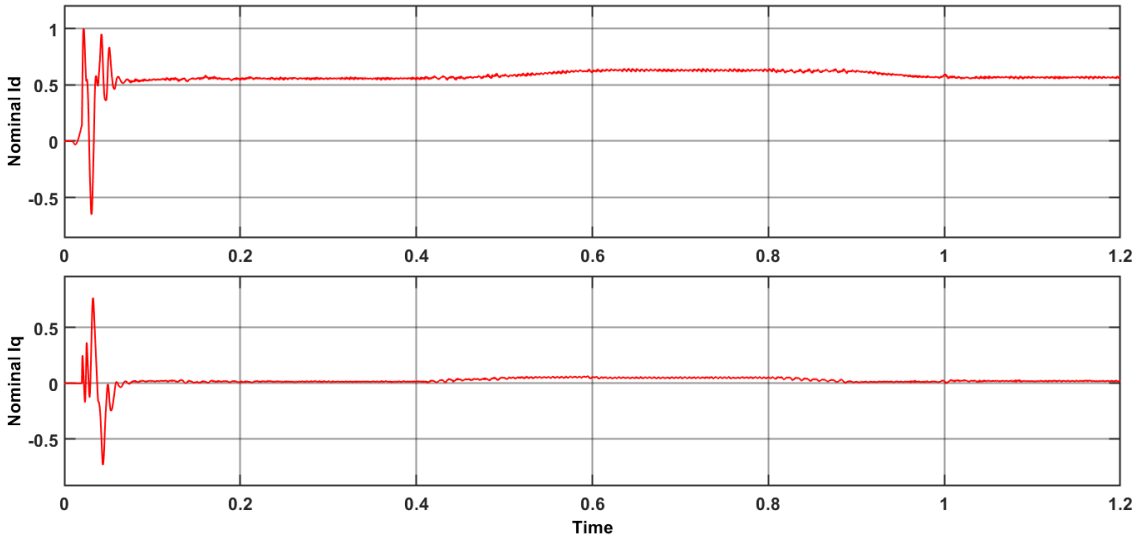

Figure 4.15: Id and Iq nominal values

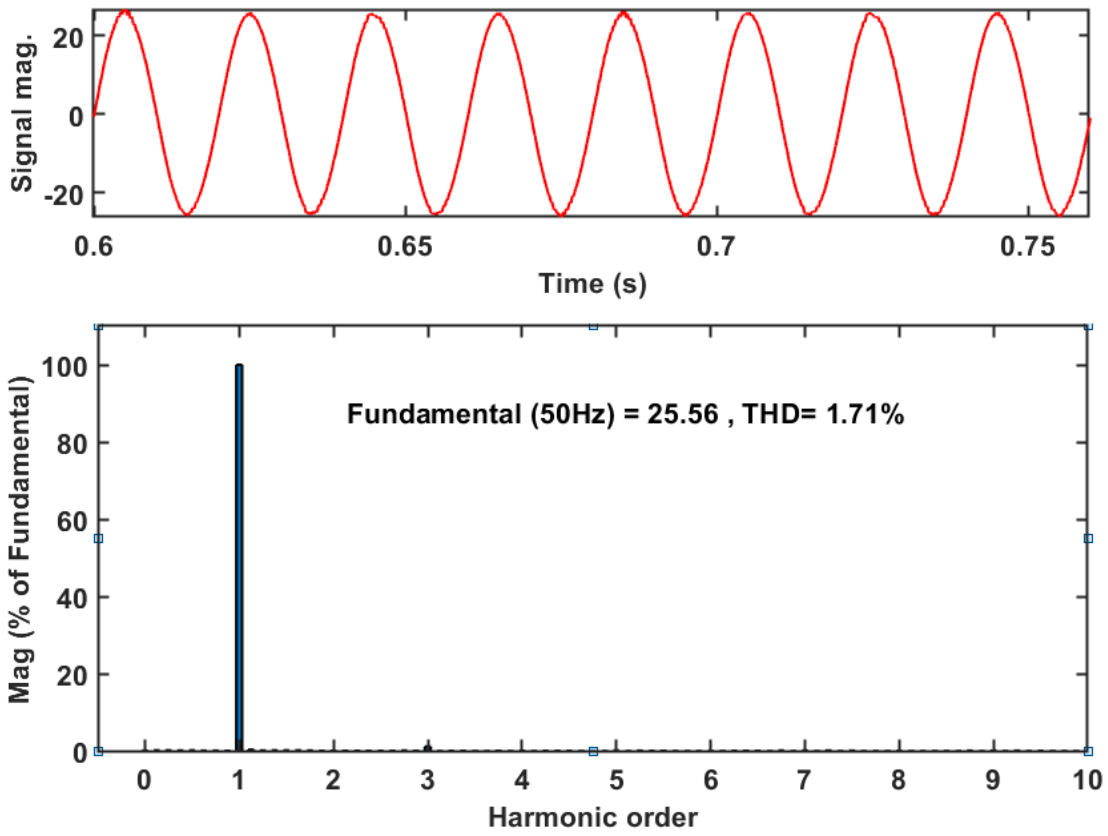

Figure 4.16: Grid current % THD (FLC)

4.4.2 Model Predictive Controller

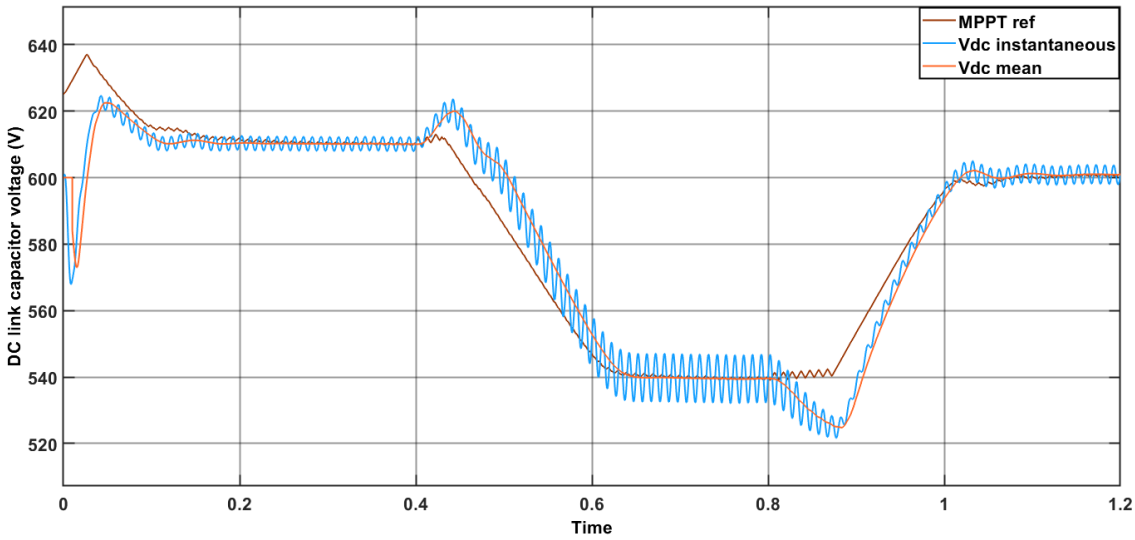

Figure 4.17: DC link capacitor voltage variations (MPC)

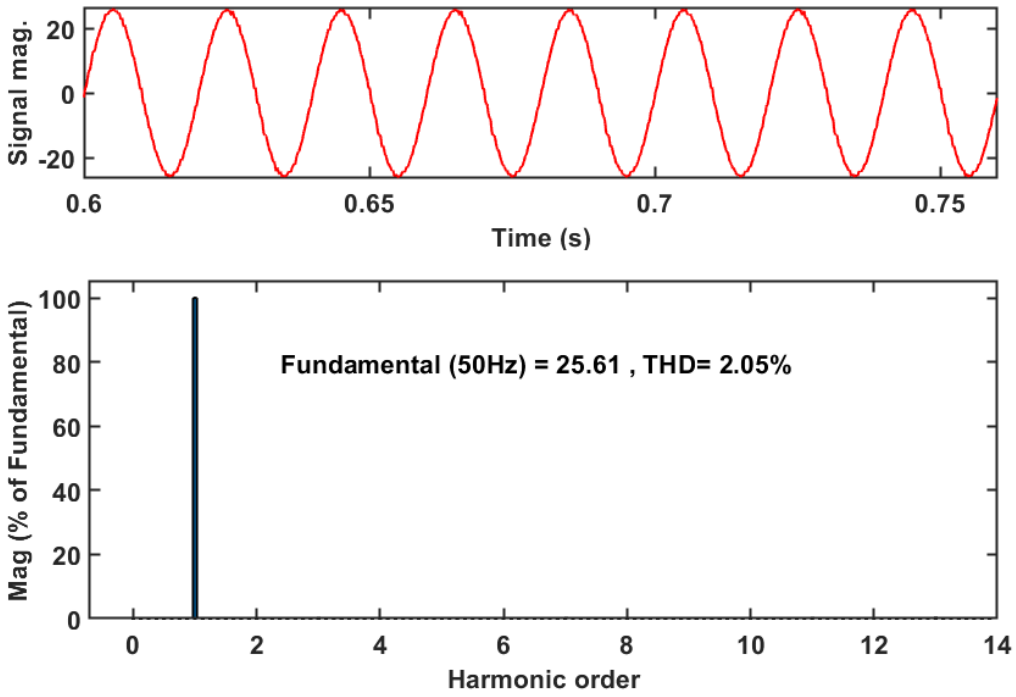

Figure 4.18: Grid current Total Harmonic Distortion (%THD)

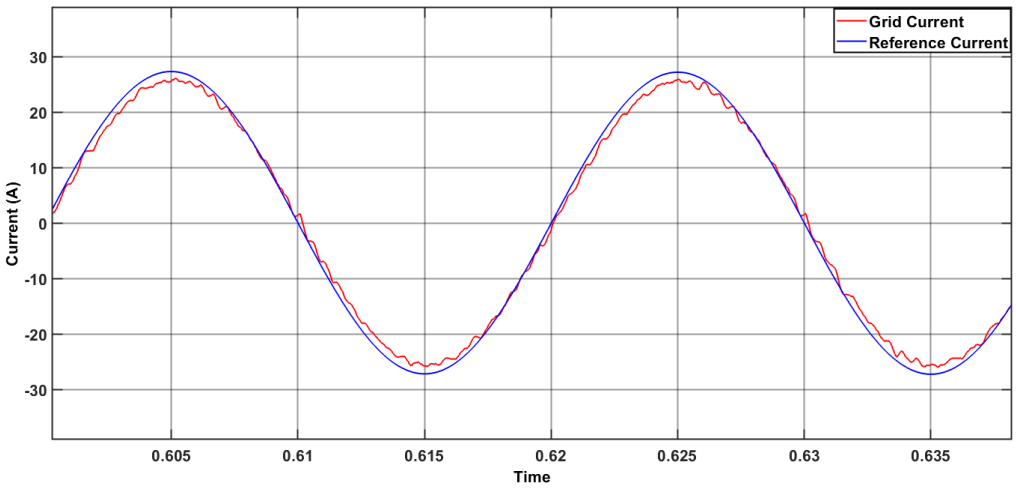

Figure 4.19: Plot of reference current and grid current

4.5 Conclusion

The results shows that both the controllers are stable for all the applied disturbances. There are few observations that can be drawn from the resultant graphs. These difference are tabulated in the below table 4.4:-

Parameters	**Fuzzy controller**	**MPC controller**
Initial Overshoot	High	low
Settling time	low	Medium
Computational complexity	High	low
Grid current %THD	low (1.71%)	Medium (2.05%)

Table 4.4: Modern controllers performance

- The initial response of MPC is better than the FLC. The overshoot is very negligible in case of model predictive controller.Whereas there is a huge dip initially in case of FLC
- From the DC link capacitor voltage graphs(Fig. 4.14 and Fig. 4.17), the settling time of the FLC is less than the MPC.
- The computational power required by FLC is very high, compared to the MPC. This is observed by recording the time it takes to run the simulation. For each sample, the fuzzy needs to check 49 rules simultaneously. Therefore it takes a lot of processing power.
- The %THD of the grid current is lower than 5% in both cases, but it is minimum for the FLC (1.71%)
- Out of the two discussed modern current controllers, FLC provides better performance qualities than its counterpart.

Chapter 5

HARDWARE DESIGN OF A SINGLE PHASE INVERTER WITH LC FILTER

5.1 Overview

This chapter discusses about the hardware implementation of a standalone single phase inverter with an LC filter supplying a resistive load (similar to an uninterrupted power supply). This hardware is built as a stepping stone for implementing a grid connected PV inverter. This setup can act as a basic structure upon which a grid connected inverter can be constructed. Section 5.2 deals with the H-bridge topology and its intuitiveness and simplicity. It also presents the design of auxiliary power circuit and level shifter circuit required by the IGBT driver. The next section 5.3, discusses about the procedure of designing the LC filter, as standalone inverter does not really require an LCL filter. Section 5.4 takes account of the microcontroller used and its features are discussed briefly. The next two sections 5.5 and 5.6 presents the implemented setup and output results. .

5.2 H-Bridge Topology

Inverter circuits form an intergral part in many technological applications, namely renewable energy resources, HVDC power transmission, Electric drives, and many more modern applications. In all the applications, the goal of an inverter remains the same, that is to convert DC power to AC power in an efficient way possible. There are many inverter topologies in the literature to convert the power. And the most common of the topology is the H-bridge topology, which is simple and efficient. The schematic of the H-bridge topology and working is presented in the Fig. 5.1. This topology can be controlled using either a square wave signal or a PWM signal [67] [68].

Four IGBT are used for the configuration. Each IGBT have an anti parallel diode internally, which is useful in case of a R-L load, so these diodes are also known as feedback diodes.

Positive half cycle (0-T/2):

- For square wave control, switch S_1 and S_2 are turned ON, whereas switch S_3

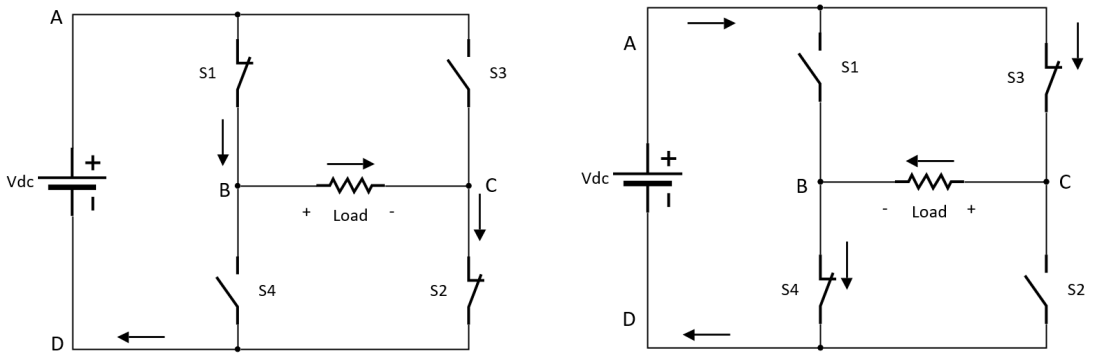

Figure 5.1: (a) when S_1 and S_2 are switched ON (b) when S_3 and S_4 are switched ON

and S_4 are turned OFF.

- current flow is given by A-B-C-D.
- V_{dc} is the voltage across the load resistor.

Negative half cycle (T/2-T):

- For square wave control, switch S_1 and S_2 are turned OFF, whereas switch S_3 and S_4 are turned ON.
- current flow is given by A-C-B-D.
- $-V_{dc}$ is the voltage across the load resistor.

As the load shown in the Fig. 5.1 is purely resistive, therefore feedback diodes do not come into play.

5.2.1 IGBT specification

SKM75GB12T4 – SEMIKRON

Properties:

- IGBT4 = 4^{th} generation Infineon IGBT.
- CAL4 = 4^{th} generation CAL diode
- Direct Bonded Copper (DBC) technology for insulated base plate
- Gate resistor is internally integrated
- Switching frequency is upto 20kHz

The IGBT module parameter's maximum value are shown in the table 5.1, and the IGBT module used in the hardware setup is shown in the Fig. 5.2

Parameter	Max. value
V_{ces}	1200 V
I_{cnom}	75 A
V_{ges}	-20 ... 20 V
$V_{ce(sat)}$	2.1 V ($@Ic = 75A$)
R_{ce}	22 $m\Omega$

Table 5.1: Maximum value of IGBT module parameters

Figure 5.2: IGBT – SKM75GB12T4 (SEMIKRON)

5.2.2 Driver circuit

The interface between the controller and the IGBT modules constitutes the SKYPER PRO 32 driver circuit core. It is used to control half bridge modules. The integration of protection, potential separation, and driving the switch is internally designed withing. Therefore, it can be easily be used to drive the IGBT module. The driver module has the following properties:

- Channel output is two in number
- Potential free power supply for the secondary side is integrated
- Short Pulse Suppression (SPS)
- Protection of under voltage for both primary and secondary side
- Under Voltage Reset (UVR)
- Drive interlock
- Short circuit protection
- Soft Turn-Off (STO)
- Handle voltage (DC) up to 1200V

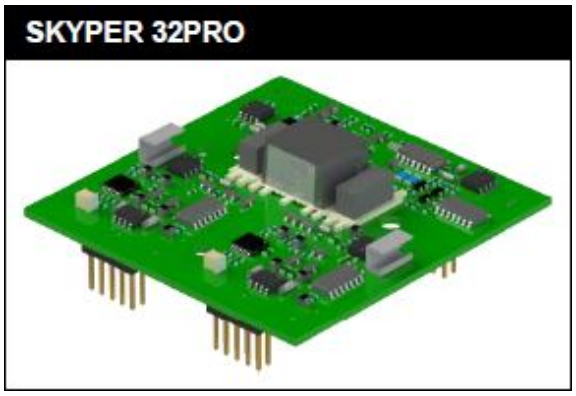

Figure 5.3: Skyper 32PRO 3D model (SEMIKRON)

5.2.3 Auxiliary power and level shifter circuit

The auxiliary power circuit is required to supply 15 V power to the driver circuit and 5 V to Arduino UNO board. It is implemented using LM7805CT/15CT linear regulator IC. It also supplies power to the level shifter circuit.

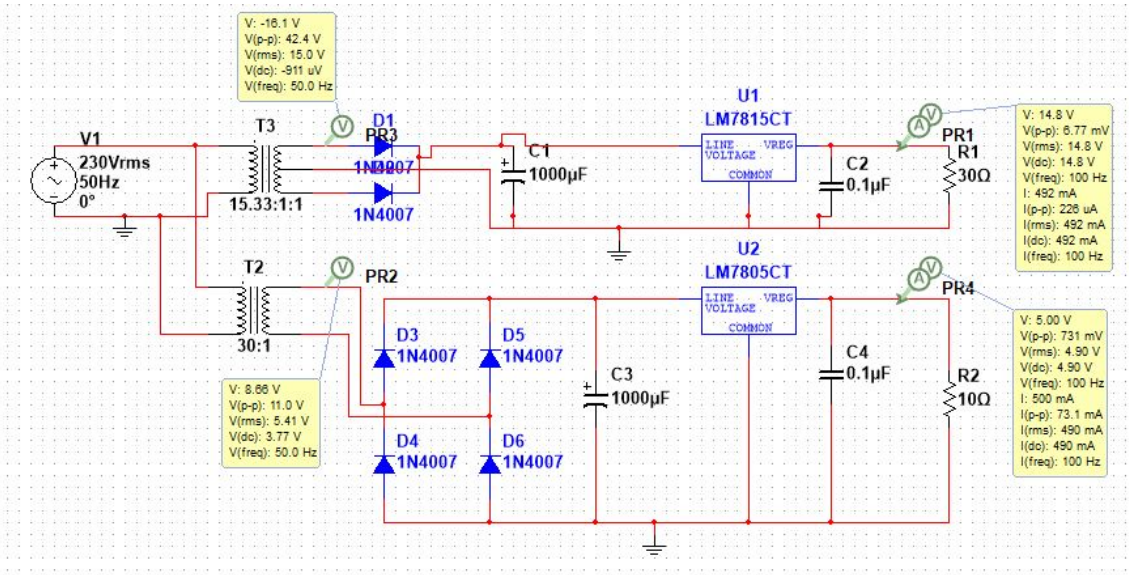

Figure 5.4: Auxiliary power circuit schematic (MULTISIM)

The level shifter circuit is used to perform two important functions. First, it converts the 5V pulses from the Arduino to 15V pulses for the driver circuit. Second, it isolates the Arduino from the power circuit so as to protect the low power control circuit from any damage. This is implemented using opto-isolator IC MCT2E. The schematic diagram for both the sub-systems is shown in the Fig. 5.4 and Fig. 5.5. The simulation of both circuits is performed on the MULTISIM software.

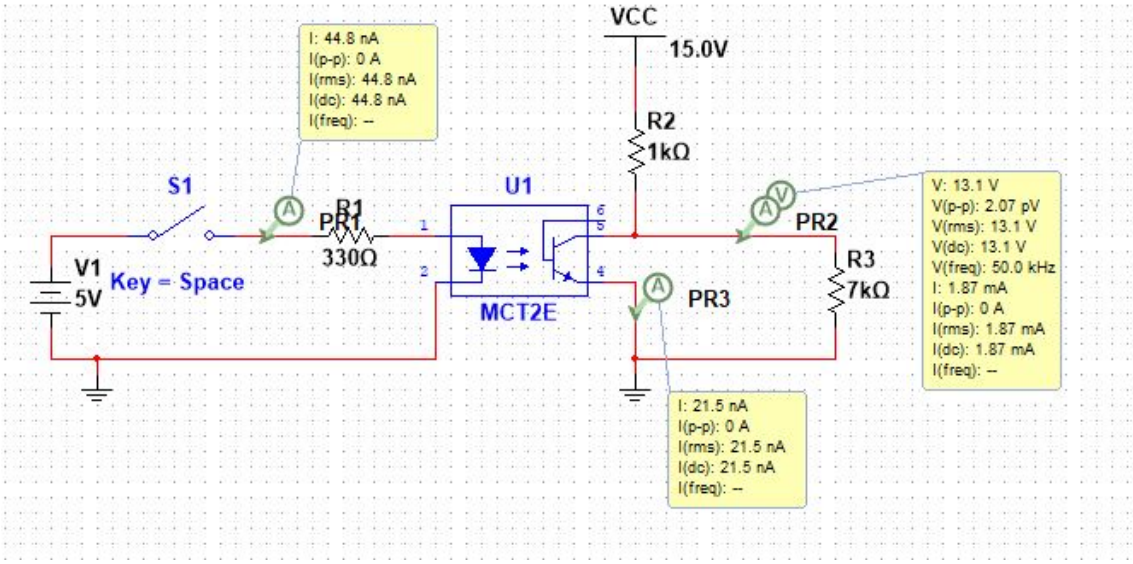

Figure 5.5: Level shifter circuit schematic (MULTISIM)

5.3 LC filter design

In this section, a procedure for designing a single phase inverter with a LC filter is presented. First, derivation of the total harmonic inductor current and capacitor voltage is performed along with its analysis. As the solution of designing the LC values results into infinite solutions, another criteria of reactive power absorbed by the filter is used to find specific design values. The hardware setup is built upon the calculated values from the procedure described in[69].

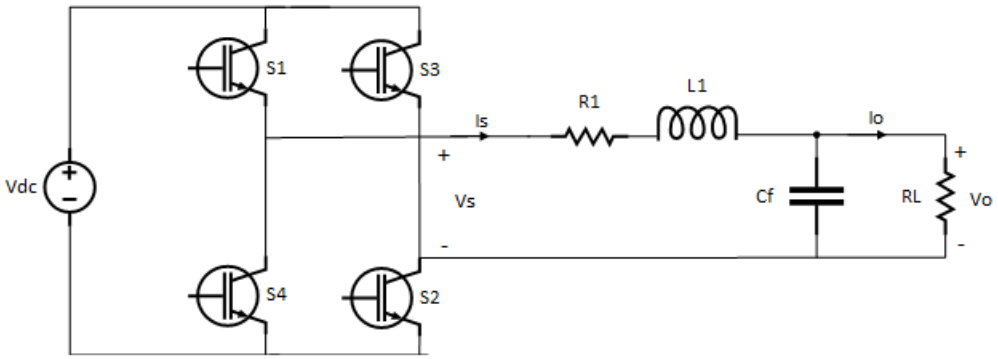

Figure 5.6: Schematic of Single phase inverter with LC filter

In Fig. 5.6, the schematic of single phase inverter with LC filter and load is given, and this is used as the reference circuit. Following assumptions are used for the derivation [70] :

- The input dc source V_{dc} is constant and ripple free.
- Semiconductor switching devices are considered ideal in nature.
- The ESR of filter capacitor is neglected.

- Linear load (a resistance) is connected.

The voltage equation can be written as in eqn. (5.1). It is with reference to shown as per Fig. 5.6.

$$v_s = v_o + R_1 i_s + L_1 \frac{di_s}{dt} \tag{5.1}$$

Where, v_o represents the capacitor or output voltage; v_s is the inverter output voltage; i_1 is the current through filter inductor, and R_1 is the internal resistance of the inductor.

5.3.1 Design procedure

Based on the analysis shown in [71], the steps to design the LC filter values are as follows:-

1. The nominal modulation index (k) is calculated on the basis of input dc voltage (V_{dc}), and output load voltage (V_o). The voltage drop across the filter inductor is assumed to be negligible, as the value of L_1 is not known yet. This is a fairly valid assumption because the drop in inductor is compensated by the shunt capacitor. Therefore, the rms value of inverter output voltage can be approximated to be equal to the rms value of load voltage, thus we get,

$$k = \sqrt{2}\frac{V_o}{V_{dc}} \tag{5.2}$$

   The nominal modulation index (k) in eqn. (5.3) is used to find the factor K,

$$K = \left[\frac{k^2 - \frac{15}{4}k^4 + \frac{64}{5\pi}k^5 - \frac{5}{4}k^6}{1440}\right]^{1/2} \tag{5.3}$$

2. Based on the factor K calculated above, fundamental output and switching frequency, f_r and f_s; nominal load current $I_{o,rms}$, and the rms value of total harmonic of load voltage $V_{o,rms}$, the optimal value of L_1 is calculated using the eqn. (5.4).

$$L_1 = \frac{V_{o,rms}}{I_{o,rms} f_s}\left\{K\frac{V_{dc}}{V_{o,av}}\left[1 + 4\pi^2\left(\frac{f_r}{f_s}\right)^2 K\frac{V_{dc}}{V_{o,av}}\right]\right\}^{1/2} \tag{5.4}$$

3. Finally, using the eqn. (5.5) the value of filter capacitor is calculated.

$$C_f = K\frac{V_{dc}}{L_1 f_s^2 V_{o,av}} \tag{5.5}$$

Just to note that if the DC input voltage source is varying, then the value used should be the one that gives the most worse harmonic value. This way design will still remain validated [71].

5.4 Micro-controller unit

5.4.1 Arduino Uno

The controller used is Arduino Uno for generating the unipolar SPWM gating pulse. The micro-controller unit (MCU) integrated in Arduino Uno is Atmega328p from AVR [72]. The board's pin description is as shown in the Fig. 5.7. The SPWM program coded into the Arduino is such that it can change three parameters of the inverter output voltage as per the user via UART (serial communication). The three parameters are namely:-

1. Modulation Index
2. frequency
3. Phase angle

These parameters flexibility makes the system appropriate for manual synchronization with the grid as the system needs to synchronize the wave with that of grid waveform. This automation also paves the way for automatic synchronization program in future.

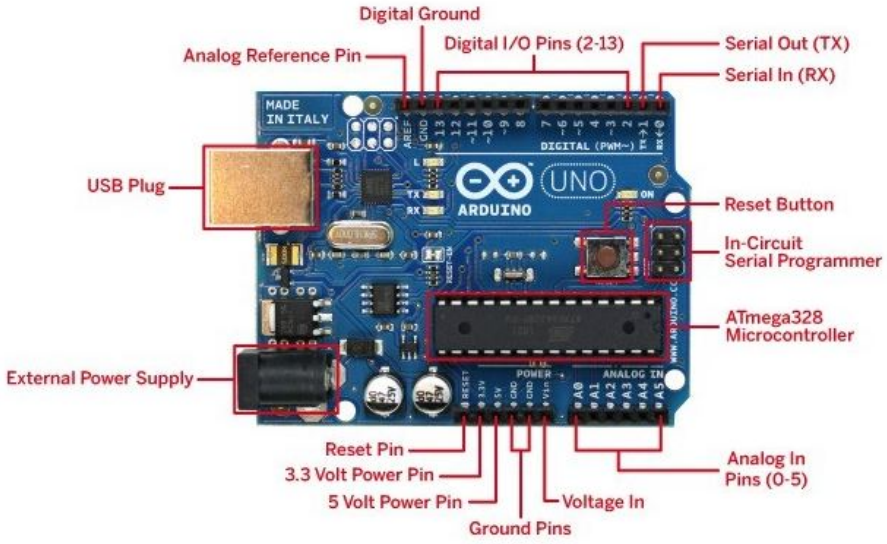

Figure 5.7: Arduino UNO Pin Configuration [72]

AtMega 328P specifications

The ATmega 328P is a low cost CMOS, 8 bit micro controller by AVR, which is based on the RISC architecture. Most of the instructions are executed in one cycle. This fact improves the speed of the controller, and thus giving a throughput of million instructions per second (MIPS). The power consumption is also very low due to the use of CMOS technology

Some of the peripheral features of the 8 bit microcontroller family are:-

- Two timers/counters of 8 bit size, along with prescalar and compare mode options
- Two timers/counters of 16 bit size, along with prescalar and compare mode options
- Real Time Counter with Separate Oscillator
- PWM channels - 6
- 10 bit ADC - 8 (SOIC package)
- Programmable I/O pins - 23

5.5 Hardware setup

The complete hardware setup is shown in the Fig. 5.8. The two half bridge IGBT modules are placed on top of a heat-sink in the center. The snubber capacitors are also connected with them. On the right side of the setup, the micro-controller and level shifter circuits are kept. They are also shown in the Fig. 5.9. Four opto-isolators are used for four switch signals. On the left hand side of the Fig. 5.8 are the LC filter components. Four $5\mu F$ capacitors are connected in parallel to form $20\mu F$ filter capacitor. The filter is followed by a DPST switch to connect the system to load.

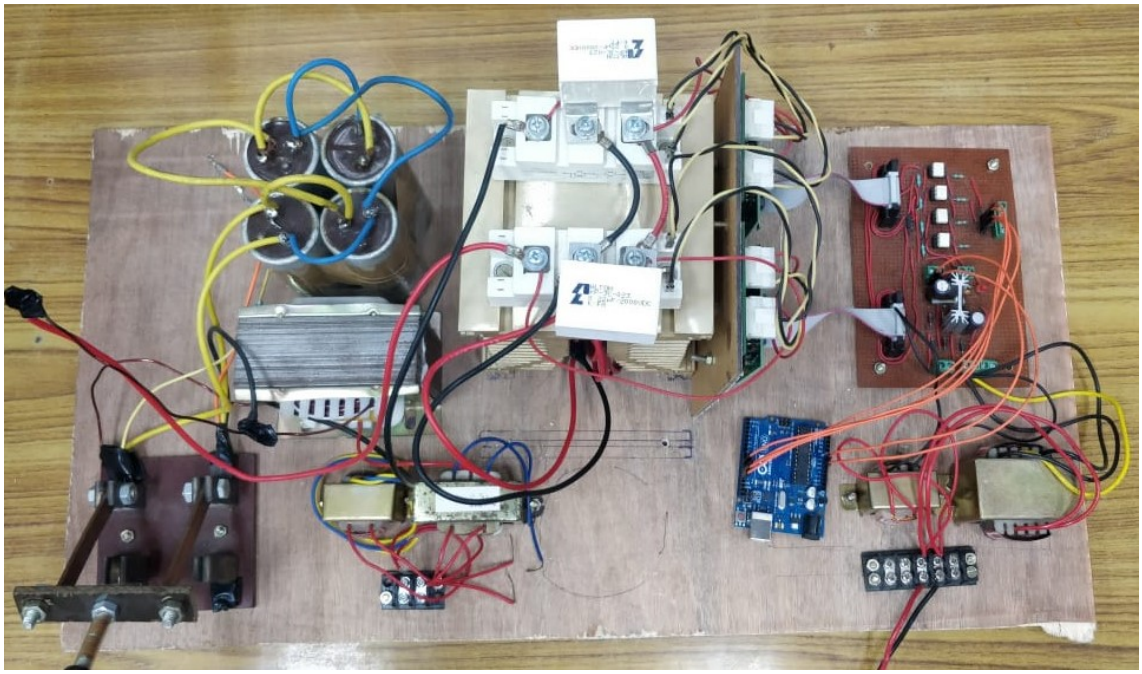

Figure 5.8: Complete Hardware setup

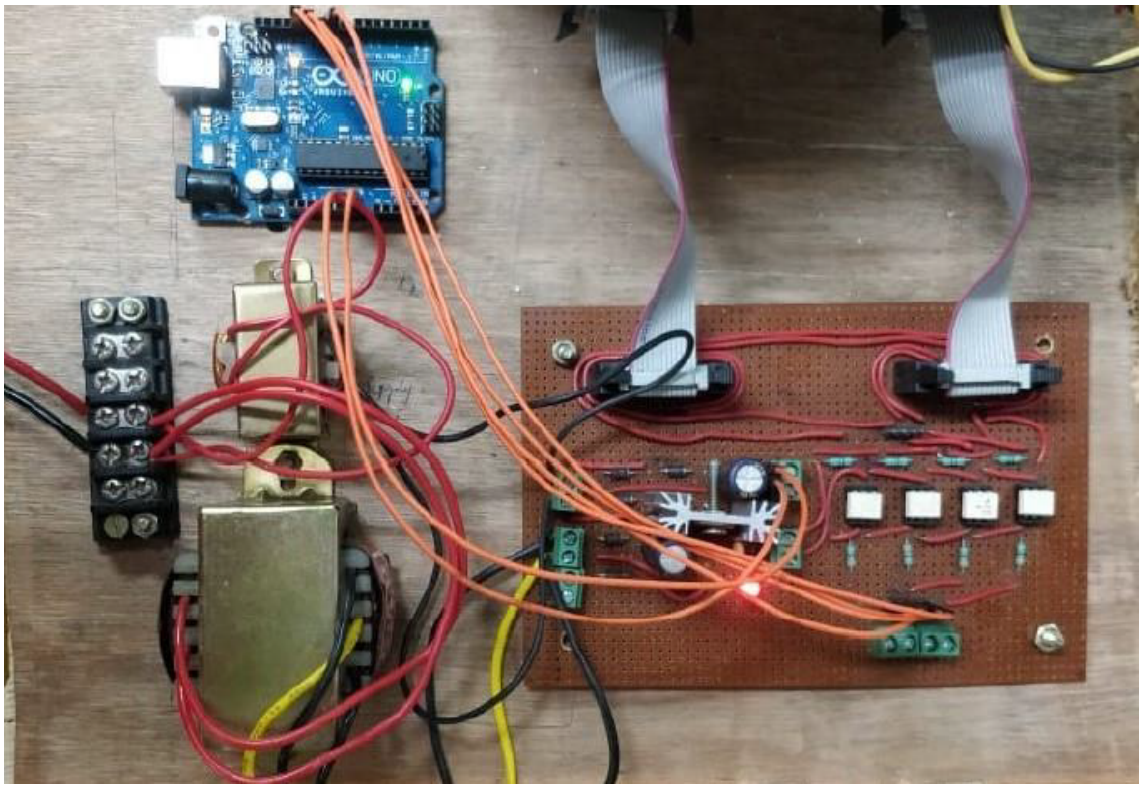

Figure 5.9: Auxiliary power supply and level shifter circuit

5.6 Results

The design parameters for the implemented hardware setup and the simulation in MATLAB is shown in the table 5.2. The dead band given in the Arduino code to the switches is $16\mu s$ which is much larger than their on/off time. The results are divided into two subsections; the first part shows the inverter output voltage without any filter connected, whereas second part shows the same quantity with the LC filter present. Thus, it becomes easy to visualize the difference.

Parameter	Value
Voltage source (V_{dc})	20 V
Filter inductance (L_1)	4.4 mH
Filter Capacitance (C_f)	20 uF
ESR of Filter inductance (R_1)	0.01 Ω
Load Resistance (R_L)	14 Ω
Switching frequency (f_s)	1 kHz

Table 5.2: Parameter values for the hardware setup

5.6.1 Without filter

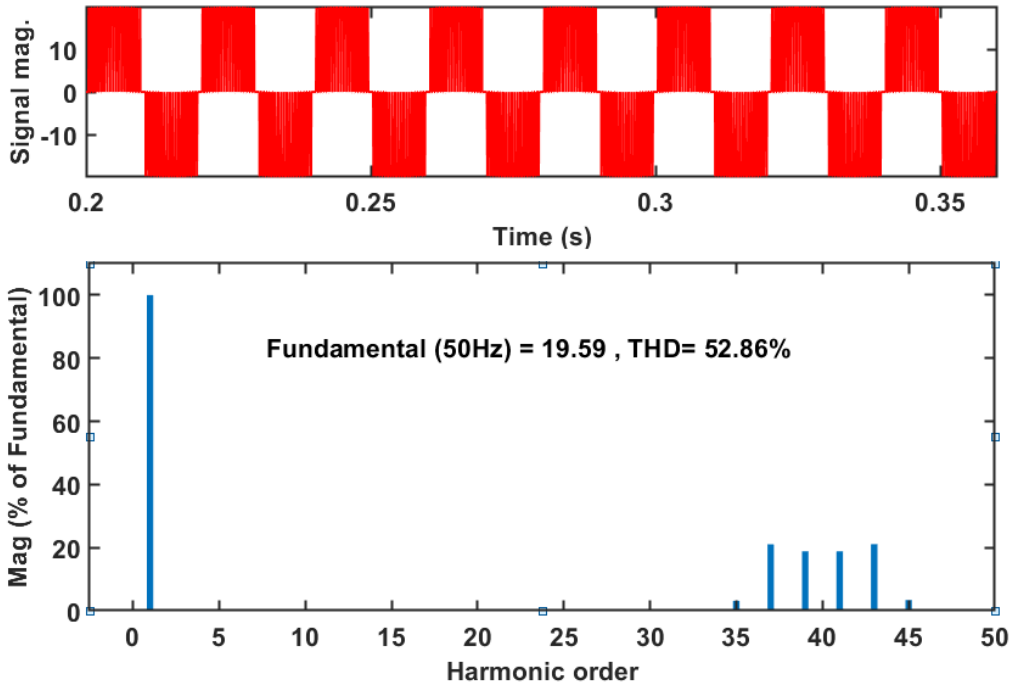

Figure 5.10: FFT analysis of Unfiltered inverter output voltage (MATLAB)

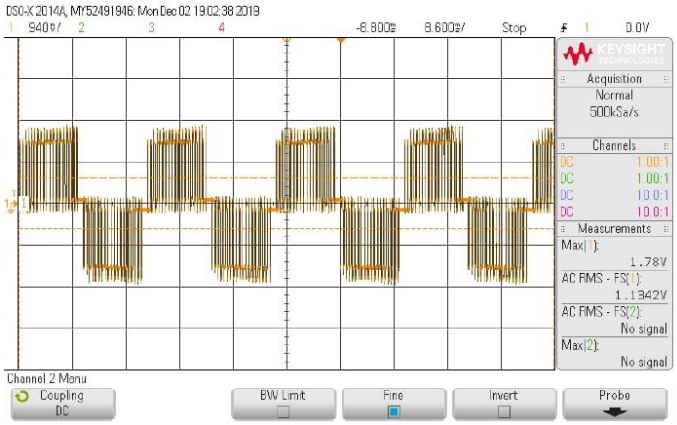

Figure 5.11: Output Voltage without LC Filter

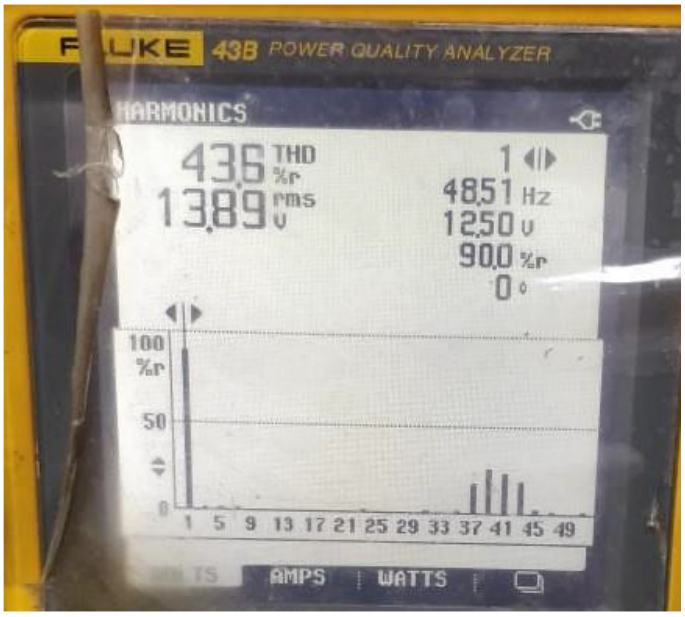

Figure 5.12: FFT Analysis of inverter output voltage without LC Filter (Hardware)

5.6.2 With filter

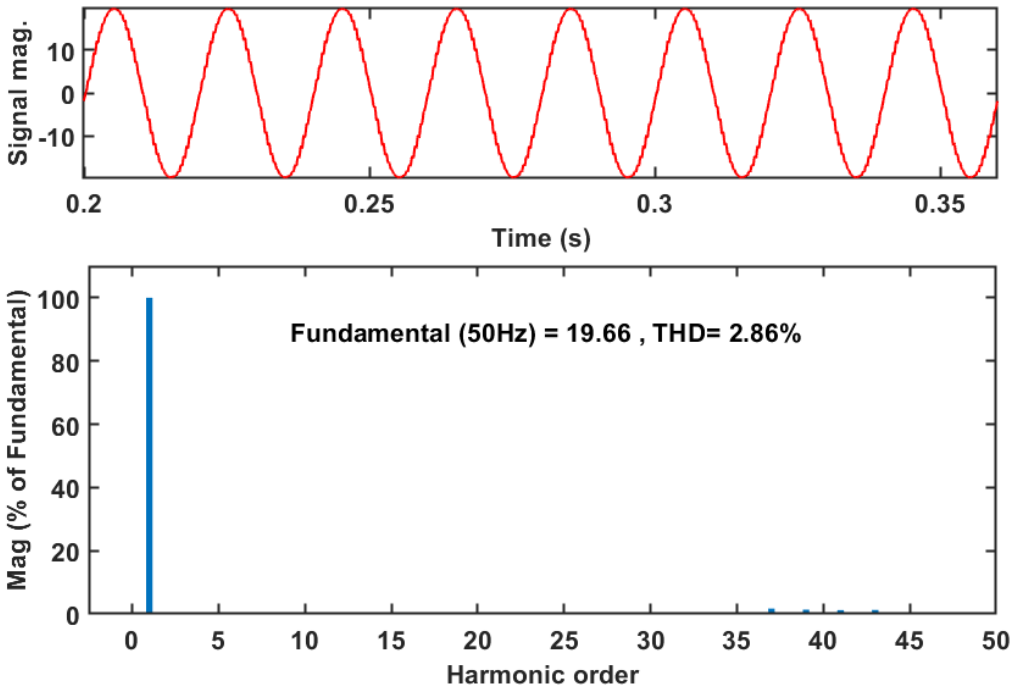

Figure 5.13: FFT analysis of Filtered inverter output voltage (MATLAB)

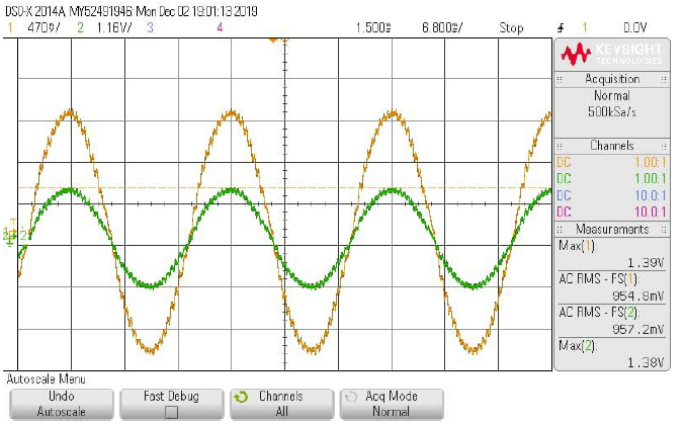

Figure 5.14: Output Voltage and Current with Filter

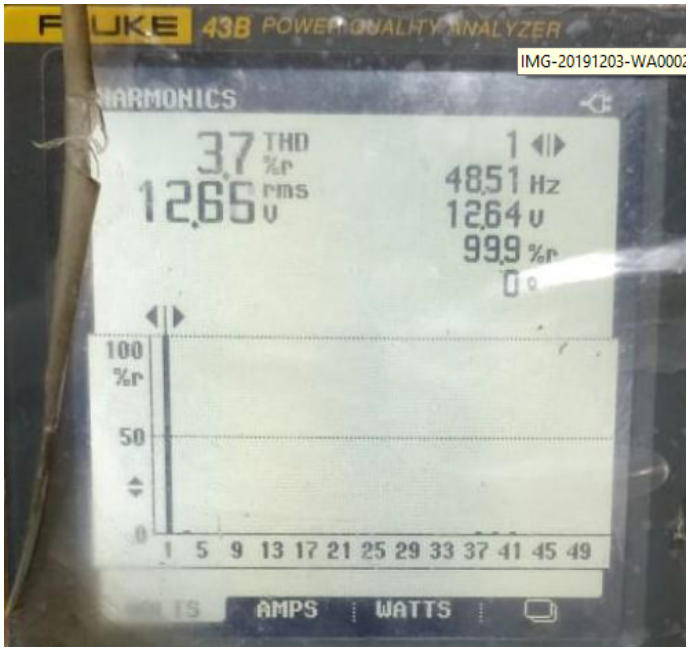

Figure 5.15: FFT Analysis of inverter output voltage with Filter (Hardware)

5.7 Conclusion

This hardware deals with the analysis and design of Single Phase H-Bridge inverter with Unipolar SPWM. The Simulink model has been designed in MATLAB with two states(with and without filter). The SPWM switching shifts the harmonics to higher order and hence the filter size required reduces. The %THD has also reduced to less than 5% with filter.The is in agreement with the simulation results obtained for the same .In addition to it,the controller used(Arduino Uno) is fully capable of generating as well as manual controlling SPWM pulses in open loop configuration.

Chapter 6

CONCLUSION AND FUTURE SCOPE

6.1 Conclusion

Four current controllers have been designed and simulated. Their performance is analyzed and compared under varying atmospheric conditions. The following conclusion can be drawn from the presented thesis:

- Before the design of the control system, the simulation of the power circuit is built with stable results. The design of LCL filter, Bipolar SPWM, and DC link capacitance is carried out and a working model is obtained successfully.
- Proportional Resonant control gives better performance than the d-q controller. Though its response is not as good as the modern controllers but the ease of implementing it makes it a good option.
- Fuzzy logic control transient response is fastest of all but requires high computational power to go through all the rules in each sample. Also, It produces the grid current with least %THD.
- Model Predictive control modeled is a simpler form of the more complex type. It is an approximate model with reduced computation and the performance is comparable to the classical control methods.
- Single phase inverter prototype have been developed in laboratory and circuits such as level shifter, auxiliary power supply, and micro-controller programming have been implemented. Performance of inverter is tested satisfactorily in an open loop configuration.
- From the results it is observed that modern controllers performance is better than that of the conventional controllers. Due to the advancements and reduction in prices of digital micro-processors, such techniques can be realized easily.

6.2 Future Scope

The presented system in the thesis is an assembly with very much simplicity, so as to observe the performance of the current controllers easily, without making it complex. This project can be extended in the following direction of work:-

- A look into active damping methods of LCL filter, as passive damping results into reduction in system efficiency.
- Complete hardware implementation of the described power circuit and its control system, to verify the simulation results.
- Response of the control system in case of non-linear loads and practical grid supply (with harmonics present).
- Use of the adaptive MPPT algorithms, which unlike P&O method, do not have steady state oscillations, .

REFERENCES

[1] G. Tiwari and R. Mishra, *Advanced Renewable Energy Sources*. Royal Society of Chemistry, 2015, ISBN: 9781782625780.

[2] U. S. Energy Information Administration, *International Energy Outlook 2019*. Office of Energy Analysis U.S. Department of Energy Washington DC 20585.

[3] International Energy Agency and International Energy Agency Staff, "Electricity information 2002," *With 2001 Data IEA StatisticsOECD International Energy Agency 9 Rue de la Federation 75015 Paris France*, 2002.

[4] ——, "Electricity information 2010," *With 2009 Data IEA StatisticsOECD International Energy Agency 9 Rue de la Federation 75015 Paris France*, 2010.

[5] ——, "Electricity information 2017," *With 2016 Data IEA StatisticsOECD International Energy Agency 9 Rue de la Federation 75015 Paris France*, 2017.

[6] U. S. Energy Information Administration, *International Energy Outlook 2017*. Office of Energy Analysis U.S. Department of Energy Washington DC 20585, 2017.

[7] ——, *International Energy Outlook 2017*. Office of Energy Analysis U.S. Department of Energy Washington DC 20585, 2017.

[8] Secretariat UNFCCC, "Report of the conference of the parties on its fifteenth session," United Nations Framework Convention on Climate Change, held in Copenhagen, 2009.

[9] Secretary, "In conversation with MNRE," *Akshay Urja*, vol. 12, 5 2019.

[10] J. Twidell and T. Weir, *Renewable Energy Resources*, 3rd ed. Taylor and Francis, 2015, ISBN: 9781317660378.

[11] O. Ellabban, *Renewable energy resources Current status future prospects and their enabling technology, Renewable and Sustainable Energy Reviews*. 2014, pp. 748–764.

[12] A. Qamer. (2016). "Solar (PV)," [Online]. Available: `http://www.alqamer.com/index.php/2016-02-01-19-25-41/solar-pv`.

[13] Wikipedia the free encyclopedia. (2020). "Renewable energy in india," [Online]. Available: `https://en.wikipedia.org/wiki/Renewable_energy_in_India`.

[14] ——, (2020). "Solar cell," [Online]. Available: `https://en.wikipedia.org/wiki/Solar_cell`.

[15] T. Salmi, M. Bouzguenda, A. Gastli, and A. Masmoudi, "MATLAB/Simulink based modelling of solar photovoltaic cell," *International Journal of Renewable Energy Research*, vol. 2, no. 2, 2012.

[16] P. Patil, V. Jadhav, and S. Sharma, "Solar Photovoltaic Plant with single quadrant DC-DC converter equipped with maximum power point tracker," B.Tech. College of Engineering, Pune, 2015.

[17] J. Carrasco, "Power electronic systems for the grid integration of renewable energy sources: A survey," *IEEE Transactions on Industrial Electronics*, vol. 53, no. 4, pp. 1002–1016, 2006, ISSN: 0278-0046.

[18] J. Rodriguez and P. Cortes, *Predictive Control of Power Converters and Electrical Drives*. Wiley-IEEE Press, 2012, pp. 3–39, ISBN: 9781119963981.

[19] T. Ohnishi, "Three phase pwm converter by means of instantaneous active and reactive power control," *Electronics Control and Instrumentation 1991 Proceedings IEEE*, pp. 819–824, 1991.

[20] P. Cortes, "Predictive control in power electronics and drives," *IEEE Transactions on Industrial Electronics*, vol. 55, no. 12, pp. 4312–4324, 2008, ISSN: 0278-0046.

[21] L. Haoyan, "Control Design of a Single-Phase DC/AC Inverter for PV Applications," Thesis and Dissertations, University of Arkansas Fayetteville, 2016.

[22] X. Zong, "A Single Phase Grid Connected DC/AC Inverter with Reactive Power Control for Residential PV Application," University of Toronto Canada, 2011.

[23] T. Esram, "Comparison of photovoltaic array maximum power point tracking techniques," *IEEE Proceedings*, 2007.

[24] Q. Zhang, "A Center Point Iteration MPPT Method With Application on the Frequency-Modulated LLC Microinverter," *IEEE Transactions on Power Electronics*, vol. 29, pp. 1262–1274, 3 2014.

[25] F. Roberto, "Energy comparison of MPPT techniques for PV Systems," *WSEAS transactions on Power Systems*, vol. 3, 6 2008.

[26] R. F. Coelho, F. M. Concer, and D. C. Martins, "A MPPT approach based on temperature measurements applied in PV systems," in *2010 IEEE International Conference on Sustainable Energy Technologies (ICSET)*, 2010, pp. 1–6.

[27] N. Anuja and W. Harshal, "Unipolar and Bipolar PWM Inverter," in *IJIRST –International Journal for Innovative Research in Science and Technology*.

[28] O. Lopez, "Eliminating ground current in a transformerless photovoltaic application," in *IEEE transactions on energy conversion*, vol. 25, 2010.

[29] B. Chenlei and R. Xinbo, "Stepby- Step Controller Design for LCL-Type Grid-Connected Inverter with Capacitor–Current- Feedback Active-Damping," in *Power Electronics IEEE Transactions*, 23 vols., 2014, pp. 1239–1253.

[30] J. Sosa, G. Escobar, M. Rodriguez, P.R., G. Vazquez, M. Juarez, and M. Diosdado, "Comparative evaluation of L and LCL filters in transformerless grid tied converters for active power injection," in *Power Electronics and Computing (ROPEC)*, I. I. A. Meeting, Ed., 2014.

[31] C. Hanju and V. Trung-Kien, "Comparative analysis of low-pass output filter for single phase grid-connected photovoltaic inverter," in *Applied Power Electronics Conference and Exposition (APEC)*, 2010.

[32] M. Bhardwaj, S. Choudhury, V. Xue, and B. Akin, "Online LCL filter compensation using embedded FRA," in *2014 IEEE Applied Power Electronics Conference and Exposition - APEC 2014*, 2014, pp. 3186–3191.

[33] A. Houari, "Large signal stability analysis and stabilization of converters connected to grid through LCL filters," in *IEEE Trans. Ind. Electron*, vol. 61, 2014, pp. 6507–6516.

[34] K. Jalili and S. Bernet, "Design of LCL filters of active-front-end two level voltage-source converters," in *IEEE Trans. Ind. Electron*, vol. 56, 2009, pp. 1674–1689.

[35] R. Pena-Alzola, M. Liserre, F. Blaabjerg, R. Sebastian, J. Dannehl, and F. W. Fuchs, "Analysis of the passive damping losses in LCL-filter based grid converters," in *IEEE Trans. Power Electron*, vol. 28, 2013, pp. 2642–2646.

[36] J. Dannehl, M. Liserre, and F. W. Fuchs, "Filter-based active damping of voltage source converters with LCL filter," in *IEEE Trans. Ind. Electron*, vol. 58, 2011, pp. 3623–3633.

[37] J. Xu, S. Xie, and T. Tang, "Active damping-based control for grid connected LCL filtered inverter with injected grid current feedback only," in *IEEE Trans. Ind. Electron*, vol. 61, 2014, pp. 4746–4758.

[38] P. C. Krause, O. Wasynczuk, and S. D. Sudhoff, *Analysis of Electric Machinery*. IEEE press, 1995.

[39] B. Crowhurst, E. El-Saadany, L. Chaar, and L. Lamont, "Single-phase grid-tie inverter control using dq transform for active and reactive load power compensation," in *IEEE International Conference on Power and Energy (PECon)*, 2010, pp. 489–494.

[40] X. Fu and S. Li, "Control of Single-Phase Grid-Connected Converters With LCL Filters Using Recurrent Neural Network and Conventional Control Methods," in *IEEE Transactions on Power Electronics*, 31 vols., 2016, pp. 5354–5364.

[41] R. Teodorescu, M. Liserre, and P. Rodriguez, *Grid Converters for Photovoltaic and Wind Power Systems*. Chichester, West Sussex, United Kingdom: John Wiley and Sons, 2011.

[42] M. Liserre, F. Blaabjerg, and S. Hansen, "Design and control of an LCL filter-based three-phase active rectifier," in *IEEE Trans. Ind. Appl*, 41 vols., 2005, pp. 1281–1291.

[43] MATLAB Help. (2013). "PLL," [Online]. Available: `https://in.mathworks.com/help/physmod/sps/powersys/ref/pll.html`.

[44] V. Trung-Kien and S. Se-Jin, "Comparison of PI and PR Controller Based Current Control Schemes for Single-Phase Grid-Connected PV Inverter," in *IEEE conference*, 11 vols., 2010, pp. 2968–2974.

[45] R. Teodorescu, F. Blaabjerg, M. Liserre, and P. Loh, "Proportional-resonant controllers and filters for grid-connected voltage-source converters," in *IEE Proc.-Electr. Power Appl*, 153 vols., 2006.

[46] D. Zmood, D. Holmes, and G. Bode, "Frequency-domain analysis of three-phase linear current regulators," in *IEEE Transactions on Industry Applications*, 37 vols., 2001, pp. 601–610.

[47] V. Trung-Kien and S. Se-Jin, "PR Controller based Current Control Scheme for Single-Phase Inter-Connected PV Inverter," in *Journal of the Korean Academic Industrial Society*, 10 vols., 2009, pp. 3587–3593.

[48] Z. Ningyun, T. Houjun, and Y. Chen, "A Systematic Method for Designing a PR Controller and Active Damping of the LCL Filter for Single-Phase Grid-Connected PV Inverters," *Open access energies*, pp. 3934–3954, 2014, ISSN: 1996-1073.

[49] MATLAB Help. (2020). "What is fuzzy logic?" [Online]. Available: `https://in.mathworks.com/help/fuzzy/what-is-fuzzy-logic.html`.

[50] V. Novák, I. Perfilieva, and J. Močkoř, *Mathematical principles of fuzzy logic*. 1999, ISBN: 978-0-7923-8595-0.

[51] Stanford Encyclopedia of Philosophy. (2006). "Fuzzy logic," [Online]. Available: `https://plato.stanford.edu/entries/logic-fuzzy/`.

[52] Tutorialpoint. (2019). "Fuzzy logic - inference system," [Online]. Available: `https://www.tutorialspoint.com/fuzzy_logic/fuzzy_logic_inference_system.htm`.

[53] S. Islam, K. Zeb, W. Din, I. Khan, M. Ishfaq, A. Hussain, T. Busarello, and H. Kim, "Design of robust fuzzy logic controller based on the levenberg marquardt algorithm and fault ride trough strategies for a grid-connected PV system," in *Electronics*, 2019.

[54] M. Hannan, M. Lipu, P. Ker, R. Begum, V. Agelidis, and F. Blaabjerg, "Power electronics contribution to renewable energy conversion addressing emission reduction: Applications issues and recommendations," in *Appl. Energy*, 2019.

[55] R. Wai, M. Chen, and Y. Liu, "Design of adaptive control and fuzzy neural network control for single-stage boost inverter," in *IEEE Trans. Ind. Electron.*, vol. 62, 2015, pp. 5434–5445.

[56] J. Zhang, P. Shi, J. Qiu, and S. Nguang, "A novel observer-based output feedback controller design for discrete-time fuzzy systems," in *IEEE Trans. Fuzzy Syst.*, 23 vols., 2015, pp. 223–229.

[57] Y. Wang, Y. Yang, G. Fang, B. Zhang, H. Wen, H. Tang, L. Fu, and X. Chen, "An advanced maximum power point tracking method for photovoltaic systems by using variable universe fuzzy logic control considering temperature variability," in *Electronics*, 7 vols., 2018.

[58] J. Holtz and S. Stadtfeld, "A predictive controller for the stator current vector of AC machines fed from a switched voltage source," in *International Power Electronics Conference*, 1983, pp. 1665–1675.

[59] P. Mutschler, "A new speed-control method for induction motors," in *Conference Record of PCIM*, 1998, pp. 131–136.

[60] T. Kawabata, T. Miyashita, and Y. Yamamoto, "Dead beat control of three phase PWM inverter," in *IEEE Transactions on Power Electronics*, 5 vols., 1990, pp. 21–28.

[61] S. Kouro, P. Cortes, R. Vargas, U. Amman, and J. Rodriguez, "Model predictive control – a simple and powerful method to control power converters," in *IEEE Transactions on Industrial Electronics*, 56 vols., 2009, pp. 1826–1838.

[62] J. M. C. Geldenhuys, H. du Toit Mouton, A. Rix, and T. Geyer, "Model predictive current control of a grid connected converter with LCL filter," in *2016 IEEE 17th Workshop on Control and Modeling for Power Electronics (COMPEL)*, 2016, pp. 1–6.

[63] C. E. Garcia, D. M. Prett, and M. Morari, "Model predictive control: Theory and practice – a survey," in *Automatica*, vol. 25, 1989, pp. 335–348.

[64] Y. Xingwu, J. Hongchao, and G. Wei, "Model predictive control of single phase grid-connected inverter," in *2014 IEEE PES Asia-Pacific Power and Energy Engineering Conference (APPEEC)*, 2014, pp. 1–4.

[65] M. Mosa, H. Abu-Rub, M. E. Ahmed, A. Kouzou, and J. Rodriguez, "Control of single phase grid connected multilevel inverter using model predictive control," in *4th International Conference on Power Engineering, Energy and Electrical Drives*, 2013, pp. 624–628.

[66] E. Z. Bighash, S. M. Sadeghzadeh, E. Ebrahimzadeh, Y. Yang, and F. Blaabjerg, "A novel model predictive control for single-phase grid-connected photovoltaic inverters," in *017 IEEE Energy Conversion Congress and Exposition (ECCE)*, 2017, pp. 461–467.

[67] M. H. Rashid, *Power electronics circuit device and application*, ch. 6, pp. 253–256.

[68] P. S. Bimbhra, *Power Electronics*, 4th edition. New Delhi: Khanna Publishers, 2003.

[69] S. B. Dewan and P. D. Ziogas, "Optimum Filter Design for a Single-phase Solid-state UPS System," in *IEEE Trans. Ind. Appl*, 15 vols., 1979, pp. 664–669.

[70] H. van der Broeck, "Untersuchung des oberschwingungsverhaltens eines hochtaktenden vierquadmntstellers," in *ET2 Archiv*, 8 vols., 1986, pp. 195–199.

[71] P. A. Dahono, A. Purwadi, and Qamaruzzaman, "An LC Filter Design Method for Single-phase PWM Inverters," in *IEEE Catalogue*, 1995.

[72] Arduino Project Hub. (2002). "Getting started," [Online]. Available: `https://www.arduino.cc/en/guide/introduction`.